Spring 12-6-2017

# Dynamics of Solute Transport and Rare Earth Element Behavior in Acid Mine Drainage Impacted Alpine Rivers, Snake River CO

Jordan Elizabeth Carroll
*University of Colorado at Boulder*, jordan.carroll@colorado.edu

# DYNAMICS OF SOLUTE TRANSPORT AND RARE EARTH ELEMENT BEHAVIOR IN ACID MINE DRAINAGE IMPACTED ALPINE RIVERS, SNAKE RIVER CO

By

JORDAN ELIZABETH CARROLL

A thesis submitted to the Faculty of the Graduate School of the University of Colorado in partial fulfillment of the requirement for the degree of Master of Science

Environmental Engineering

Master of Science

May 2017

**This Thesis entitled:**
**DYNAMICS OF SOLUTE TRANSPORT AND RARE EARTH ELEMENT BEHAVIOR IN ACID MINE DRAINAGE IMPACTED ALPINE RIVERS, SNAKE RIVER CO**
**written by Jordan Carroll**
**has been approved for the Environmental Engineering Program**

Dr. Diane M. McKnight, University of Colorado at Boulder
Committee Chair

Dr. Roseanna Neupauer, University of Colorado at Boulder

Dr. Robert L. Runkel, United States Geological Survey

The final copy of this thesis has been examined by the signatories, and we find that both the content and the form meet acceptable presentation standards of scholarly work in the above mentioned discipline.

DYNAMICS OF SOLUTE TRANSPORT AND RARE EARTH ELEMENT BEHAVIOR IN ACID MINE DRAINAGE IMPACTED ALPINE RIVERS, SNAKE RIVER CO

Jordan Carroll (M.S., Environmental Engineering)

*Thesis Directed By Dr. Diane M. McKnight*

**Abstract**

Quantifying and understanding the transport of rare earth elements (REEs) in relation to heavy metals within acidic alpine rivers is relatively understudied. However, employing solute transport models, specifically One-Dimensional Transport with Inflow and Storage (OTIS) can provide insight on the reactivity and transport of REEs. The Snake River is located along the Colorado Mineral Belt in Summit County, Colorado and drains into metropolitan Denver's drinking water source – Dillon Reservoir. The Snake River is of particular interest due to its hydrological and geochemical similarity to other alpine streams impacted by acid mine drainage throughout Colorado.

In previous studies, most REEs were found to behave conservatively at lower pH. In general, the higher concentrations of REEs were found at the headwaters containing lower pH levels with decreasing concentrations as pH increased from 4.13 to 8.52. Using size-partitioning experiments, the composition of colloidal and dissolved metal oxides were obtained to determine the dominant state of Fe and Al, and subsequent interaction with REEs. Fractionation experiments showed that REEs are proportionally more abundant in their

dissolved form at lower pH < 5. The distribution between colloidal and dissolved phases increased as pH increased.

The influence of pH on metal complexation, precipitation/dissolution and oxidation/reduction was investigated using simulations, and parameter estimation to analyze data collected from synoptic sampling and tracer injection experiments. Modeling the transport of these REEs of industrial importance will significantly resolve issues concerning acid mine drainage remediation and future mineral extraction.

**Acknowledgements**

I cannot express enough thanks to my advisor Dr. Diane McKnight – a person who is truly dedicated to the advancement of science and engineering. It has been an honor to work with Diane, and I would not have been able to complete such research without her expert guidance and encouragement. Through her invaluable insight and unconventional approach to solving problems, I have progressed as both a researcher and a well-rounded individual. She is the primary motivation for this research, and progression into stream ecology hereafter.

I would like to give special thanks to Dr. Robert Runkel for his patience and expertise on the Snake River watershed, and in hydrological modeling. He has provided a solid framework and necessary support for establishing my research. He has provided me opportunities to work with his team, and not only is a great teacher with an open door policy, but a brilliant hydrologist.

Thank you, Dr. Roseanna Neupauer for setting aside time from a busy schedule to sit on my committee, and offer much appreciated feedback.

My sincere thanks to Garrett Rue for discovering sources of REEs in the Snake River watershed, showing me the ropes, and clarifying complex geochemical principles. This research is an extension of his own, and I owe him many thanks.

I could not have collected synoptic and tracer data without the help from Maggie Baker and the graduates of Applied Stream Ecology. Thank you so much for making this research possible.

Thank you, Dr. Fred Luiszer for swift water quality analysis at The Laboratory for Environmental and Geological Sciences, and many great stories.

Sabre Duren has provided great feedback regarding revisions. She is an excellent writer and communicator. She has, through patience and time, encouraged me to develop as a science writer.

I would also like to thank the Institute of Arctic and Alpine Research (INSTAAR) and the American Water Resources Association (AWRA) for their financial support in extensive sample analyses.

Thanks to Debra and Brian Carroll for being the most supportive and loving parents any graduate student could ask for.

**TABLE OF CONTENTS**

**Motivation**

Acid mine drainage (AMD) is a global issue, and among the most significant environmental challenges facing the mining industry today. In order to better utilize our resources and protect our surface water systems, we need to improve our forecasting and modeling of post-mining conditions. The Snake River is a major tributary to Dillon Reservoir—Denver's major metropolitan drinking water source. The Snake is heavily impacted by the surrounding area's rich history of mining and subsequent limitation in regulatory oversight. Like many rivers in Colorado, the Snake is still under the influence of fleeting mining operations resulting in enhanced acidity and increased metal loading. Water quality in these problem areas can only be anticipated to worsen over time. With decreasing water quality, remediation will have to consider more extreme conditions than those found in the past or, possibly past extremes in runoff and highest metal loading observed may become typical of average conditions. Overall, remediation will become more expensive, and water treatment plants will become more expensive to operate because the capacity of treatment and water resource management (dams, diversion, re-vegetation, etc.) will have to be expanded and/or modified to handle increased contaminant loading.

Previous investigations conducted by Rue (2015) identified concentrations of rare earth elements three orders of magnitude higher than the average of rivers worldwide. Despite being heavily understudied, rare earth elements (REEs) are essential in technological applications throughout the globe. The high concentrations of these

metals make the Snake River an ideal system for studying the behavior and transport of REEs in surface water. The Snake River provides an environment that is pH sensitive, which encourages oxidation/reduction, and sorption mechanisms that in turn could alter the behavior and transport of REEs downstream. This investigation hopes to add insight to the strong foundation of previous investigations of this critically impacted, alpine river (Theobald et al., 1963; McKnight and Feder 1984; Runkel et al., 1996; McKnight et al., 1990; Sullivan et al., 1998; Boyer et al., 1999; Belanger, 2002; McKnight and Duren, 2004; Todd et al., 2005; Crouch, 2011; Rue, 2015).

**FIGURES**

**TABLES**

# CHAPTER 1:

# ACID ROCK DRAINAGE (ARD) AND ACID MINE DRAINAGE (AMD)

## *1.1 Introduction*

Acid Rock Drainage (ARD) and Acid Mine Drainage (AMD) are pervasive water quality issues in areas with histories of intensive mining. ARD is a process by which naturally exposed metal sulfides, such as pyrite ($FeS_2$), within native bedrock reacts with water and oxygen creating sulfuric acid and ferrihydrite ($Fe_2O_3*3H_2O$). Acid mine drainage (AMD) is an anthropogenically-induced route of acid production created by the increased exposure of pyrite (and other sulfidic minerals) from previous mining endeavors. Both ARD and AMD are long-term processes continuing until pyrite and other sulfide-based minerals in the host rock are weathered away—a process taking place over tens of thousands of years (Crouch, 2011). Mining involves the extraction of metals from bedrock and tunnel systems leaving behind waste rock, tailings, and drainage adits. These mining remnants greatly increase the reactive surface area of pyrite further accelerating acid production. AMD and ARD are created from, and promoted by the following reactions (Kleinman et al., 1981):

$$\mathbf{FeS_2 + 7/2\ O_2 + H_2O \rightarrow Fe^{2+} + 2SO_4^{2-} + 2H^+} \quad \textit{(1-1)}$$

**(slow, abiotic reaction)**

$$\mathbf{Fe^{2+} + 1/4\ O_2 + H^+ \rightarrow Fe^{3+} + 1/2\ H_2O} \quad \textit{(1-2)}$$

**(faster, biotic)**

$$\mathbf{4Fe^{2+} + 10\ H_2O + O_2 = 4Fe(OH)_3 + 8H^+} \quad \textit{(1-3)}$$

$$FeS_2 + 14Fe^{3+} + 8H_2O = 15Fe^{2+} + 2SO_4^{2-} + 16H^+ \quad \textit{(1-4)}$$

This results in the release of $H^+$ ions, and a decrease in the pH of the water. The water flowing through abandoned mine tailings eventually enters tributaries of potentially less acidity. The mixing of mine waters with less contaminated tributaries can result in the precipitation of colloids, specifically hydrous iron oxides (HFOs) (Kimball et al., 1995). This can result in the deposition of hydrous iron oxides onto the streambed or the transportation of HFOs in the water column downstream. In Colorado, ARD is mostly associated with rivers draining metalliferous hydrothermal deposits stretching from Boulder County to the La Plata Mountains, also known as the Colorado Mineral Belt (CMB) (Tweto and Sims, 1963).

The first reaction **(1-1)** shows the oxidation of minerals in the host rock, primarily pyrite ($FeS_2$). In the presence of $H_2O$ and $O_2$, $FeS_2$ is dissolved and oxidized producing dissolved ferrous iron (Fe (II)) and sulfuric acid. The first reaction releases hydrogen ions, which decreases the pH.

Generally, at low pH (< 4.5) the oxidation of ferrous iron is assisted by acidophilic, chemosynthetic bacteria, such as *Thiobacillus ferroxidans*. Otherwise, this reaction would proceed too slowly to have any notable effects on stream health (Todd et al., 2005; Crouch, 2011). Naturally occurring bacteria of the genus *Thiobacillus spp*. can accelerate AMD production by assisting in the breakdown of sulfide minerals (Nordstrom and Southam, 1997). Acidophiles can dramatically alter the reaction rates and therefore, the suppression of microbial activity can significantly reduce acid generation (McKnight et al., 2001).

The second reaction **(1-2)** will occur if the system is sufficiently oxidized. Much of the ferrous iron will then be oxidized to ferric iron.

In the third reaction **(1-3)**, at pH levels between 2.3 and 3.5, Fe (III) will precipitate as $Fe(OH)_3$ (Akcil and Koldas, 2006). The result is a decreased concentration of Fe (III) in solution and lower pH. When the pH is raised above 3.5, generally from the inflow of less contaminated streams, the iron precipitates out of the water column or as colloids transported downstream. If not precipitating out of solution, the hydroxide will be mobilized farther downstream.

The fourth reaction **(1-4)** dictates that the remaining Fe (III) that does not precipitate from solution, may react to promote further pyrite oxidation acting as a terminal electron acceptor when oxygen is low; as shown in reaction **(1-4)**.

The simplified reaction of ferric iron oxidizing additional pyrite is shown below:

$$\mathbf{FeS_2 + 15/8O_2 + 13/2Fe^{3+} + 17/4H_2O \rightarrow 15/2Fe^{2+} + 2SO_4^{2+} + 17/2H^+} \qquad \mathbf{(1\text{-}5)}$$

However, the aforementioned reactions assume oxygen as the single oxidant and pyrite as the primary sulfide mineral. There are many other sulfide minerals that contribute to AMD, but pyrite is among the most commonly found within the Snake River watershed.

*1.2 Colorado Mining History*

The discovery of gold in the South Platte and Cherry Creek circa 1850 marked the beginning of resource extraction in Colorado (Colorado Geological Survey, 2016). As prospectors found more gold in vein deposits, mineral excavation and settlement expanded throughout Colorado. Originally, precious metals such as gold (Au) and silver (Ag) were extracted from streams and bedrock, but after exhaustion of these sources, more rigorous mining techniques were used. As deposits were depleted from over-mining, settlers would pan elsewhere leaving behind what would later become ghost towns.

There are estimated 23,000-abandoned mines throughout Colorado that range in their severity as point sources to surface water systems (Colorado Mining Water Quality Task Force, 1997). Many of these abandoned mines still drain into headwater streams at high elevations. In general, these contaminated watersheds have limited road access, no sources of power and avalanche dangers during winter. It is difficult to gather empirical data necessary to study the effects of ARD in high elevation streams.

*1.3 Health Impacts of ARD/AMD Impacted Systems*

The upper Snake River and Peru Creek are highly stressed ecosystems. The increased acidity and dissolved metal concentrations associated with ARD and AMD, in streams and groundwater can endanger aquatic life, specifically invertebrates, periphyton, bacteria, and fish. Not only are in-stream biotic communities affected, but the inputs from mine adits negatively impact drinking water supplies.

Some metals found in some sulfide minerals such as zinc, copper, and cadmium exhibit relatively conservative behavior in streams remaining in solution at neutral pH. Thus, these metals are transported greater distances downstream compared to more reactive metals such as iron and aluminum (Stumm and Morgan, 1981; Crouch, 2011). The conservative nature of these metals result in contamination of river reaches far downstream from original point sources.

Other trace metals with higher reactivity such as Fe and Al begin to precipitate as pH increases downstream, forming metal oxide deposition along the streambed and bank. These metal oxides and hydroxides can be detrimental to stream ecology. Metal oxide deposition provides an artificial substrate that can shift benthic invertebrate communities, and limit periphyton colonization (McKnight and Feder, 1984). McKnight and Feder (1984) found much lower abundances of periphyton and benthic invertebrates below the confluence of the Snake River and Deer Creek due to the streambed being coated with Fe and Al oxides. The study concluded that the destabilization of natural substrate with metal deposition could have more adverse effects than low pH and high metal concentration (McKnight and Feder, 1984). In addition, the increased deposition of metal oxides can result in greater scavenging of trace metals – the precipitating hydroxides cause co-precipitation of metals such as zinc and lead, resulting in increased zones of toxic metal accumulation. These consequences are shown to lower abundance and diversity of benthic invertebrates (Hynes, 1970; McKnight and Feder, 1984). The shift in water chemistry results in systems dominated by acid-tolerant invertebrates, such as beetles, true bugs, and chironomids (Hogsden and Harding, 2011). The more sensitive species

of mayflies and caddisflies are precluded from growing, and successfully fulfilling their roles as filter feeders, collector-gatherers, scrapers and shredders. The low species richness and abundance are a result of stress from sudden pH shifts, resulting in impaired regulation of ions and metabolically active metals (Hogsden and Harding, 2011).

In most ARD/AMD systems, fish life is not supported. Dissolved metals can accumulate in fatty tissues of fish causing chronic toxicity (Todd, 2005). Acute fish toxicity occurs when metals are at high enough concentrations to begin out-competing required ions such as calcium and sodium for adsorption sites on the gills of the fish. The displacement of these major ions can result in prompt osmotic imbalance.

In summary, the ecological instability caused from headwater stream segments having significantly lower pH levels is often evident farther downstream as more pristine inflows neutralize the system. This pH change can be drastic resulting in the precipitation of metal oxides onto the streambed, and inhibition of microbial respiration, algal biomass, and invertebrate viability and growth. The removal of these organisms can cause absences in important niches, and shifts in organisms of higher trophic levels, such as fish. The shift in community structure, although occurring potentially kilometers upstream, can adversely affect downstream fish populations.

### *1.4 Field Site*

The Snake River is a high altitude headwater stream located just west of the Continental Divide in the eastern portion of the Colorado River basin in Summit County, CO. The upper Snake River begins above the town of Montezuma, CO, and flows through the former mining district before terminating into Dillon Reservoir. In the early 2000s, the Snake River was placed on Colorado's 303(d) list of impaired waters due to high concentrations of zinc, cadmium, copper lead and manganese, primarily caused by ARD and AMD (CDPHE, 2008).

The Snake River watershed ranges in elevation from 3350 to 4120 m. The headwaters are impacted by the natural weathering of disseminated pyrite (Theobald et al., 1963; McKnight and Duren, 2005). This study focuses on the Snake River at the confluences with Deer Creek and Peru Creek, which are two tributaries of equivalent flow. Deer Creek provides inflow of relatively pristine water, and farther downstream Peru Creek contributes a significant degree of acidity and metal loading. Peru Creek drains a heavily mined portion of the watershed (Sullivan et al., 1998; Runkel et al., 2013). This tributary has an extensive mining history, and houses the Pennsylvania Mine, which is considered one of the largest sources of metal loading and acidity within the Snake River watershed. Sts John, a smaller tributary with its confluence with the Snake River at Montezuma, is also of interest in distinguishing the effects of geochemical processes. Various portions of the Snake River, specifically at confluences or areas of notable pH increases are coated in iron and aluminum hydroxides.

Recent work has documented increasing metal concentrations over the past 30 years, in particular a four-fold increase in zinc concentrations during low flow periods of September and

November (Crouch, 2011; Todd et al., 2012). Not only have metal concentrations been increasing, the sulfate concentrations have also increased suggesting that the increases are caused by an increase in pyrite weathering (Crouch, 2011). The increase in pyrite weathering could be contributed by a hydrological transition, with peak snowmelt occurring 2-3 weeks earlier than in the past. The earlier snowmelt results in an extended period of low flows, and drier soils later in the season, which may cause greater exposure of pyrite to oxygenated conditions (Crouch et al., 2013).

*1.5 Geology*

The Snake River catchment has been mined for Au, Ag, and various sulfide minerals since the 1860s. The catchment is characterized by steep sided glacial valleys underlain by metamorphic granitic rocks (Lovering and Goddard, 1950; Wood, 2005; Crouch, 2011). The Snake River basin

drains the Idaho Springs Formation, as shown in Figure 1-1.

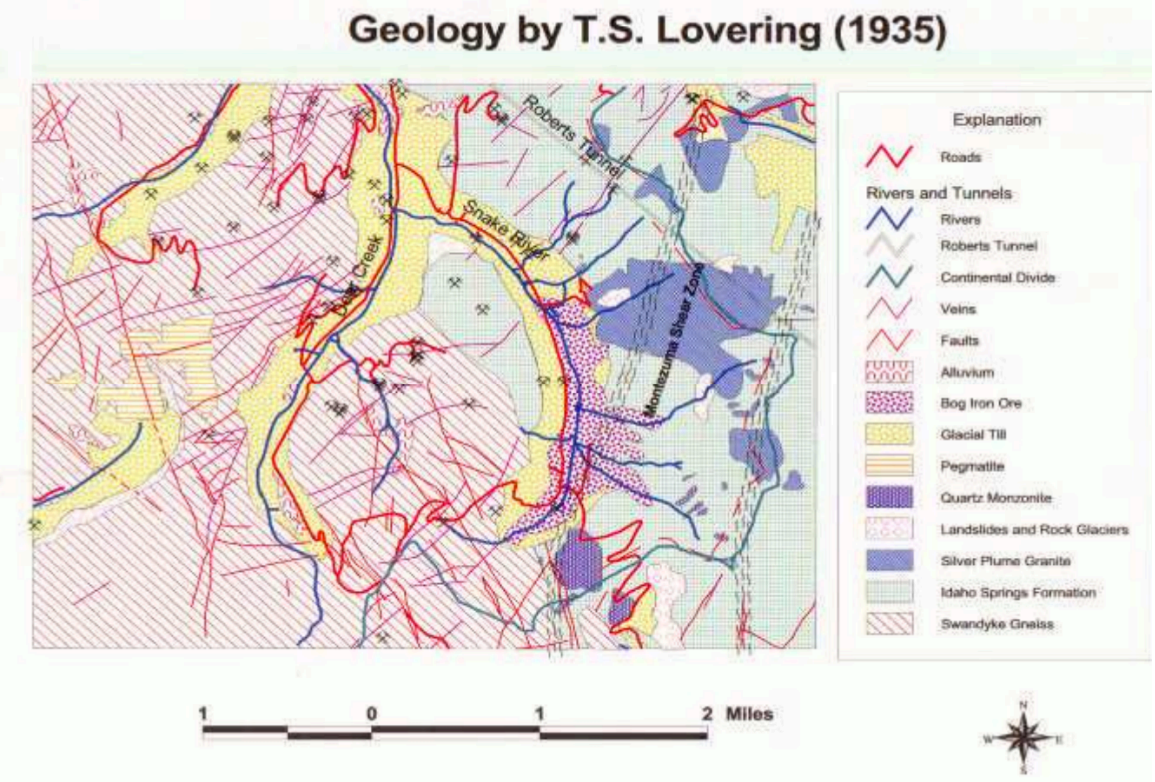


**Figure 1-1. Geology of Upper Snake River and Deer Creek (Adapted from Loverling 1935)**

The upper Snake River runs through naturally occurring ferricrete, providing a rich source of iron oxides. The Deer Creek basin drains the Swandyke Hornblende Gneiss. Idaho Springs Formation is Al- and Si-rich, while the Swandyke Hornblende Gneiss is Ca, Mg, and Fe rich. The Montezuma sheer zone crosses the Snake River drainage basin, where mineralization is concentrated. Mineralization of this host rock is associated with the intrusion of the Tertiary Montezuma quartz monazite Stock, also composed of aplite and monzonite (Neuerburg and Botinelly, 1972).

Rare earth elements are present in minor accessory minerals such as allanite, apatite, and monazite (Johannesson, 2005). Generally, there is an enrichment of light REEs in basic to acidic rocks; however, this varies across mineral types (Johannesson, 2005).

*1.6 Hydrology*

The Snake River is an alpine headwater stream of the Rocky Mountains, and has a seasonally dependent hydrologic regime. This means that certain times of the year have more influence on the water availability throughout the remainder of the year (Crouch, 2011). The contribution of overland flow, groundwater recharge, and subsurface flows vary according to the season. In the Rocky Mountains, up to 80% of annual precipitation falls as snow, and the hydrograph is heavily influenced by spring melt (Brooks et al., 2001; Crouch, 2011). The hydrograph, shown in Figure 1-2, reflects the flow conditions during the year 2015 and beginning of 2016:

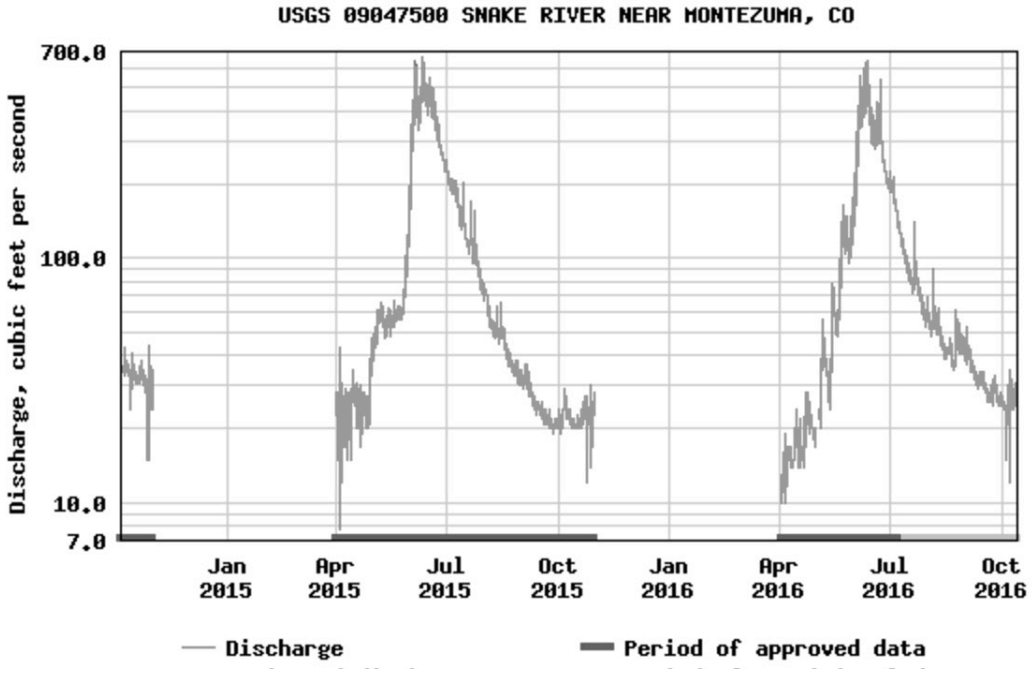


**Figure 1-2. Hydrograph of the Snake River, near Montezuma, CO during the years 2015-2016**

The Snake River hydrology is snowmelt driven, with peak flows commonly occurring in late April-early June (McKnight and Bencala, 1990). A model to explain the relationship between seasonal flow contributions to overall stream flow is provided by Liu et al. (2004). The stages are as follows: initiation of snowmelt, rising limb of hydrograph until maximum discharge is reached, and the recession limb of the hydrograph to low flow conditions (Liu et al 2004; Nordstrom, 2009; Crouch, 2011). During the first stage, soils quickly become saturated. The moisture holding capacity of the soil decreases, and results in overland flow. When soils reach their maximum moisture capacity, water-dependent reactions producing ARD/AMD are accelerated, and solute concentrations within the stream increase (Crouch, 2011). The second stage involves the dilution of solute concentrations due to higher flows from snowmelt. The third stage involves the shift to groundwater dominated flow, presumably from fractured bedrock storage (Liu et al., 2004; Crouch, 2011).

In general, low flows are observed from the months of September to March. However, peak snowmelt is occurring 2-3 weeks earlier than historical averages (Clow, 2010). As the flows begin to decrease over time, and during prolonged dry periods of summer, the acidity and metal concentrations will increase due to a greater surface area of pyrite in contact with oxidizing conditions over a longer duration of time (Crouch, 2011).

Precipitation events in summer can cause increases in metal loading in AMD-impacted systems (Nordstrom, 2009). Studies have shown that after precipitation events, there is a flushing of

soluble material (i.e. dissolution of salts along the river bank) from soils and sediments, which can lead to significantly higher concentrations of metals (Nordstrom, 2009). Some metal concentrations spike during first snowmelt, and during rainstorms due to the flushing of accumulated salts and shallow acidic groundwater. After first snowmelt and intermediate rainstorms, metal concentrations will steadily decrease until low flow conditions (Nordstrom, 2009; Crouch, 2011).

Subsurface flows can also contribute to metal loading, as noted by Belanger (2002) who suggested that in mid-summer, subsurface inflows could be more significant than surface tributary flows. Hyporheic exchange can play an important role in increased metal concentrations. The hyporheic zone is defined as the area in which water is exchanged between shallow groundwater and the surface, typically visualized as a region directly beneath or lining the stream bed. Lateral inflow can significantly increase metal concentrations in the main channel because of the greater exposure of the subsurface water with surrounding rocks, soils and sediment (Crouch, 2011).

*1.7 In-stream Geochemistry*

pH is considered a master variable in which many processes vary according to its fluctuations. The pH of a stream will increase downstream due to inflows of water with higher pH, assuming the stream of interest is impacted with AMD. An increase in pH above approximately 3.5 causes iron precipitation. Colloids, generally referred to as hydrous ferric oxides (HFOs) and hydrous aluminum oxides (HAOs), either coat the streambed or suspended in the water column.

Therefore, the composition of oxides and oxy-hydroxides in the mobile or immobile phase will vary with the mineral composition of the bedrock. Precipitating HFOs and HAOs have large sorption capacities, compared to many environmental materials (Jenne, 1968 and Jenne, 1977; Dzombak and Morel, 1990; Verplanck et al., 2004). As pH increases above 5, aluminum hydroxides begin to precipitate. The presence of metal hydroxide precipitates can affect the chemistry of other metals by sorption and co-precipitation (McKnight et al. 1992, Runkel et al. 1999). The primary mechanism of metal (e.g. As, Cu, Pb, and Zn) removal within ARD/AMD-impacted channels is by sorption to HFOs (Chapman et al., 1983; Johnson, 1986; McKnight and Bencala, 1990; Webster et al., 1994; Smith et al., 1998; Verplanck et al., 2004). The removal capacity is controlled by pH with each metal being removed in a specific pH range. For example, studies show that in AMD impacted streams, metals such as cadmium, copper, and manganese were scavenged more frequently by iron-rich colloids than reported in surrounding soils (Johnson, 1986; Kimball et al., 1992). In contrast, studies show zinc to be impacted less by sorption and co-precipitation to Fe and Al colloids. HFOs precipitate out of solution at relatively low pH and have the potential to accumulate in regions forming thick iron ore deposits. This can be seen in areas of river confluences such as the confluence of the Snake River and Deer Creek (Crouch, 2011). These HFO sinks sorb other metals increasing total residence times within storage zone and downstream.

In the Coeur d'Alene mining district in northern Idaho, geochemical modeling indicates that removal of dissolved metals (Cd, Cu, Pb, and Zn) by Fe and Al oxyhydroxides is a function of the physical state of the mixing and reaction zone (Balistrieri et al., 2002). Using flow and mass

balance calculations in two mixing zones in the Animas River, Colorado, dissolved metals such as Ca, Mg, Mn, Si and $SO_4^{2-}$ were found to behave conservatively, whereas dissolved Cu, Pb and Zn co-precipitated or adsorbed onto Fe and Al phases (Schemel et al., 2000). In the mixing zone at the Pecos mine in New Mexico, geochemical modeling suggested pH and Ca were dependent upon calcite dissolution (Schemel et al., 2000). Therefore, high concentrations of Ca could indicate a system draining a zone of concentrated calcite. Schemel et al. suggested that Mg, Mn, $SO_4^{2-}$, and Zn behave conservatively and Al, Cu, and Fe precipitate as aluminium hydroxide, alunite, tenorite, and HFOs. Also, Pb concentrations are influenced by Al hydroxide sorption (Schemel et al., 2000).

*1.8 Changing Climate in the West*

The western United States is particularly susceptible to climate change, and has been experiencing an increase in average temperature over the past five years that is 70% greater than the United State's 20$^{th}$ century average (Saunders et al., 2003). The Rocky Mountain Climate Organization (RMCO) found that during the 2003 through 2007 period, western states such as Colorado had average temperatures 1.7 °C warmer than the region's 20th century average of 1 °C.

The effects of climate change, specifically air temperature, precipitation, and maximum snow water equivalent (SWE) in the western U.S. have been studied in regards to the Pacific Decadal Oscillation (PDO), El Niño Southern Oscillation (ENSO), North American Monsoon (NAM), and global warming (Clow, 2010; Mote, 2006; Hanson et al., 2006). Weather patterns on the scale

of a few years are strongly influenced by ENSO and patterns on the scale of 1–2 decades are influenced by PDO (Clow, 2010). Also, snowmelt in the Sierra Nevada and Rocky Mountains is being observed to arrive 1-4 weeks earlier than previously documented from data collected between 1948–2000 (Dettinger and Cayan, 1995). In parallel to earlier snow melt, average temperatures in the Rockies have been found to have increased more than 0.34 °C per decade between the years 1979 to 2005 (Folland et al., 2001). Greatest temperature increases are expected between November and January and could result in greater levels of thawing (Folland et al., 2001; Crouch, 2011). The PDO and the longer-term process of global warming attribute to earlier snowmelts, confirmed from SNOTEL SWE data. Stream flow timing using gauge discharge recordings from the region encompassing the Snake River was found to be on average 4.0-5.9 days earlier per decade (Clow, 2010; Crouch, 2011). This transition to earlier snowmelt and stream timing in the Rocky Mountains can result in a longer summer dry period, decreasing the flow allowing for greater sediment erosion, and thus increases in contaminants. Ground waters will have increased concentrations of soluble constituents. Another pattern of global warming will be the transition of snowfall to rainfall, possibly decreasing the snow pack in the Rockies (Knowles et al., 2006). It is projected that precipitation events may become less frequent, but more likely to occur in greater intensity than historical averages (Trenberth, 1999).

*1.9 ARD/AMD Remediation*

Often, remediation efforts can prove inadequate in terms of longevity, and too expensive rendering much of AMD left untreated. Every mine is unique in terms of its AMD generating potential; therefore, the nature and size of the associated risk, and applicability of mitigation

will vary from site-to-site. There are no standardized methods for ranking, measuring and reducing the risk of AMD. In future mining regions where AMD is not yet an issue, research should be carried out to identify ways in which it can be prevented, not reduced.

Mineral extraction is a water quality issue prevalent across the globe; it is likely that many parts of the world laden with abandoned mine waste will experience similar climate patterns with similar consequences. Extended dry periods will result in decreases in surface runoff and lower carbonate-buffering systems triggering increases in metal concentrations, sulfate, and acidity. More intense precipitation events could also increase these soluble constituents. If left untreated, the toxicity could render many streams uninhabitable to aquatic life and lowering the overall experience of recreational activities. Remediation efforts must account for more severe extreme conditions than have been encountered in the past. Treatment plants may need greater capacities and passive treatment schemes may require greater capacities (wetlands, dams, diversions, re-vegetation) and more resistance to erosion. Finally, urgency for remediating mine sites may intensify not only because we can expect these more extreme conditions, but also because the need for adequate supplies of water in the Rocky Mountain region is increasing.

*1.10 Rare Earth Elements (REEs)*

The rare earth elements (REEs) are the largest periodic group of chemically similar metallic elements comprising the lanthanide series plus scandium and yttrium. They are commonly referred to as YREEs, which stands for yttrium and the rare earth elements. They encompass

the following elements in order of increasing atomic number: cerium (Ce), dysprosium (Dy), erbium (Er), europium (Eu), gadolinium (Gd), holmium (Ho), lanthanum (La), lutetium (Lu), neodymium (Nd), praseodymium (Pr), promethium (Pm), samarium (Sm), scandium (Sc), terbium (Tb), thulium (Tm), ytterbium (Yb) and yttrium (Y). Despite their name, they are not especially rare, and generally occur close together in nature with varying abundances. They are more often than not found in an even distribution within the earth's crust (Dutta et al., 2016).

### *1.10.1 REE Characteristics*

The YREEs vary in character, with many possessing advanced nuclear, metallurgical, chemical, catalytic, electrical, magnetic, and optical properties. These varying properties make YREEs valuable resources in many applications such as lighter flints, glass polishing, phosphors, lasers, magnets, batteries, high temperature superconductivity, and the safe storage and transport of hydrogen (Haxel et al., 2002). The optimal properties of the YREEs can be attributed to their systematic changes in character with increasing atomic number. These shifts in electron configuration are also transferrable to how they react in aqueous environments. Chemical reactivity is heavily influenced by atomic number and spatial distribution of electrons as these control how easily electron bonds and electrostatic interactions form. The empty ($La^{3+}$), half-filled ($Gd^{3+}$), and completely filled ($Lu^{3+}$) 4f electron shells have increased stability and therefore may exhibit similar chemical behavior compared to the remaining REEs (De Baar et al., 1991; McLennan, 1994; Sholkovitz, 1995). The decrease in ionic radius, coinciding with the filling of the f-electron shell, with increasing atomic number, known as the lanthanide contraction is the most notable change that should be considered when investigating aqueous chemistry and

complexation (Sholkovitz, 1995). In aqueous environments, YREEs ions are present in their trivalent state with the exception of Ce and Eu, which also exist in tetravalent and divalent states (Sholkovitz, 1995).

In general, acidic waters contain higher concentrations of REEs that potentially provide geochemical signatures reflective of the flow path's bedrock composition (Verplanck et al., 2004). Until recently, the geochemical behavior of REEs has been relatively understudied. The evolution of Inductively Coupled Plasma Mass Spectrometry (ICP-MS) has provided the analytical power to measure metal concentrations on the level of parts per million, and without pretreatment and chemical separation (Smedley, 1991; Taylor et al., 1983; Verplanck et al 2001; Verplanck et al., 2004). Usually, concentrations of REEs are normalized to a reference standard, such as chondrite or North American Shale Composite (NASC)—this is to account for the variation in geochemical behavior associated with the decreasing ionic radius across the Lanthanide series (Verplanck et al., 2001)

Over the past 40 years, REEs have been used as geochemical tracers to constrain processes involving cosmogenic evolution, mantle and crustal evolution, magma genesis, sedimentary petrology and ore genesis (Henderson, 1984; Verplanck et al., 2004). However, there are some inconsistencies in using REEs as conservative tracers in some areas containing fractions of REE in bedrock. Groundwater can become REE enriched due to extended contact with REE-bearing minerals providing higher concentrations in lateral inflow.

*1.10.2 REE Commercial Mining*

Up until 1999 and 2000, the United States was able to sustain the country's REE demand, but since then has become more reliant on REE ore deposits imported from China. Rare earth ore mining and concentration are performed using intricate methods that involve grinding and cracking the REE- bearing ores, such as monazite, to produce mixed, concentrated rare earth oxides (REO) (Dutta et al., 2016). This is followed by physical and/or chemical separation and purification of oxides resulting in industrial grade REEs (Dutta et al., 2016). It is difficult to obtain REE concentrates from ore deposits because they often occur with radioactive elements such as uranium and thorium, potentially producing radioactive stockpiles (Dutta et al., 2016).

*1.10.3 REE Presence in the Snake River*

In the case of the Snake River, REEs are especially prevalent due to the presence of monazite. Re-analysis of archived water samples by Rue (2015) suggest a near fourfold increase in rare earth elements. In 2015, REEs were discovered in the upper Snake River and Peru Creek to be several orders of magnitude higher than major freshwater rivers wordwide, shown in Figure 1-3 (Rue, 2015):

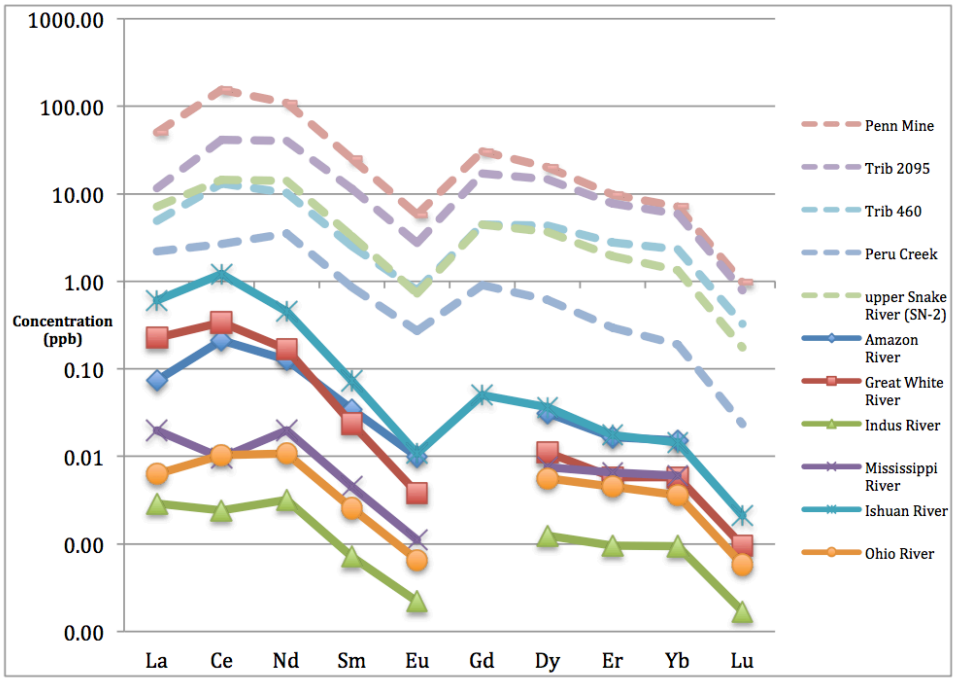


**Figure 1-3. Rare earth Element enrichment patterns of the Snake River and tributaries of interest relative to major freshwater rivers worldwide (Adapted from Rue, 2015)**

REEs are considered emerging contaminants, which are being introduced into the environment to a greater extent, by increasing demands for 'technology' metals to support advancements in applied sciences. The future demand for these metals should encourage further investigation in regards to associated toxicity and metal transport, as well as behavior in surface water. Currently, the REEs are unregulated by the Environmental Protection Agency (EPA) as their concentrations are considered low in drinking water sources.

*1.11 Rare Earth Element Solution and Surface Water Chemistry*

In order to predict how rare earth elements are entering Denver's drinking water supply – Dillon Reservoir, it is essential to understand their adsorption behavior. The primary sources of

YREEs are from ARD in the upper Snake River, and AMD from Peru Creek, with mobilization dependent on their solution chemistry.

Adsorption of YREE depends on environmental variables such as pH, ionic strength, temperature, the presence of additional ligands such as carbonate or organic species, and surface coverage (Music and Ristic, 1988; Koeppenkastrop and De Carlo, 1992; Kosmulski, 1997; Marmier et al., 1997, 1999a,b; De Carlo et al., 1998; Rabung et al., 1998; Marmier and Fromage, 1999; Yoshida et al., 2004; Zhang et al., 2004b; Ridley et al., 2005; Tang and Johannesson, 2005). Adsorption onto Fe precipitates and co-precipitation is predicted to be the primary YREE scavenging mechanisms in ARD/AMD-impacted systems (Verplanck et al., 2004). The type of metal hydroxide or oxide present, as well as variation in properties affects REE attenuation across the lanthanide series. Coagulation and aggregate precipitation of HFOs and HAOs may be among the most effective mechanisms to YREE removal in AMD impacted waters (Zhao et al., 2007).

In addition to sorption, aqueous complexation plays an important role in YREE distribution. Zhao et al. (2007) found through speciation modeling of coal mining induced AMD that YREE sulfate complexes denoted as $LnSO_4^+$ were the primary form of dissolved YREE concentration, followed by free metal cations ($Ln^{3+}$). The partitioning of dissolved YREE onto sulfate complexes decreased as atomic number increased (Zhao et al., 2007). The study also found that the partitioning of free metal cations ($Ln^{3+}$) increased as atomic number increased (Zhao et al., 2007). The dissolved YREE present in other forms such as $LnCl^{2+}$, $LnF^{2+}$ and $LnOH^{2+}$ accounted

for less than 1 % (Zhao et al., 2007). The study found that after normalizing concentrations to the NASC standard, removing Ce and Eu anomalies, the middle rare earth elements (MREE) are more enriched compared to LREE and HREE – however, this trend varied throughout the study. This observation varies from Sholkovitz (1995) who found the sequence of YREE adsorption onto particle surfaces as LREEs>MREEs>HREEs. The YREE-sulfate complexes possibly adsorb onto Fe-Al-Mn oxide and hydroxide, subsequently co-precipitating with them. As previously mentioned, REE geochemical behavior may be strongly influenced by surface complexation but little research has been done on YREE adsorption behavior in the absence of primary ligands.

*1.12 Objectives*

The hypothesis of this research is that the transport and behavior of REEs can be quantified based on pH variation, and understanding the scavenging mechanisms associated with heavy metal speciation. It is expected that a strong correlation between metal redox, complexation, dissolution and precipitation of Fe and Al, and to a lesser extent Mn, exists to determine the mobilization of YREEs. Sediment suspension and re-suspension plays an important role in the availability of heavy metals such as Fe, Al, Cu, Zn and Pb in the water column. Element removal within the mixing zone is observed if reaction rates are faster or similar to transport rates, and no removal is observed when transport rates are faster than reaction rates (Kimball et al., 1994). These reaction rates are pH depenent. The time scale of these hydrological transport and chemical reaction rates allow for the study of heavy metal and rare earth element cycling.

ARD/AMD impacted systems will have characteristically low pH, high specific conductivity, high concentration of Fe, Al and Mn. To delineate YREE behavior and mine drainage remediation, it is essential to model the fate of iron, aluminum and manganese in solution to determine the possibility of insoluble precipitate formation. The primary objectives of this thesis are the following:

**1.)** Investigate heavy metal and rare earth element behavior downstream in a stream system receiving ARD and AMD inputs (Chapter 2)

**2.)** Compare conservative solute behavior to more reactive metals and investigate heavy metal redox, complexation, dissolution and precipitation of heavy metals in relation to REE concentration (Chapter 2)

**3.)** Employ a solute transport models, specifically One-Dimensional Transport with Inflow and Storage (OTIS) to adequately predict hydrological parameters that could be transferrable to remediation decisions intended to reduce AMD loading and REE transport (Chapter 3)

The research approaches to achieve these objectives were to conduct a synoptic study reflective of high flow conditions from Upper Snake to Dillon Reservoir, and to conduct a tracer injection on the Upper Snake River to model breakthrough curves with OTIS

# CHAPTER 2:

# SNAKE RIVER SYNOPTIC STUDY

## *2.1 Introduction*

Synoptic studies of streams and rivers are important for profiling changes in biogeochemical and microbial processes associated with major tributary inflows. Synoptic studies provide a "snap-shot" of the underlying processes occurring throughout a stream, and insight into the influences of lateral inflow and stream-groundwater exchange on stream characteristics (Bencala and McKnight, 1987; Runkel et al., 2013).

A synoptic study was conducted on June 6$^{th}$ 2015 investigating an approximate 11 km stretch of the Snake River to its terminus with Dillon Reservoir. The stretch was sampled over the course of eight hours at high flow conditions. The Snake River has four major tributaries—Deer Creek, Sts John, Peru Creek and the North Fork. The study began at the confluence with Deer Creek, continued below Peru Creek to the Snake's terminus at Dillon Reservoir. The objective was to provide insight into how pH changes and stream dilution affect trace metals and REE transport and reactivity, and quantify the metal concentrations entering Dillon Reservoir from AMD and ARD.

In order to investigate the response of heavy and rare earth elements with changing water chemistry, samples at each site underwent fractionation experiments to better understand the influence of heavy metals on REE scavenging. The samples were separated based on particle

diameter resulting in three phases: particulate, colloidal, and dissolved. The fractionation experiment determined metal speciation at the following particle diameters: particulate phase ($d_p$>10 µm particle), colloidal (0.45 µm < particle < 10 µm), and dissolved phase ($d_p$ < 0.45 µm particles). Colloidal phase was defined as solids that do not directly settle from the aqueous phase having diameters between $10^{-9}$ to $10^{-6}$ m. In contrast, in previous studies, such as Kimball et al. (1995), the colloidal concentrations were determined by the difference between the total-recoverable and dissolved metal concentrations. The dissolved phase was defined using the filtrate of the traditional 0.45 µm break point (Kimball et al., 1995). However, for Fe-rich AMD impacted streams, the 0.45 µm threshold is not always an effective cutoff for the separation of dissolved and particulate concentrations. Even at low pH much of the Fe-rich colloidal material formed can have diameters much smaller than 0.45 µm. As particle diameter decreases, the smaller size results in larger surface areas, which in turn can influence partitioning of toxic metals by sorption, and co-precipitation.

*2.2 Field Site*

Sampling began in the upper reaches of the Snake River at the confluence with Deer Creek and samples were taken at varying distances downstream until reaching the Snake River's terminus with Dillon Reservoir. To create a spatial profile of pH variance, metal concentration, and REE fractionation behavior, 11 sampling sites were chosen based on relative location of prior studies, accessibility, areas with uniform flow, and sites with consistent morphology. A map, and table outlining the properties of each sampling site can be seen below:

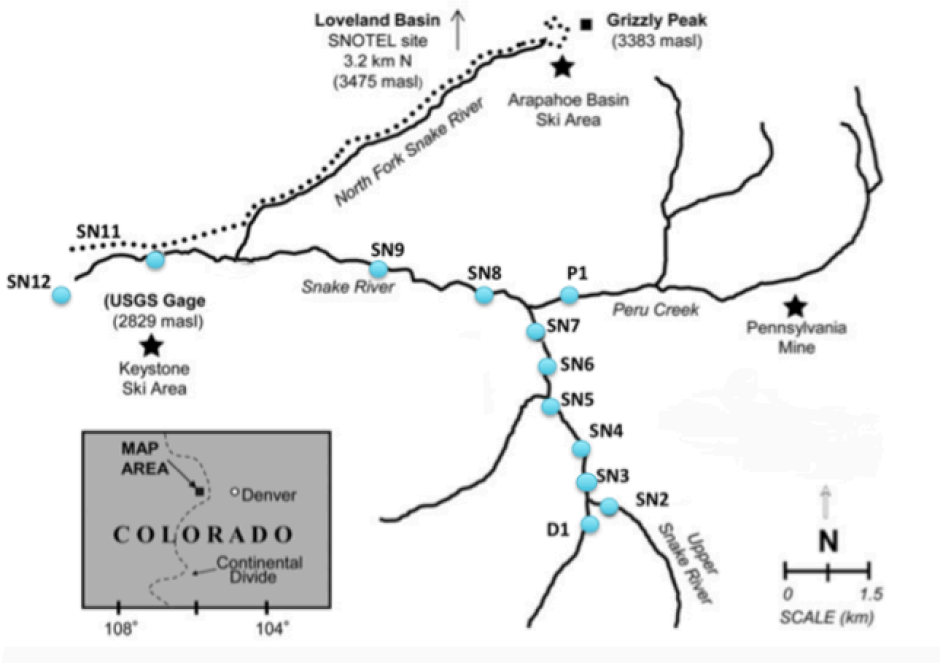


**Figure 2-1. Snake River map with sampling sites of synoptic study and tracer injection**

**Table 2-1. Characteristics of sampling sites in 2015 synoptic study and tracer injection**

| Site | Description | pH | Conductivity (uS) | DO (mg/L) |
|---|---|---|---|---|
| D1 | wetland | 6.98 | 25.5 | 1.26 |
| SN2 | iron precipitate, high flow, above split, rocky, shady | 4.13 | 108.3 | 1.1 |
| SN3 | rocky, conifers, high flow, steepish bed | 5.7 | 53.9 | 1.07 |
| SN4 | rocky, Shady, smaller rocks, bed erosion, 20 ft from road | 6.66 | 41.4 | 1.47 |
| SN5 | steep bank, show melt, sunny, bend | 6.8 | 57.4 | 1.6 |
| SN6 | conifers, shady, sunny in flow, rocky, wide, fast | 6.72 | 60.5 | 1.49 |
| P1 | gauge site, open, Al precipitate, run off from snow melt | 6.11 | 67.2 | 2.18 |
| SN8 | deep, high flow, not much sed., flat, shady | 8.52 | 67.5 | 3.34 |
| SN9 | condos, below bridge, keystone, wide, flat | 8.5 | 60.9 | 3.39 |
| SN11 | wide, housing developments, deep | 7.4 | 83.1 | 2.8 |
| SN12/DR | very wide, near highway 6 | 7.38 | 58.08 | 2.64 |

## *2.3 Methods*

### *2.3.1 General Water Quality*

The parameters collected were pH, conductivity, temperature, dissolved oxygen, total and ferrous iron, and major and trace metals. On-site measurements of pH, specific conductance, and temperature were obtained at each site. The pH and temperature at each site were measured using a YSI 60 multi-parameter field probe. Salinity, conductivity and temperature were measured using a YSI 30 multi-parameter field probe. Dissolved oxygen (DO) was measured using YSI 55 field probe.

All measurements taken using the YSI probes were recorded after the field probe equilibrated for a few minutes in the sampling area. Before entering the field, the pH electrode was calibrated using three buffers (4.01, 6.86, 9.18) that validated the range of pH expected for the Snake River system. Also, before collection, the high-density polyethylene bottles (HDPE) were rinsed three times with the stream water at each sampling site.

*2.3.2 Cations*

The water samples were collected at all 11 sites (can be identified on the field map, excluding SN7) using EPA method 200.8. Before entering the field, 250 mL and 60 mL HDPE bottles were rinsed three times with DI water, and then soaked in a 5% reagent grade nitric acid bath over night, followed by three additional DI rinses. All samples were collected after rinsing the bottle three times with the water being collected, and were then completely filled to eliminate headspace.

A 250 mL HDPE bottle was filled at each site for total and dissolved samples, 60 mL of sample was collected and labeled for total, and the remaining 190 mL were passed through a 10 µm Whatman filter. The 60 mL of the filtrate from the 10 µm filter was collected and labeled. The used 10 µm filter from each site was preserved in aluminum foil and stored in the Kiowa freezer. The remaining 130 mL from the 10 µm filter was passed through a 0.45 µm filter, and 60 mL was collected and labeled for dissolved phase. The 0.45 µm filter was preserved in aluminum foil and stored in the freezer to identify percent mass loss. After collection, the pH of the sample was adjusted to less than 2 with trace grade concentrated nitric acid ($HNO_3$), and pH was further confirmed using litmus paper.

Samples were kept on ice in a cooler to limit the influence of light and ambient heat until taken to the Laboratory for Environmental and Geological Studies (LEGS). The cations were analyzed using Inductively Coupled Plasma Mass Spectrometry (ICP-MS) analysis

*2.3.2.1 Fe Speciation*

Total iron, Fe (II) and Fe (III) were measured using the Hach DR-2800 Field Spectrophotometer in the field. Total Iron was measured using the USEPA FerroVer method in which the FerroVer iron reagent converts all soluble and most insoluble forms of iron within the sample to soluble ferrous iron. The Fe (II) iron reacts with 1,10 Phenanthroline to form an orange color with an absorbance proportional to iron concentration. The absorbance is taken at a wavelength of 510 nm. The Fe (III) does not react, and can be calculated by subtracting the Fe (II) concentration from the total iron concentration.

*2.3.2.2 Cation Fractionation*

In order to obtain the metal partitioning profile downstream: unfiltered, 10 µm filtrate, and 0.45 µm filtrate samples were collected at each sampling site. The particulate phase was determined using the concentration obtained from the difference between the unfiltered samples and the filtered samples (both the 10 µm and 0.45 µm filtrates). Metal concentrations in the dissolved fraction with a nominal 0.45 µm cutoff were subtracted from the 10 µm filtrate concentration to obtain final colloidal measurements. This was further compared to the concentration of the 10 µm filtrate to confirm the calculations provided reasonable measurements. The indirect measurement was reliable for Fe, Mn, and Zn at each of the sites. The dissolved phase was determined by measuring the filtrate of the 0.45 µm water sample.

*2.3.3 Anions*

Samples were also kept on ice in a cooler to limit the influence of light and ambient heat until taken to LEGS. Anions ($Cl^-$ and $SO_4^{2-}$) were measured using ion chromatography (IC). Field blanks and duplicates taken at Peru Creek due to high metal concentrations and analyzed for QA/QC.

*2.4 Results*

*2.4.1 Water Chemistry (pH, Conductivity and Sulfate)*

The pH profile, shown in Figure 2-2, depicts the pH increasing downstream due to the higher pH of Deer Creek, and lateral inflow.

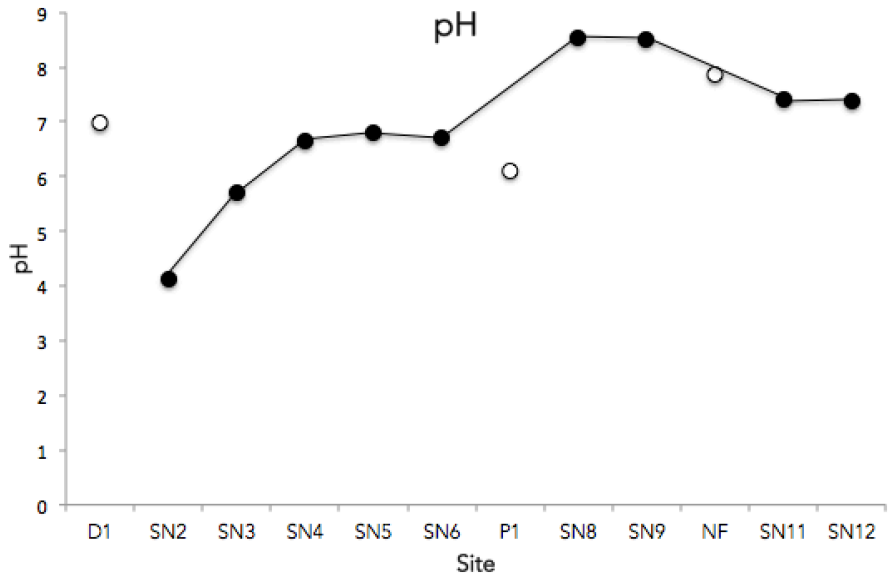


**Figure 2-2. pH variation downstream**

The water samples from the Snake River range in pH from 4.13 above the confluence with Deer Creek to 8.52 farther downstream. The pH was lowest at 4.1 at SN2. The pH was highest at a value of 8.52 between SN9 and before the inlet to Dillon Reservoir at SN11.

Conductivity was highest above the Deer Creek and Snake River confluence at SN2 with 108.3 µs and lowest at SN4 at values 41.4 µs, respectively, shown in Figure 2-3:

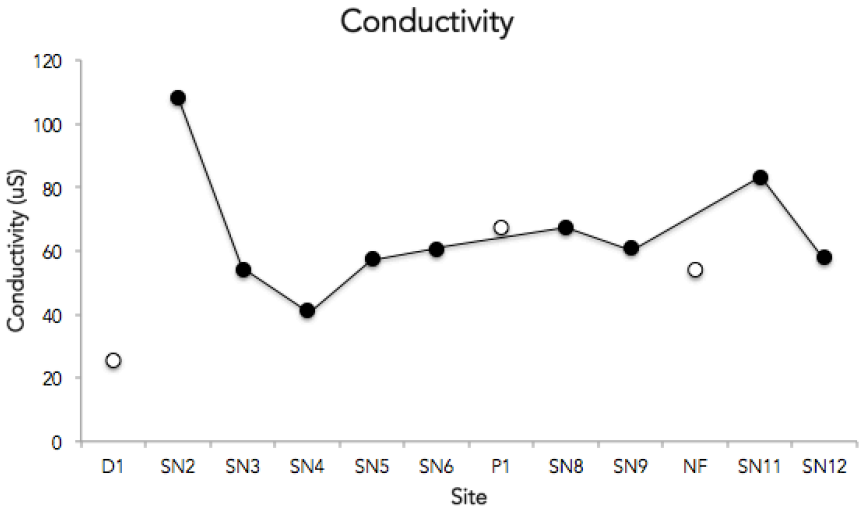


**Figure 2-3. Conductivity variation downstream**

Sulfate concentrations were highest at SN2 and below the confluence of the Snake River and Peru Creek, as shown in Figure 2-4:

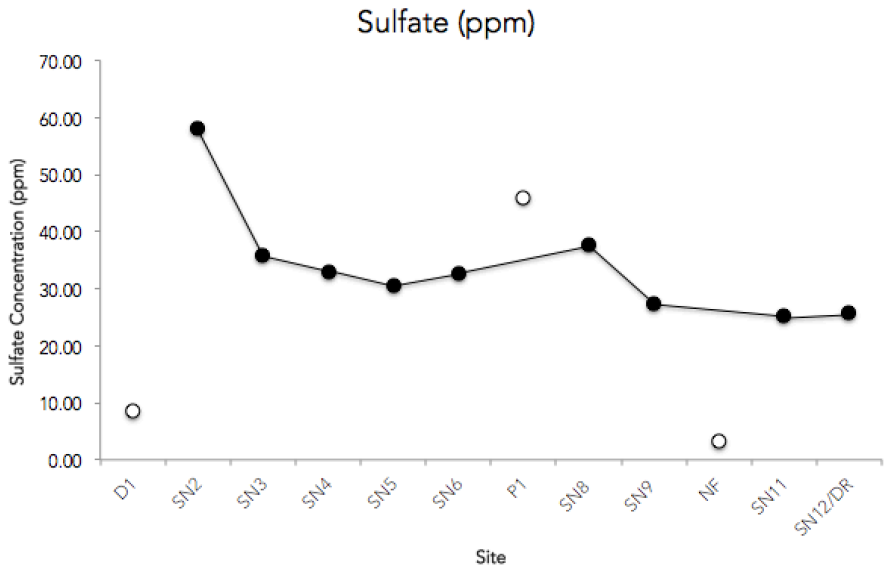


**Figure 2-4. Sulfate concentrations (ppm) downstream**

Sulfate decreased by nearly half from SN2 to SN3, and then remained between 25 to 35 ppm. There was a slight peak in concentration at SN8.

*2.4.2 Cations and Anions*

Figure 2-5 shows that concentrations of Fe were highest at SN2 and SN3, and then proceeded to decrease until inflow from Peru Creek at SN8. The lowest concentrations of Fe were found in the Deer Creek and closer to Dillon Reservoir (SN12) at 0.14 ppm and 0.28 ppm, respectively.

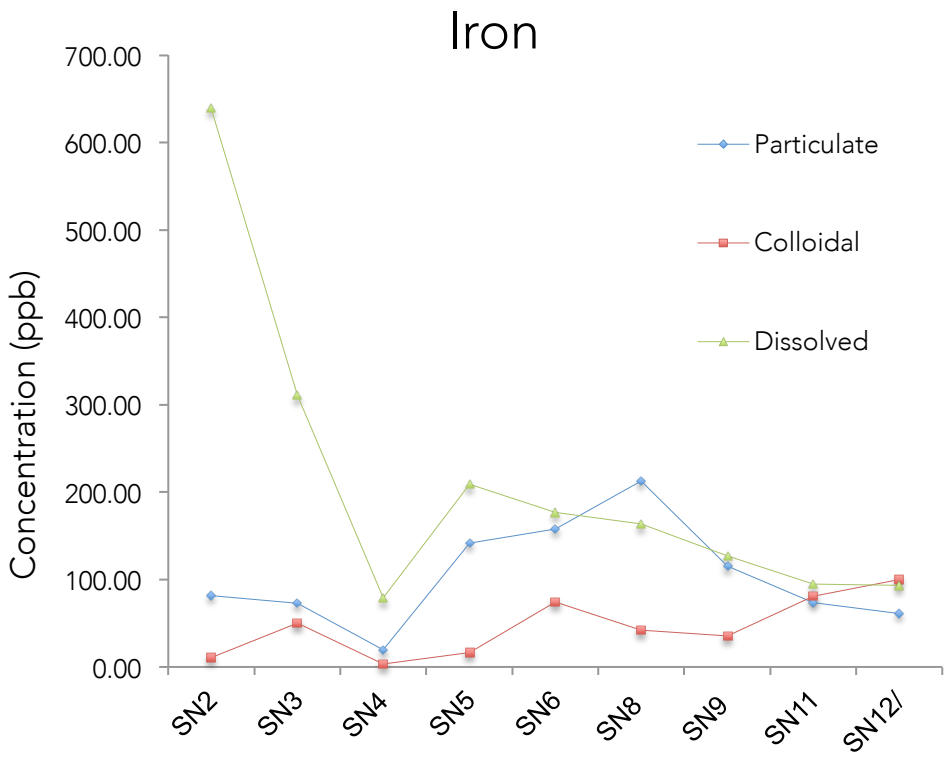


**Figure 2-5. Iron variations downstream. Particulate phase (Particulate = Unfiltered Sample - Colloidal - Dissolved), colloidal phase (Colloidal phase = 10 µm filtrate - .45 µm filtrate), and dissolved phase (filtrate of 0.45 µm) shown**

Concentrations of Al were highest in particulate phase at SN8 at 771.3 ppb, and lowest at SN2 at 0.0 ppb, as shown in Figure 2-6.

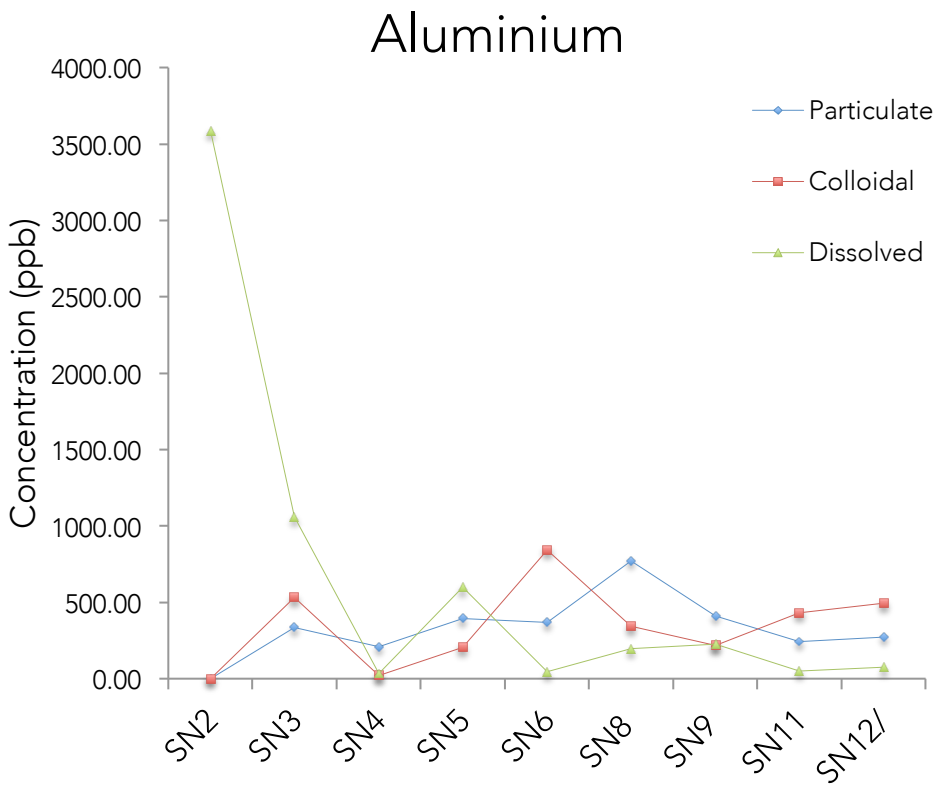


**Figure 2-6. Aluminum (Al) variations downstream. Particulate phase (Particulate = Unfiltered Sample - Colloidal - Dissolved), colloidal phase (Colloidal phase = 10 µm filtrate - .45 µm), and dissolved phase (filtrate of 0.45 µm) shown**

Concentrations of Al were highest in colloidal phase at SN6 at 841.3 ppb, and lowest at SN2 at 0.0 ppb. Concentrations of Al in dissolved phase were highest at SN2 at 3585.6 ppb, and lowest at SN4 at 33.9 ppb. Concentrations decreased until inflow from Peru Creek. After the acidic inflow from Peru Creek, Fe and Al decreased until terminating into Dillon Reservoir, as shown in Figures 2-5 and 2-6.

*2.4.2.1 Zinc (Zn) and Copper (Cu)*

Overall, the highest concentration of particulate Zn was at SN8 at 51.2 ppb, and lowest at SN2 at 0.0 ppb, as shown in Figure 2-7.

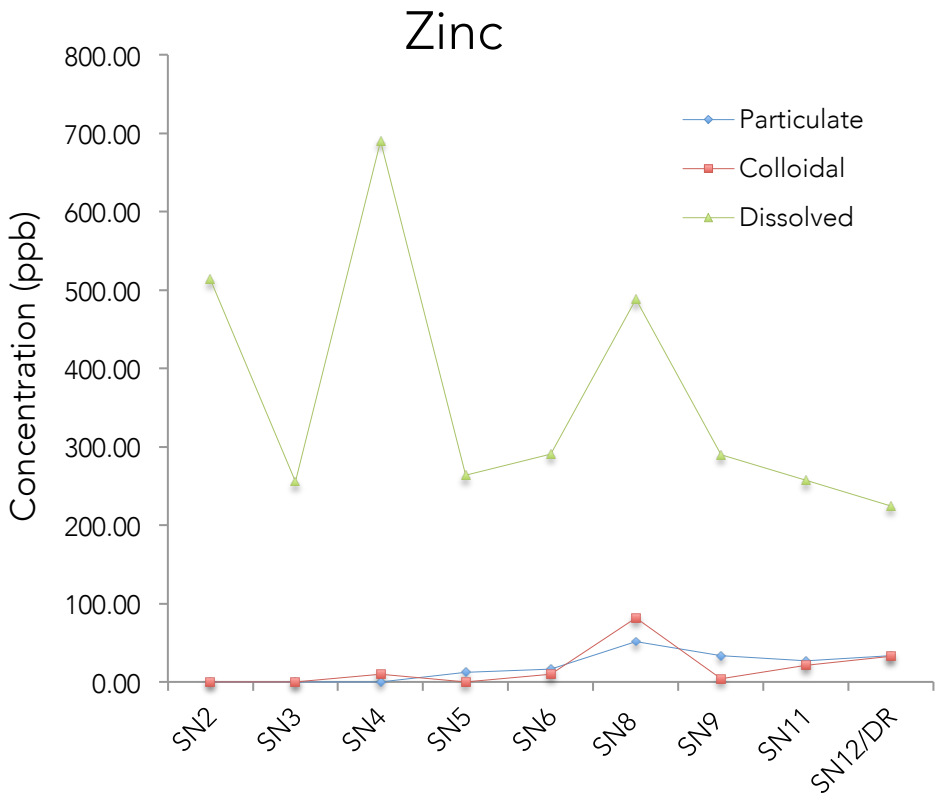


**Figure 2-7. Zinc (Zn) variations downstream. Particulate phase (Particulate = Unfiltered Sample - Colloidal - Dissolved), Colloidal phase (Colloidal phase = 10 µm filtrate - .45 µm), and dissolved phase (filtrate of 0.45 µm) phases shown**

The highest concentrations of Zn in colloidal phase were at SN8 at 81.8 ppb, and lowest at SN2 at 0.0 ppb. The highest concentrations of dissolved Zn were found at SN4 at 690.3 ppb, and lowest at SN12/DR at 224.3 ppb. Concentrations of zinc were highest in the dissolved phase for the entire study area. Data collected from the field support the overall decrease in dissolved Zn as the pH increased above 7 at SN8, an elevated concentration of particulate Zn was observed.

As seen in Figure 2-8, Cu concentration was highest in particulate phase at SN12/DR at 20.1 ppb, and lowest at SN2 at 0.0 ppb.

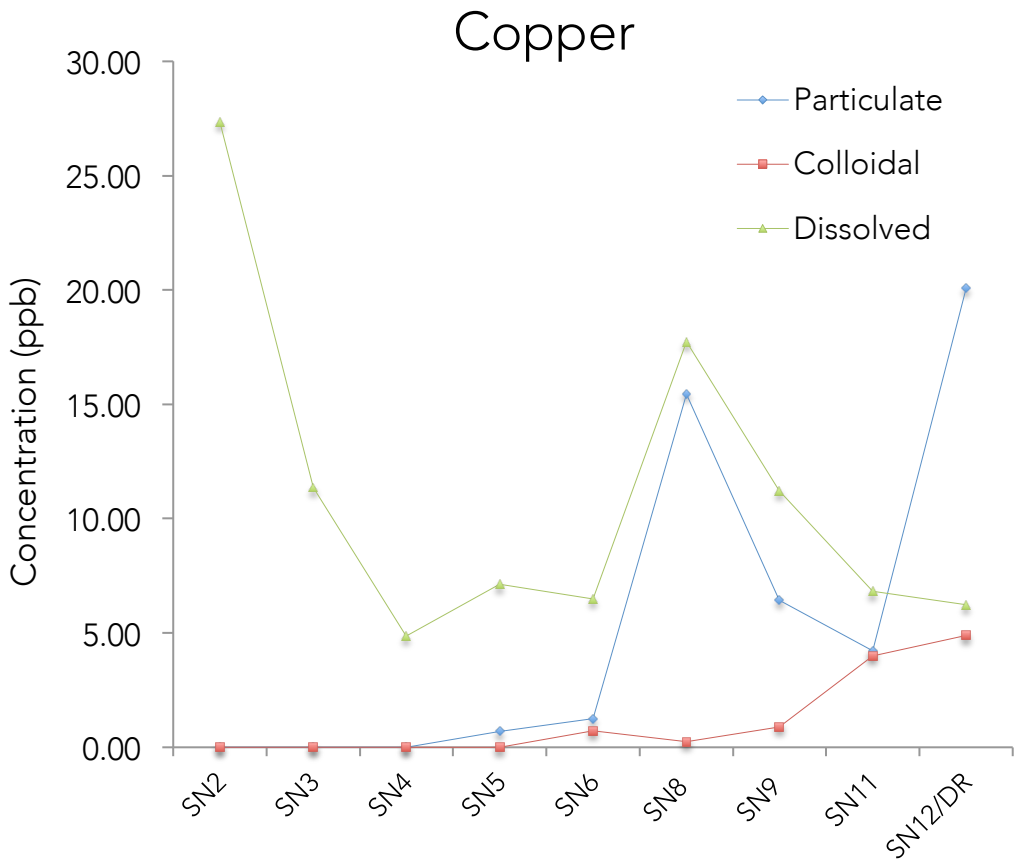


**Figure 2-8 Concentrations of copper (Cu) downstream. The particulate phase (Particulate = Unfiltered Sample - Colloidal - Dissolved), colloidal phase (Colloidal phase = 10 µm filtrate - .45 µm), and dissolved phase (filtrate of 0.45 µm) phases shown**

Cu concentration was highest in colloidal phase at SN12/DR at 4.9 ppb, and lowest at SN2 at 0.0 ppb. Cu concentration was highest in dissolved phase at SN2 at 27.3 ppb, and lowest at SN4 at 4.9 ppb. In the upper reaches, between SN2 and SN6, dissolved Cu dominated, but below SN6, particulate Cu became more prominent, with less differentiation between particulate and dissolved phases. Within each phase, the concentrations were variable.

*2.4.2.2 Fe Speciation*

Fluctuations in total Fe, Fe (II), and Fe (III) can be seen in Fig. 2-9.

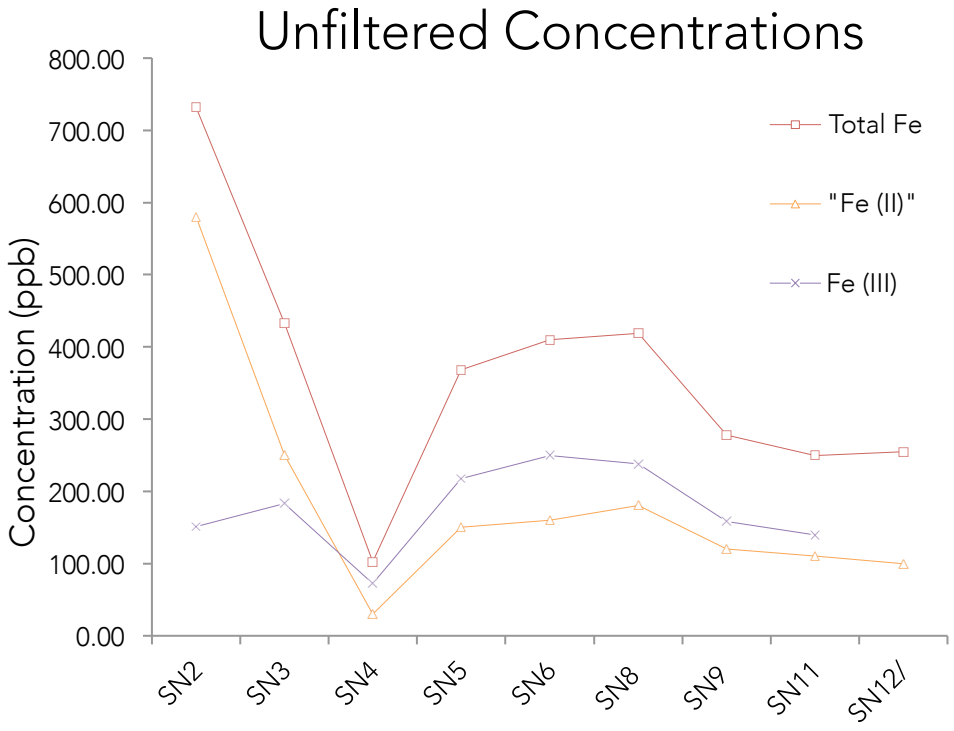


**Figure 2-9. Concentrations of total iron, ferrous ($Fe^{2+}$), and ferric iron ($Fe^{3+}$) downstream.**

Fe (II) was highest at SN2, and lowest at SN4. Fe (III) was highest at SN6, and lowest at SN4. Concentration of Fe (II) exceed Fe (III) in the upper reaches of the Snake River (SN2 and SN3); however, the Fe (III) form dominates downstream of SN4.

*2.4.2.3 Fe and Al Partitioning*

The highest concentrations of Fe in colloidal form were at SN11 and SN12. The lowest colloidal concentrations of Fe were at SN2 and SN4. The highest concentration of Al found in colloidal form was at P1 followed by SN3, and the lowest found at SN2. Fe and Al were highest in

concentration of dissolved form at SN2, and exhibited general decreasing trends in the dissolved phase downstream. The colloidal concentrations calculated can be seen in Figure 2-10.

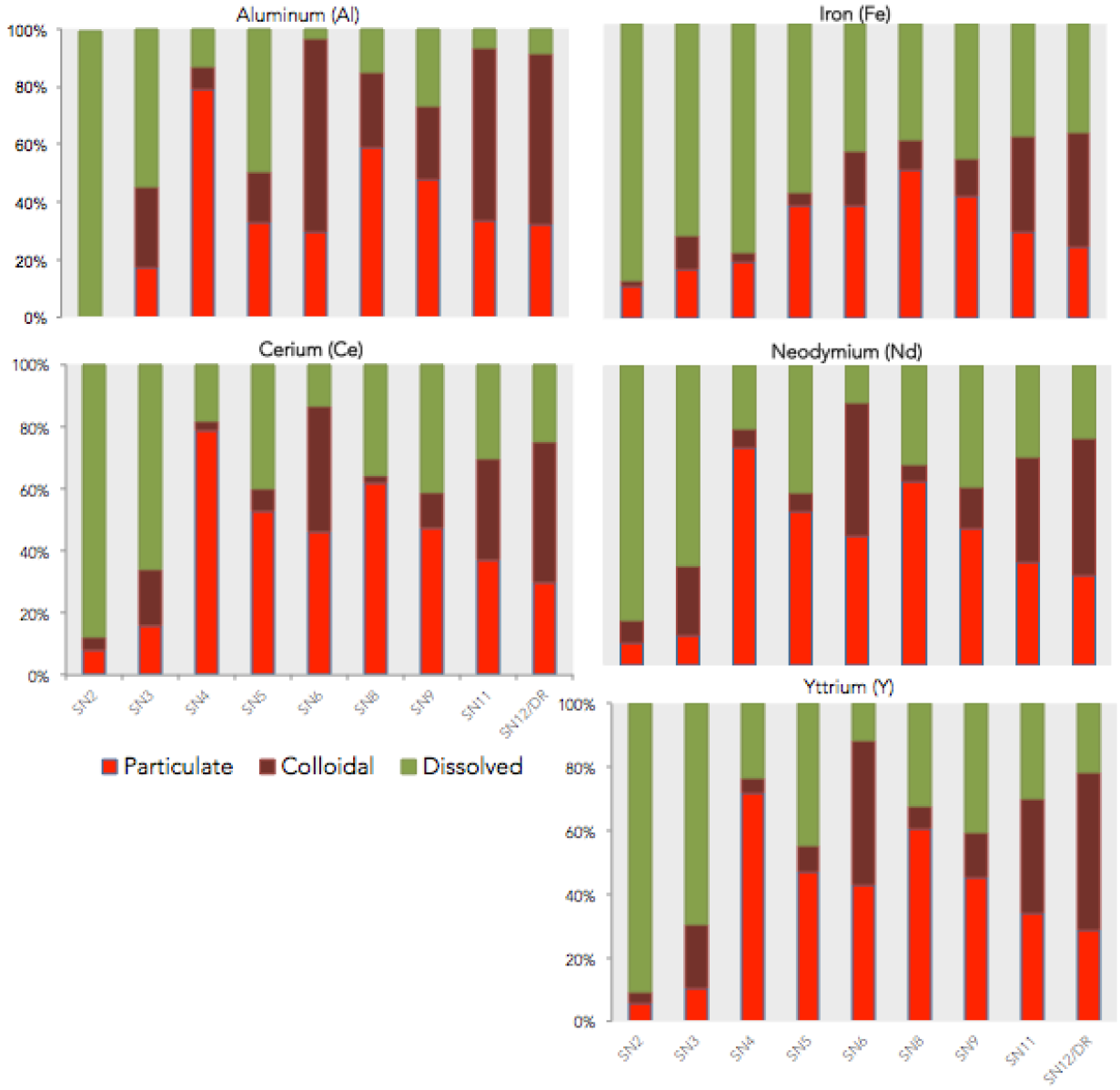


**Figure 2-10. The percentage of heavy metals and REEs in particulate phase (>10 µm particle), colloidal (.4 µm < particle < 11 µm), and dissolved phase (< 0.45 µm particle). Metal concentrations determined by ICP-MS.**

Concentrations of zero indicated the difference between the particulate and dissolved phase was too small to consider distinguishable phases, and so considered within the margin of error.

*2.4.3 Rare Earth Element Partitioning*

Figures 2-11 to 2-14 depict the concentrations of REEs at each site. The REEs selected were Cerium (Ce), Gadolinium (Gd), Neodymium (Nd), and Yttrium (Y) to represent a portion of the lanthanide series.

Ce was highest in particulate phase at SN8 at 1.8 ppb, and lowest at SN2 at 0.4 ppb, shown in Figure 2-11. Ce was highest in colloidal phase at SN12/DR at 0.6 ppb, and lowest at SN4 at 0.01 ppb. Ce was highest in dissolved phase at SN2 at 3.8 ppb, and lowest at SN4 at 0.08 ppb.

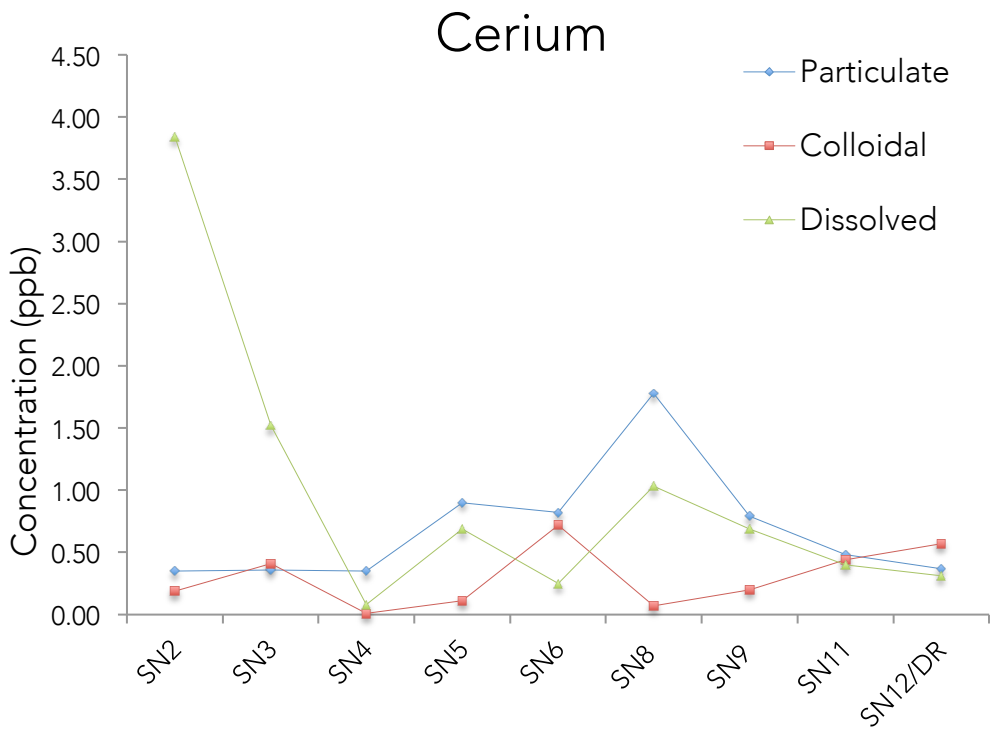

**Figure 2-11. Cerium (Ce) variations downstream. Particulate phase (Particulate = Raw Sample - Colloidal - Dissolved), colloidal phase (Colloidal phase = 10 µm filtrate - .45 µm), and dissolved phase (filtrate of 0.45 µm) shown**

Gd was highest in particulate phase at SN8 at 0.4 ppb, and lowest at SN2 at 0.1 ppb, as shown in Figure 2-12. Gd was highest in colloidal phase at SN12/DR at 0.2 ppb, and lowest at SN4 at 0.01 ppb. Gd was highest in dissolved phase at SN2 at 1.1 ppb, and lowest at SN4 at 0.04 ppb.

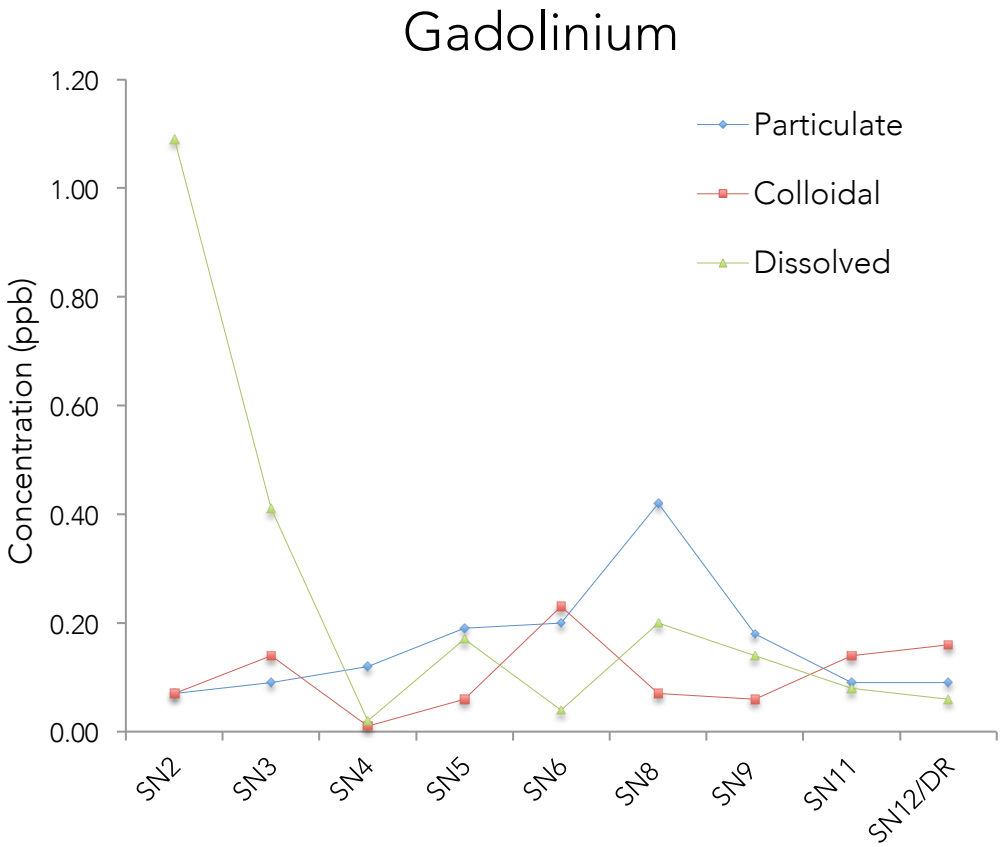


**Figure 2-12. Gadolinium (Gd) variations downstream. Particulate phase (Particulate = Raw Sample - Colloidal - Dissolved), colloidal phase (Colloidal phase = 10 µm filtrate - .45 µm), and dissolved phase (filtrate of 0.45 µm) phases shown**

Nd was highest in particulate phase at SN8 at 1.6 ppb, and lowest at SN3 at 0.2 ppb, shown in Figure 2-13. Nd was highest in particulate phase at SN6 at 0.7 ppb, and lowest at SN4 at 0.03

ppb. Nd was highest in dissolved phase at SN2 at 3.53 ppb, and lowest at SN4 at 0.1 ppb.

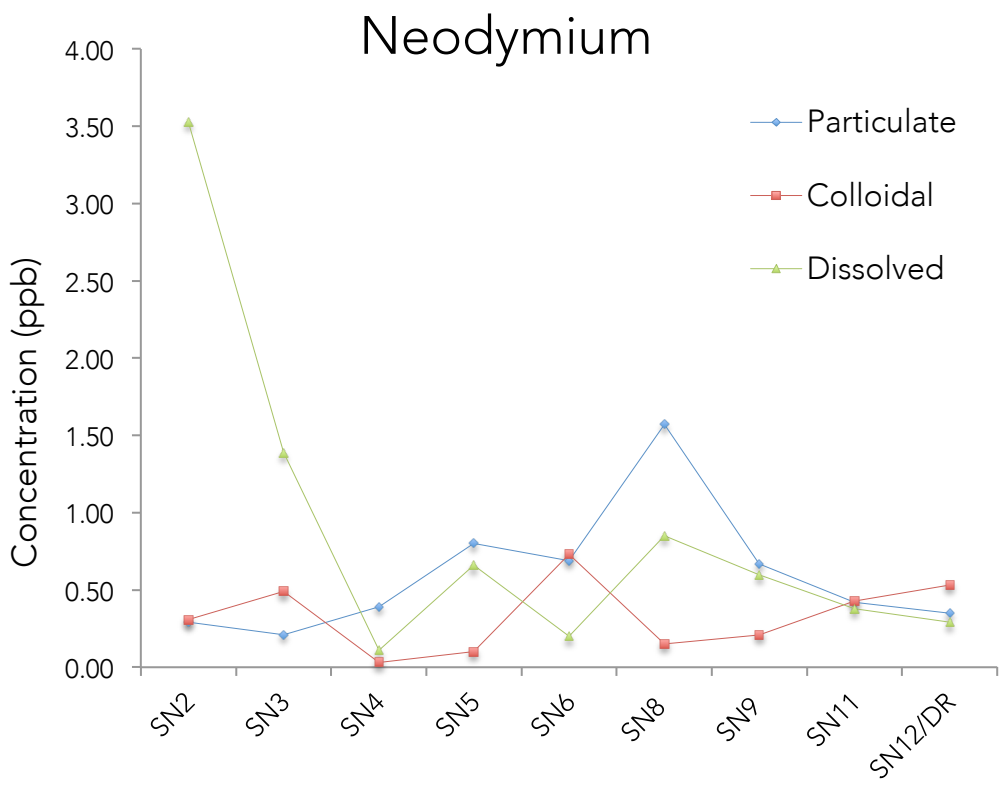


**Figure 2-13. Neodymium (Nd) variations downstream. Particulate phase (Particulate = Raw Sample - Colloidal - Dissolved), colloidal phase (Colloidal phase = 10 µm filtrate - .45 µm), and dissolved phase (filtrate of 0.45 µm) shown**

Y was highest in particulate phase at SN8 at 1.9 ppb, and lowest at SN3 at 0.4 ppb, as shown in Figure 2-14. Y was highest in colloidal phase at SN6 at 1.1 ppb, and lowest at SN4 at 0.03 ppb. Y was highest in dissolved phase at SN2 at 5.8 ppb, and lowest at SN4 at 0.2 ppb.

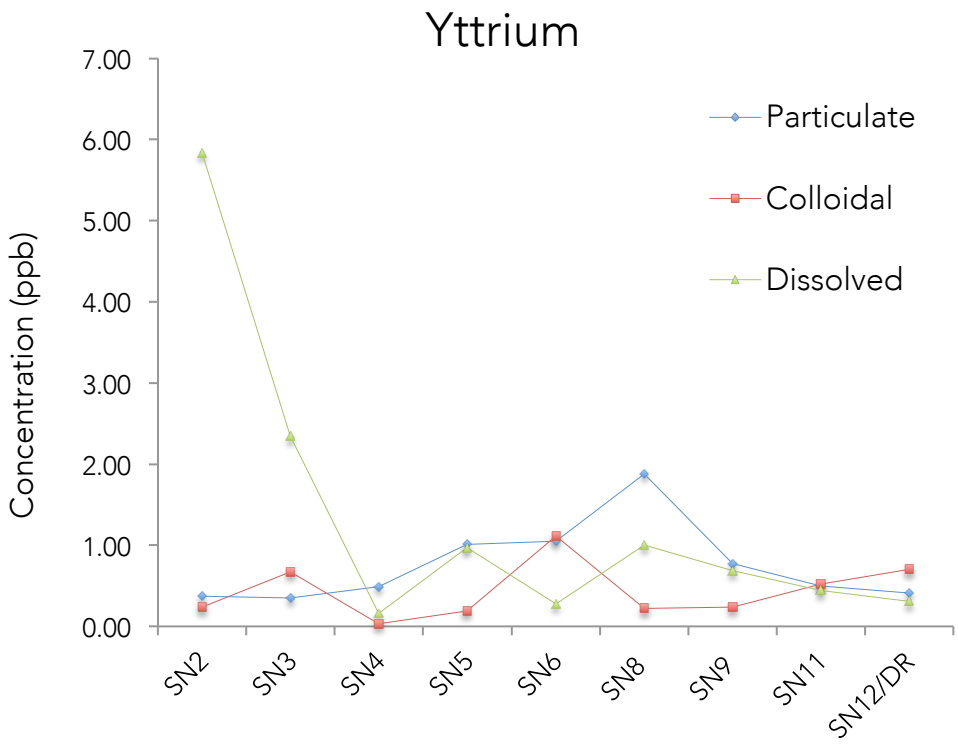


**Figure 2-14. Yttrium (Y) variations downstream. Particulate phase (Particulate = Raw Sample - Colloidal - Dissolved), colloidal phase (Colloidal phase = 10 µm filtrate - .45 µm), and dissolved phase (filtrate of 0.45 µm) shown**

The relationship of colloidal/dissolved REE concentrations in Fig. 2-15 does not show any notable pattern in heavy rare earth elements (HREE) enrichment as compared to the light rare earth elements (LREEs). SN5 and SN12 contained the highest colloidal/dissolved REE ratios

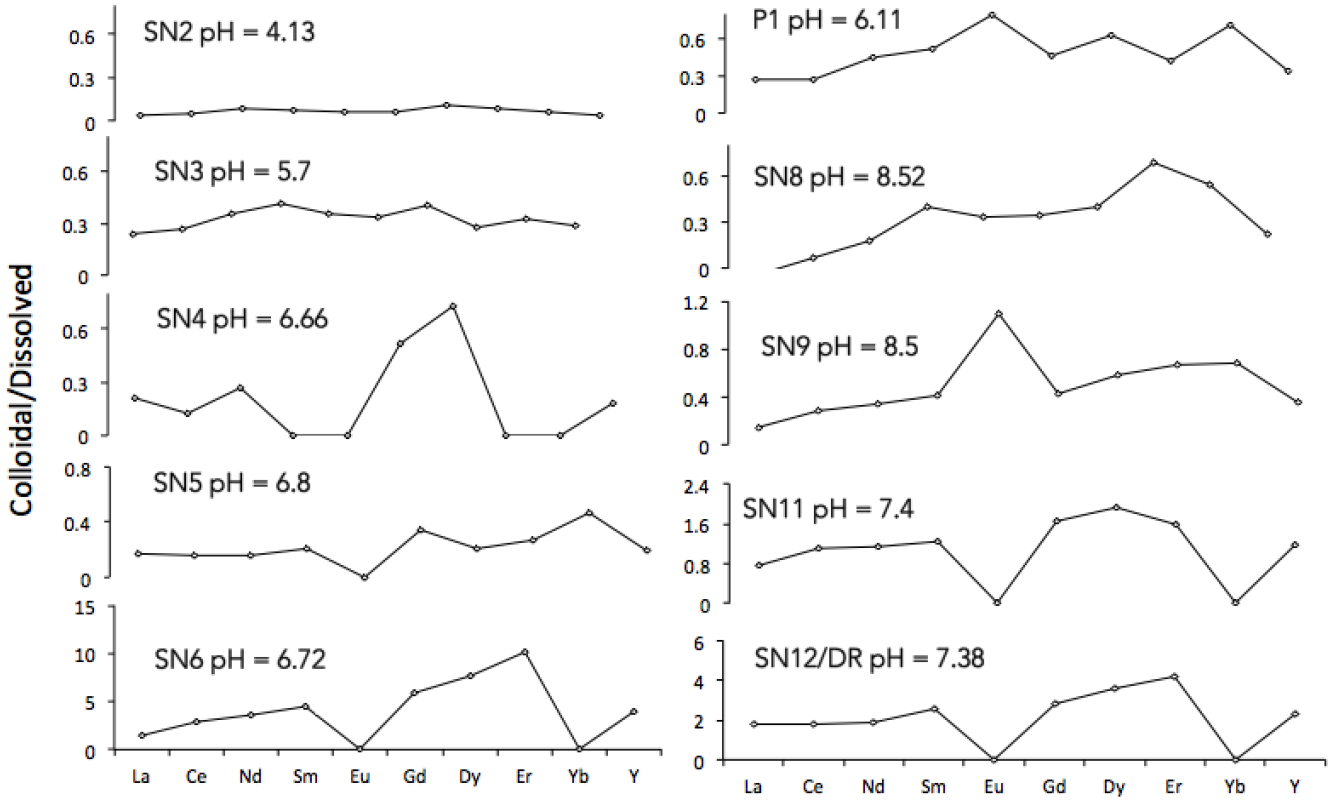


**Figure 2-15. Colloidal concentrations normalized by the concentration in dissolved form (in order of increasing atomic number: 57 (La) to 71 (Lu) with those below machine DL = 0) at each site.**

Figure 2-10 presents graphs characterizing the results of the REE fractionation experiments across the 11 sample sites. The particulate phase was most prevalent at SN4 and SN8. The colloidal phase was the most influential at SN6. The dissolved phase was the primary phase in the upper reaches at SN2 and SN3.

*2.5 Discussion*

*2.5.1 pH*

The pH influences the solubility of trace metals, and is affected by tributaries and lateral inflows. The low pH in the upper reaches of the Snake River causes greater mineral dissolution and weathering, which results in higher dissolved metal concentrations. As pH increases due to the pristine Deer Creek, metals begin to partition into the particulate and colloidal phases as oxy-hydroxides and hydroxides begin to form. The system's pH can fluctuate seasonally with changing flow.

### *2.5.2 Sulfate*

Higher concentrations of sulfate in the upper reaches of the Snake River, and under the confluence of Peru Creek are expected due to the presence of ARD/AMD. In general, sulfate is considered a conservative solute, and can act as a proxy for distinguishing the effects of dilution from sorption, and other non-conservative behavior. Overall, the sulfate concentrations vary little suggesting limited dilution effects other than equivalent flows of Deer Creek and Peru Creek as well as increased erosion. There were minor increases in sulfate at SN6, and SN8 corresponding with inflow from Sts John and Peru Creek.

### *2.5.3 Cations*

#### *2.5.3.1 Zinc (Zn) and Copper (Cu)*

Cu and Zn behavior within AMD impacted sites varies greatly. Generally, Zn tends to remain in solution until a pH of 7. As pH increases, generally a greater concentration of Zn in dissolved phase is observed. However, there is a peak in Zn concentration at SN8 potentially due to the combined metal loading of Peru Creek.

Usually, $Cu^{2+}$ remains the dominant form partitioning onto HFOs and HAOs up until pH of 6 - 7.5 after which copper hydroxides form. It has also been suggested that Cu will begin to precipitate at even lower pH (Dzombak and Morel, 1990; Smith and Huyck, 1999).

There is a much sharper contrast between particulate phase and dissolved phase when partitioning for the zinc profile as compared to the copper profile, suggesting greater scavenging influence such as sorption or preference for dissolved phase.

*2.5.3.2 Fe and Al Partitioning*

Reactive metals such as Fe and Al play an important role transport of other metals through sorption, redox reactions, and co-precipitation. For the most part, Al far exceeded Fe concentrations suggesting an Al-dominated system.

The decreases in Fe (II) due to pH increases below the Deer Creek confluence are consistent with the oxidation of Fe (II) to Fe (III) and precipitate $Fe(OH)_3$ at pH levels greater than 5. The visual observation HFO precipitates such as ferrihydrite or schwertmannite confirmed Fe speciation. The sharp decrease in metals at SN4 could reflect the result of complete mixing below Deer Creek. After comparison with a conservative solute such as sulfate, it is shown that little dilution occurs from SN4 to SN6 reflected by relatively consistent conservative sulfate concentrations. This contrasting behavior could indicate that another mechanism is attenuating

heavy metals and REEs– most likely from previously precipitated aluminum and iron hydroxides lining the streambed.

*2.5.4 Rare Earth Element (REE) Partitioning*

This work was intended to investigate the reactivity of REEs and the range at which they partition between particulate and colloidal phases. The REEs at SN2 (pH < 5) are predominantly in the dissolved phase with a minor percent partitioning to solid surfaces presumably from freshly precipitated aluminum and iron hydroxides (Verplanck et al., 2004). The REEs begin to exhibit significant fractionation after the confluence with Deer Creek at SN3 (pH = 5.7). This behavior is consistent with previous field studies that document REEs as remaining in their dissolved form in acidic, sulfate enriched waters with pH below 5.1, regardless of the degree of Fe oxidation (Verplanck et al., 2004). Both laboratory experiments and field data have supported the observation of REEs beginning to partition out of the aqueous phase between the pH levels of 5.1 to 6.6 with heavy REEs partitioning before light REEs (Verplanck et al., 2004). Previous studies have shown that, for the most part, REE concentrations decrease with increasing pH (Goldstein and Jacobsen, 1988; Elderfield et al., 1990; Dupre et al., 1996; Bau, 1999; Landa et al., 2000; Verplanck et al., 2004).

*2.5.5 Processes Controlling REE Partitioning*

The primary mechanism for REE removal is sorption onto solid phases as demonstrated at SN4, however other mechanisms such as aqueous speciation, oxidation-reduction reactions and variations in the atomic configurations can affect REE concentrations (Verplanck, 2004). REE

fractionation can be heavily influenced by solution chemistry with competition between stable aqueous complexes that reduce REE removal and the scavenging properties at solid surfaces encouraging REE removal from the aqueous phase (Verplanck, 2004). In basic waters where $CO_3^{2-}$ is the primary complexing ligand, REE removal from adsorption is reduced due to the higher stability of $HREE^{-}$ $CO_3^{2-}$ complexes (Sholkovitz, 1995; Byrne and Sholkovitz, 1996; De Carlo et al., 1996; Verplanck, 2004). The HREE carbonate complexes are more stable than LREE complexation, and also have the ability to obstruct LREE adsorption removal complexes (Sholkovitz, 1995; Byrne and Sholkovitz, 1996; Verplanck, 2004). Investigations conducted by Bau, 1999 suggest correlations in REE fractionation with HFO formation, even when free REE ions are the dominant form (Bau, 1999; Verplanck, 2004). Given these trends, the competing reactions involved in REE transport have the potential to be modeled.

In acid mine drainage impacted watersheds, $SO_4^{2-}$ complexes are the dominant aqueous species retarding REE removal and providing a complex stability constant that varies little with atomic mass (Verplanck, 2004). As pH increases, these complexes become less stable allowing the scavenging properties of oxides and hydroxides to control REE behavior.

## 2.6 Conclusions

- AMD mobilizing REEs resulting in higher concentrations in affected sites relative to pristine sites
- Transport behavior of REEs is relatively conservative at low pH (< 6) with ligand binding and adsorption reducing scavenging mechanisms

- As pH increases downstream (> 5), lower percent of Al and Fe in dissolved phase and variable percent in colloidal and particulate phases
- As pH increases, there is a higher degree of fractionation of REEs into colloidal and particulate phase

# CHAPTER 3:

# DYNAMICS OF SOLUTE TRANSPORT WITH CONTINUOUS TRACER INJECTION

## *3.1 Introduction*

In-stream injection experiments can be used to create spatial profiles of pH, metal loading, and discharge for ARD/AMD impacted systems. The quantification of discharge in mountain streams proves difficult using standard methods such as current meters and slugs as a percentage of the water flows through the cobble streambed in the hyporheic zone (Bencala et al., 1990; Harvey and Bencala, 1993; Kimball, 1997; Harvey et al., 1996). However, utilizing a tracer can provide an alternative route for measuring accurate discharge as the injected tracer follows the water through the stream's substrate, and as long as allowed to reach a steady concentration will provide a hydrological framework for calculating discharge and metal loading (Bencala et al., 1990; Kimball et al., 2002).

The tracer injection is used as a means of quantifying the significance of surface inflow from subsurface and groundwater inflow, as well as identifying the main transport characteristics. These transport characteristics can be used to determine contaminated flow contributions, thus supporting informed decisions regarding remediation of acidic, metal enriched portions of a watershed. The subsurface flows can include varying riparian seeps, springs, as well as hyporheic flow (Bencala et al., 1990; Kimball et al., 2002).

A LiCl tracer injection was performed to determine in-stream discharge and inflow sources, and calculate the representative hydrological parameters of the Snake River at low flow. Chloride based salts (tracer injectates) are commonly used as conservative tracers in mountain streams. Li works well in low pH streams; Cl works well in higher pH streams (Kimball et al., 2002). Also, there are rarely background concentrations of Li high enough in mountain watersheds to present any issues. Cl concentrations are generally low, but will occur due to atmospheric precipitation and weathering (Kimball et al., 2002). Other tracers such as dye-based tracers are unfavorable in low pH systems as they can behave non-conservatively due to sorption to solids and organic matter in the hyporheic zone and other slow moving forms of transient storage (Bencala et al., 1986; Runkel, 2015). For example, Rhodamine-WT, a dye-based tracer is less conservative than Li in the Snake River due to high levels of acidity (Runkel, 2015).

Breakthrough curves (BTCs) can be analyzed to distinguish the three dominant processes through the separation and distribution of total tracer mass over time. The breakthrough curve can be broken down into three portions: the “rising limb” which reflects initial solute transport downstream with increasing concentration; the “plateau” is seen when the solute concentration reaches steady state indicating the primary channel and the storage zones are saturated with solute; and finally, the “descending limb” reflects the decreasing concentration of the tracer after the pump is shut off (Crouch, 2011).

### *3.2. Simulation of Conservative Tracer Transport with OTIS and OTIS-P*

One-Dimensional Transport with Inflow and Storage (OTIS) is a numerical model developed by Dr. Robert L. Runkel of the United States Geological Survey that is capable of simulating the fate and sources of solutes in streams and rivers. OTIS is based on the physical processes of advection, dispersion, lateral inflow, and transient storage that together affect the transport of varying metals (Runkel, 1998). OTIS can provide an accurate mean of predicting one-dimensional (width and depth are assumed negligible) trace metal fate en route downstream.

Physical processes considered are advection, dispersion, molecular diffusion resulting in a velocity distribution, and transient storage which is the retention of stream water and associated solutes in areas other than the primary flow path, for a given period of time. Advection is the bulk transport of a solute downstream due to gravity. Dispersion is the distribution of convective velocity fluctuations around the mean solute velocity, and is generally modeled directly (Jury, 1988). The dispersion or solute spreading is also a result of molecular diffusion and sheer stresses acting within a system. Transport of conservative tracers in lotic systems is subject to the processes of advection, dispersion, transient storage, and mass loss to groundwater. Transient storage generally occurs in the form of eddies, porous areas of stream bank and slower, stagnant pools of water. Lateral inflow is also considered and is described as including groundwater inflow, overland flow and interflow or small springs (Runkel, 1998). The mass balances used in OTIS for each component are derived using two conceptual areas: the main channel and the storage zone; shown by the equations below (Runkel, 1998):

$$\frac{\partial C}{\partial t} = -\frac{Q}{A}\frac{\partial C}{\partial x} + \frac{1}{A}\frac{\partial}{\partial x}\left\langle AD\frac{\partial C}{\partial x}\right\rangle + \frac{q_{LIN}}{A}(C_L - C) + \alpha(C_S - C) \quad (3\text{-}1)$$

$$\frac{dC_S}{dt} = \alpha\frac{A}{A_S}(C - C_S) \quad (3\text{-}2)$$

A = main area cross-sectional area ($L^2$); $A_s$ = storage zone cross-sectional area ($L^2$); C = main channel solute concentration ($ML^{-3}$); $C_L$= lateral inflow solute concentration ($ML^{-3}$); $C_s$ = storage zone solute concentration ($ML^{-3}$); D = dispersion coefficient ($L^2T^{-1}$); Q= volumetric flow rate ($L^3T^{-1}$); $q_{lin}$ = lateral inflow rate ($L^3T^{-1}L^{-1}$); t= time (T); x= distance (L); α = storage zone exchange coefficient ($T^{-1}$). Figure 3-1, shown below, adapted from Runkel, 1998 shows the two interacting compartments used to develop OTIS's governing equations.

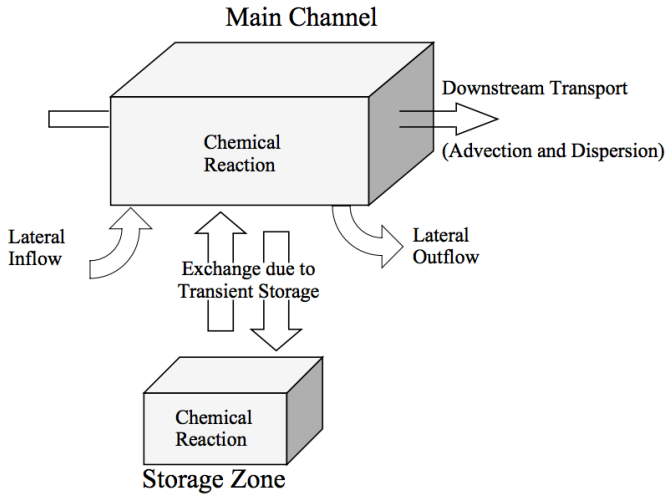


**Figure 3-1. Two conceptualized volumes used in OTIS to calculate concentration in main channel and storage zone (adapted from Runkel, 1998)**

The volume containing the main channel is a zone in which advection, dispersion, decay, and limited sorption occur that affect the solute's transport. The second, smaller box encompasses the storage zone, in which the mechanisms of decay and sorption occur. To compute the final

solute concentration, OTIS calculates the exchange and transient storage occurring between the two volumes. OTIS uses additional terms to model less conservative transport; specifically, kinetic sorption and first-order decay.

For modeling conservative solutes ($C_L$), the difference between the mass loadings of the solute at the top and bottom of the reach should be normalized by the change in flow rate across the reach, as shown by equation 3-3 below:

$$\mathbf{C_L = (C_B Q_B - C_T Q_T)/(Q_B - Q_T)} \qquad \mathbf{(3\text{-}3)}$$

In order to model more complex chemical reactions, OTIS is coupled with a chemical equilibrium sub-model based on MINTEQ, a model capable of computing the distribution of chemicals that exist within a batch reactor at equilibrium (Allison et al., 1991; Runkel et al., 1995). When modeling trace metal behavior, pH dependent processes are important to capture varying mechanisms of precipitation, co-precipitation, redox and sorption (Runkel, 1998).

*3.3 Field Site*

The sampling sites are marked in Figure 2-1, with SN2, SN3, and SN4 referred to as SN2X20, SN3X120 and SN4X520 for the remainder of the thesis. The hydrologic parameters calculated from the 2015 tracer injection were compared to parameters optimized in Bencala et al. (1990) to validate parameters obtained from a lower resolution breakthrough curve. However, before comparison, culvert additions to the field site must be addressed. Shown below, in Figure 3-2, is

an abstraction from McKnight and Feder (1984) of the Snake River and Deer Creek confluence indicating one culvert transporting water under Montezuma Road:

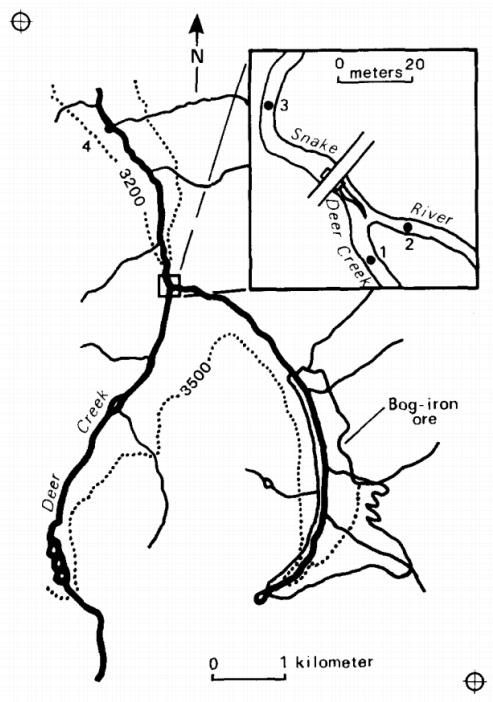


**Figure 3-2. Snake River and Deer Creek confluence in 1984 indicating one culvert (adapted from McKnight and Feder, 1984)**

Bencala et al. (1990) conducted research in 1983 and 1984 coinciding with McKnight and Feder (1984) and would indicate the presence of one culvert. Since these studies, an additional culvert has been included which alters the mixing regime, and also the water chemistry of the confluence, and will result in variable hydrological parameters. The sampling site, SN2X20 was located closer to Montezuma Road than previous SN2 sites. With the reworking of the beaver dams in the confluence since the 1980s, the site SN2X20 could reflect partial mixing of water from the upper Snake River with water from the Deer Creek (McKnight).

*3.4 Hydrological Parameter Estimation*

Determining solute transport characteristics establishes a strong foundation for accurately capturing and studying the hydrology and geochemistry of acid mine drainage systems. These parameters can be estimated using OTIS and tracer-dilution. Tracer-dilution is useful in determining the validity of OTIS's simulation accuracy, and capability through the quantification of a stream's physical processes as well as chemical equilibrium (Runkel, 1998). Tracer-dilution involves the injection of a conservative tracer at an assigned upstream site, and continuous monitoring at multiple downstream sites in order to obtain a spatial concentration profile. This method also provides insight into the degree of lateral inflow through comparison of plateau heights downstream. The higher plateau concentration suggests less dilution, and generally the plateau concentrations will decrease downstream due to lateral inflow increasing discharge.

OTIS is used widely as a means for simulating breakthrough curves created from tracer experiments using conservative solutes, such as LiCl. Parameters such as channel area (A), storage zone ($A_s$), and exchange coefficient ($\alpha$) are effective over user-specified reach lengths, and vary across reaches. Reaches are generally determined based on the stream's hydrological or geomorphological variation. These parameters will shape the rising and descending limbs of the BTC, providing insight into the mixing between the main channel and storage zones. The curvature of the BTC's "tail" reflects the outflow of the solute from transient storage such as the hyporheic zone (Crouch, 2011). OTIS can be used to quantify the dispersion, advection, and decay terms affecting relatively conservative solutes, which then can be extended to more reactive solutes such as Fe and Al.

OTIS-P provides a quantitative approach to obtaining optimized physical transport parameters defining advection-dispersion through means of Nonlinear Least Squares (NLS). NLS utilizes optimization problems to find the best parameters that minimize the difference between the observed values and the simulate values, or more specifically, the weighted residual sum of squares (RSS). OTIS-P also provides statistical measurements to validate the optimized parameters such as standard deviation, covariance matrices and the ratio of estimate to standard deviation (Runkel, 1998)

### *3.5 Methods*

#### *3.5.1 Sampling Location*

On October 3rd, 2015 a conservative (non-reactive) LiCl tracer injection was conducted on the upper to mid reaches of the Snake River. Site locations were established based on prior investigations, accessibility, and flow consistency. For the tracer injection, a total of six sites were sampled (SN2 to SN6 including Deer Creek, as shown in the site map in Chapter 2). However, only three sites (SN2, SN3, and SN4) were modeled using OTIS due to lack of tracer arrival at lower sites. Water chemistry was gathered at each site during the tracer injection, as well as at SN7, SN8, and Peru Creek. For the remainder of this thesis, sites SN2, SN3 and SN4 will be referred to as SN2X20, SN3X120, and SN4X520 to limit confusion with site names of prior tracer injections on the Snake River using similarly defined reaches with varying lengths.

#### *3.5.2 Tracer Injection*

The injection point was above the confluence of the Snake River and Deer Creek with five sampling points, shown in Figure 2-1 stretching 2.5 km downstream. A solution of LiCl was created by dissolving 1500 g of LiCl in 40 L of ultra pure DI water. The tracer of 0.9 M LiCl was continuously injected over the study area for 80 minutes. The background Li concentrations within the Snake River were approximately $5.0x10^{-3}$ ppm and Cl concentrations were less than 1 ppm.

Before the injection, the solution was sampled to verify a concentration of 31.34 g/L $Cl^-$. The injectate was also sampled at time = 0, 30 and 80 minutes to verify consistent pumping of steady, fully mixed solution. The pump was powered using a 12 V battery and calibrated before entering the field to pump at a controlled rate of 500 mL/min. The rate was tested throughout the duration of the tracer to ensure consistent pumping. The tracer injection began at noon and was designed to last 80 minutes. The samples were taken more frequently during the first 30 minutes, and in the last 30 minutes after the pump was shut off in order to obtain greater resolution of ascending and descending limbs.

*3.5.3 Field Parameters*

The pH and temperature at each site were measured using a YSI 60 multi-parameter field probe. Salinity, conductivity and temperature were measured using a YSI 30 multi-parameter field probe. Dissolved oxygen (DO) was measured using YSI 55 field probe. All measurements taken using the YSI probes were recorded after the field probe equilibrated for a few minutes in

the sampling area. Before entering the field, the pH probe was calibrated twice using pH buffer stock solutions of 4.01, 6.86, 9.18.

### *3.5.4 Cations and Anions*

The water samples were collected, and concentrations of major cations and anions were analyzed at nine sites (D1, SN2X20, SN3X120, SN4X520, SN5, SN6, SN7, SN8, P1) using EPA method 200.8. Before entering the field, 60 mL HDPE bottles were rinsed three times with DI water and then soaked in a 5% reagent grade nitric acid bath over night, followed by three additional DI rinses. All samples were collected after rinsing the bottle three times with the water being collected, and were then completely filled to eliminate headspace. A 60 mL HDPE bottle was filled at each site. After collection, the pH of the cations was adjusted to less than 2 with trace grade concentrated nitric acid ($HNO_3$), and pH was further confirmed using litmus paper. This was to reduce further chemical reaction and changes in speciation. Samples were kept on ice in a cooler to limit the influence of light and ambient heat until taken to the Laboratory for Environmental and Geological Studies (LEGS). The cations were analyzed using Inductively Coupled Plasma Mass Spectrometry (ICP-MS) analysis. Anions ($Cl^-$ and $SO_4^{2-}$) were measured using ion chromatography (IC).

### 3.5.5 *Iron Speciation Measurements*

Total iron Fe (II) and Fe (III) and Fe (II) were measured using the Hach DR-2800 Field Spectrophotometer in the field. Total Iron was measured using the USEPA FerroVer method in which the FerroVer iron reagent converts all soluble and most insoluble forms of iron within the

sample to soluble ferrous iron. The Fe (II) reacts with 1,10 Phenanthroline to form an orange color with an absorbance proportional to iron concentration. The absorbance is taken at a wavelength of 510 nm. The Fe (II) was measured using the 1,10-Phenanthroline method and utilizes the reaction between 1,10-phenanthroline and Fe (II) in the sample to form an orange color in proportion to the iron concentration. The Fe (III) does not react, and can be subsequently calculated by subtracting the Fe (II) concentration from the total iron concentration.

### *3.6 Results*

#### *3.6.1 pH*

Throughout the entire study reach, the pH varies from 4.8 to 6.23. The pH remained acidic, approximately 4.8 to 5.0 throughout the headwater reaches SN2X20 to SN4X520 (shown in Figure 3-3).

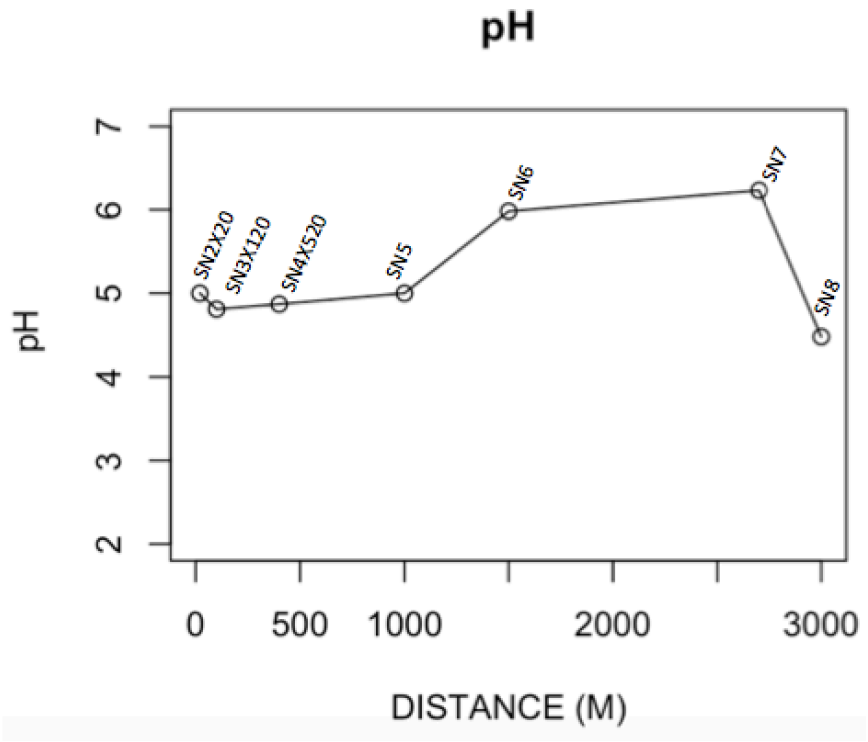


**Figure 3-3. Plot of longitudinal pH variation over the Snake River study area.**

The pH at SN2X20 was measured before the tracer injection, during, and after with values 3.3, 5.0, and 4.8, respectively. The higher pH values reflect greater contribution of water from Deer Creek at the sampling site. Below SN7, the pH dropped to 4.4 with the inflow from the Peru Creek. In general, in the Snake River, the pH increased downstream due to lateral inflow, smaller tributaries and runoff with a sharp decrease around 3000 m. This sharp decrease reflects the inflow from the even more acidic Peru Creek.

*3.6.2 Sulfate*

Much higher concentrations of sulfate were found in the headwaters of the Snake River, with relatively constant concentrations for the remaining reaches, as shown in Figure 3-4.

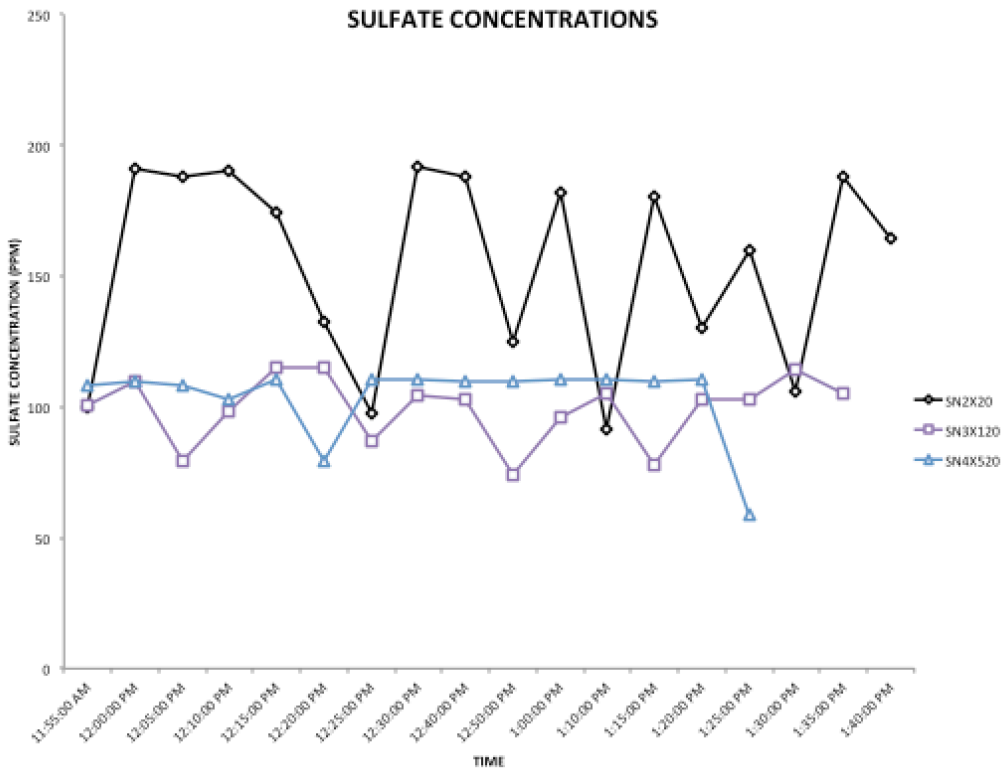


**Figure 3-4. Plot of sulfate concentrations over duration of tracer at SN2X20, SN3X120, SN4X520. Sulfate variation at site SN2X20 reflect variation in contribution of water from Deer Creek during sampling.**

At SN2X20, sulfate fluctuates similar to pH ranging between 200 ppm to 100 ppm, which also reflects greater contribution from Deer Creek when the pH was higher. SN3X120 shows sulfate variability, however, at a lower magnitude also reflecting incomplete mixing. Sulfate concentrations at SN4X520 are relatively constant, as expected in conservative solutes without additional ARD inputs or dilutions. However, the sulfate drops approximately 30% and 46% at 13.00 and 14.20 hr, respectively.

### *3.6.3 Trace Metal Transport*

Figure 3-5 contains plots showing the observed concentrations of Fe, Al, $SO_4^{-2}$, Zn, and Cu at each site until the confluence with Peru Creek, at approximately 2700 m.

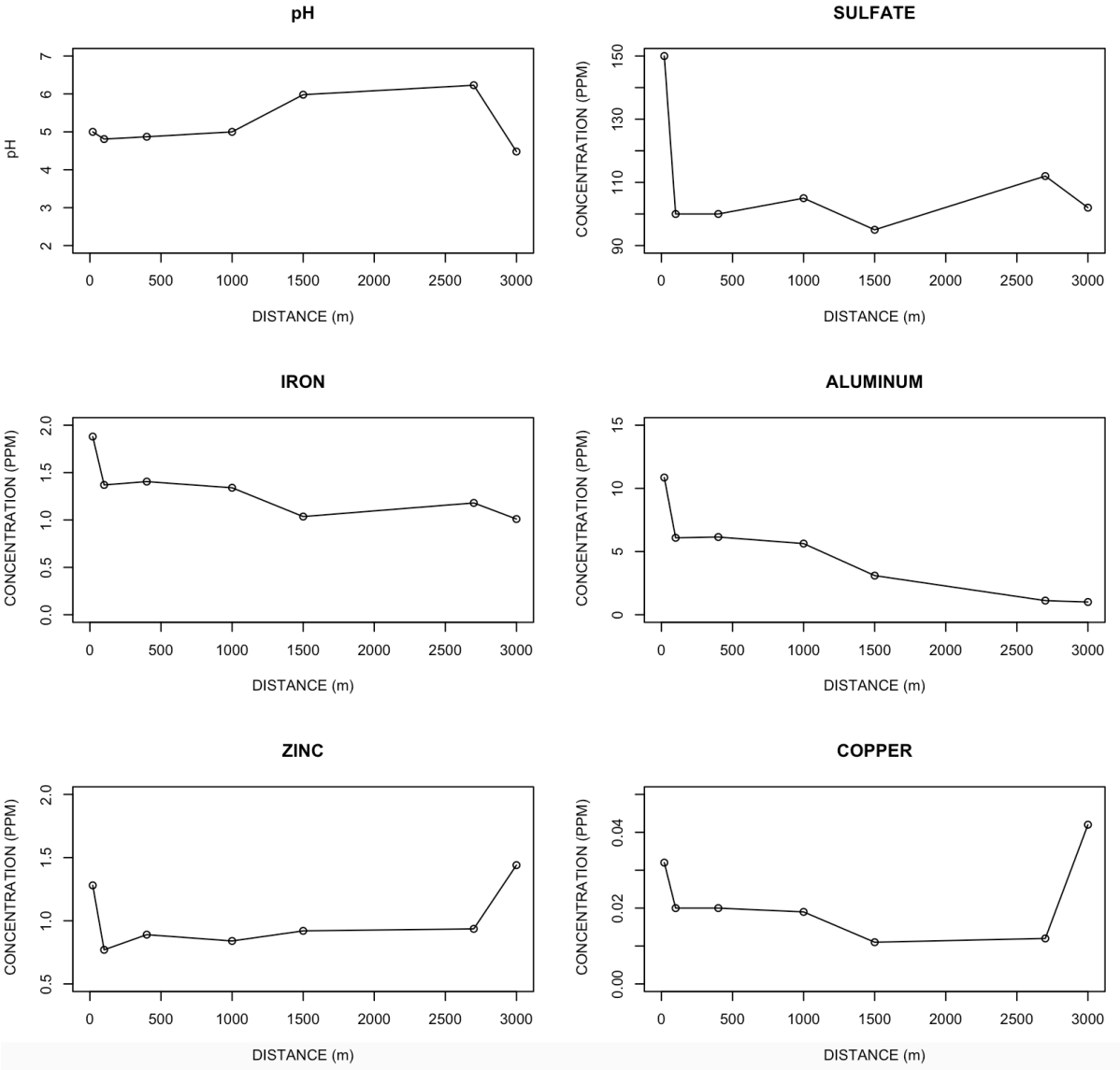


**Figure 3-5. Longitudinal variations in concentrations of total Fe, Al, Sulfate, Zn and Cu averaged over the injection area.**

The concentrations were averaged using the samples collected over the duration of tracer injection. A plot of pH variance is included for comparison. Highest average concentrations of

The concentrations were averaged using the samples collected over the duration of tracer injection. A plot of pH variance is included for comparison. Highest average concentrations of Fe are found in the headwaters at SN2, with concentrations gradually decreasing downstream until a small increase at the Peru Creek confluence. Highest concentrations of Al, shown in Fig. 3-5, were found in the ARD impacted headwaters with concentrations subsequently decreasing for the remaining study area.

The Zn and Cu profiles in Fig. 3-5 show both these two metals behaved similarly in response to pH fluctuations. However, Zn concentrations appear to be less sensitive to small pH variations around 6.0, as compared to Cu, which was found at comparatively lower concentrations at SN6 and SN7. Averaged concentrations of Zn were highest below the upper Snake River reach SN2X20, and the Peru Creek confluence at SN8; concentrations are lowest at SN3X120. Averaged Cu concentrations were highest at sites with lower pH values (SN2X20 and SN8), and concentrations were lowest at sites with higher pH levels (SN6 and SN7).

The behavior of more reactive metals, such as Fe, over the duration of the injection can be seen in Figure 3-6.

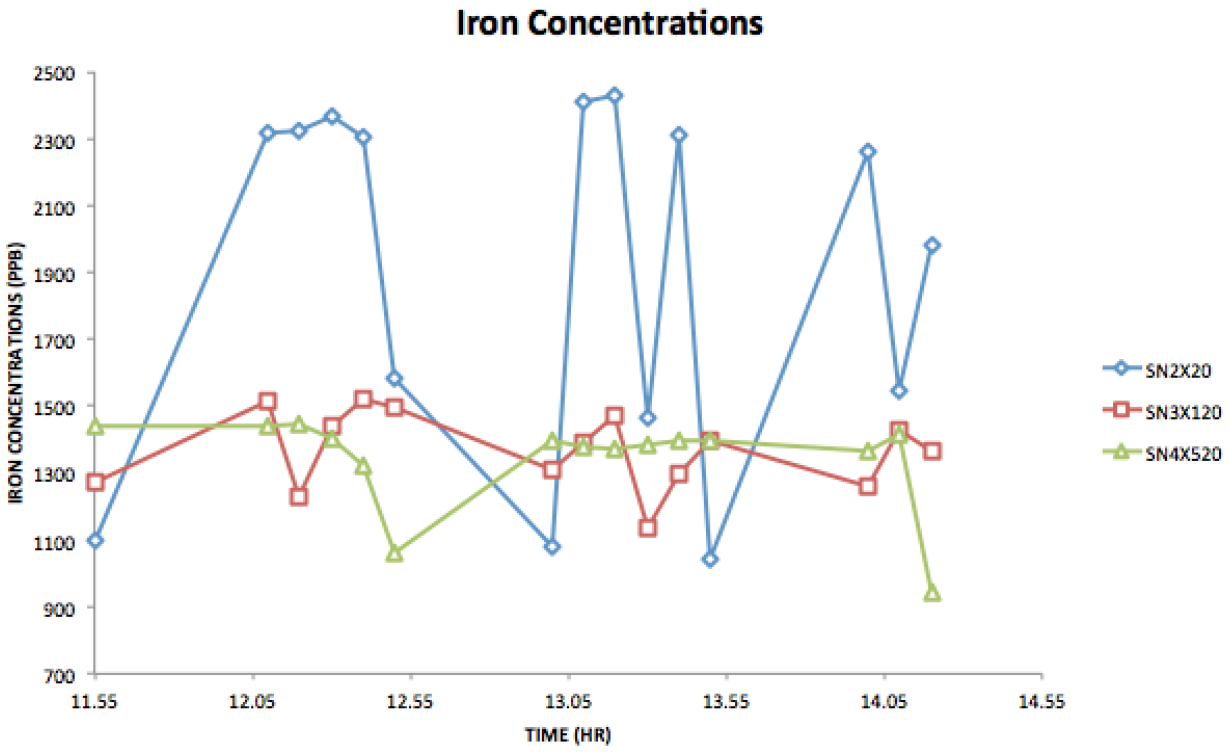


**Figure 3.6 Fe concentration (ppb) during tracer injection at SN2X20, SN3X120, SN4X520. Iron variation reflect variable mixing with Deer Creek water at the sampling site of SN2X20 in the headwaters as compared to the lower reaches.**

The mass loading of a solute is calculated by multiplying the site discharge by the solute concentration:

$$M_x = Q_x C_x \quad (3\text{-}4)$$

*3.6.4 Rare Earth Elements (REEs)*

Figure 3-7 depicts concentrations (ppb) of Ce, Nd, Y and Zn downstream.

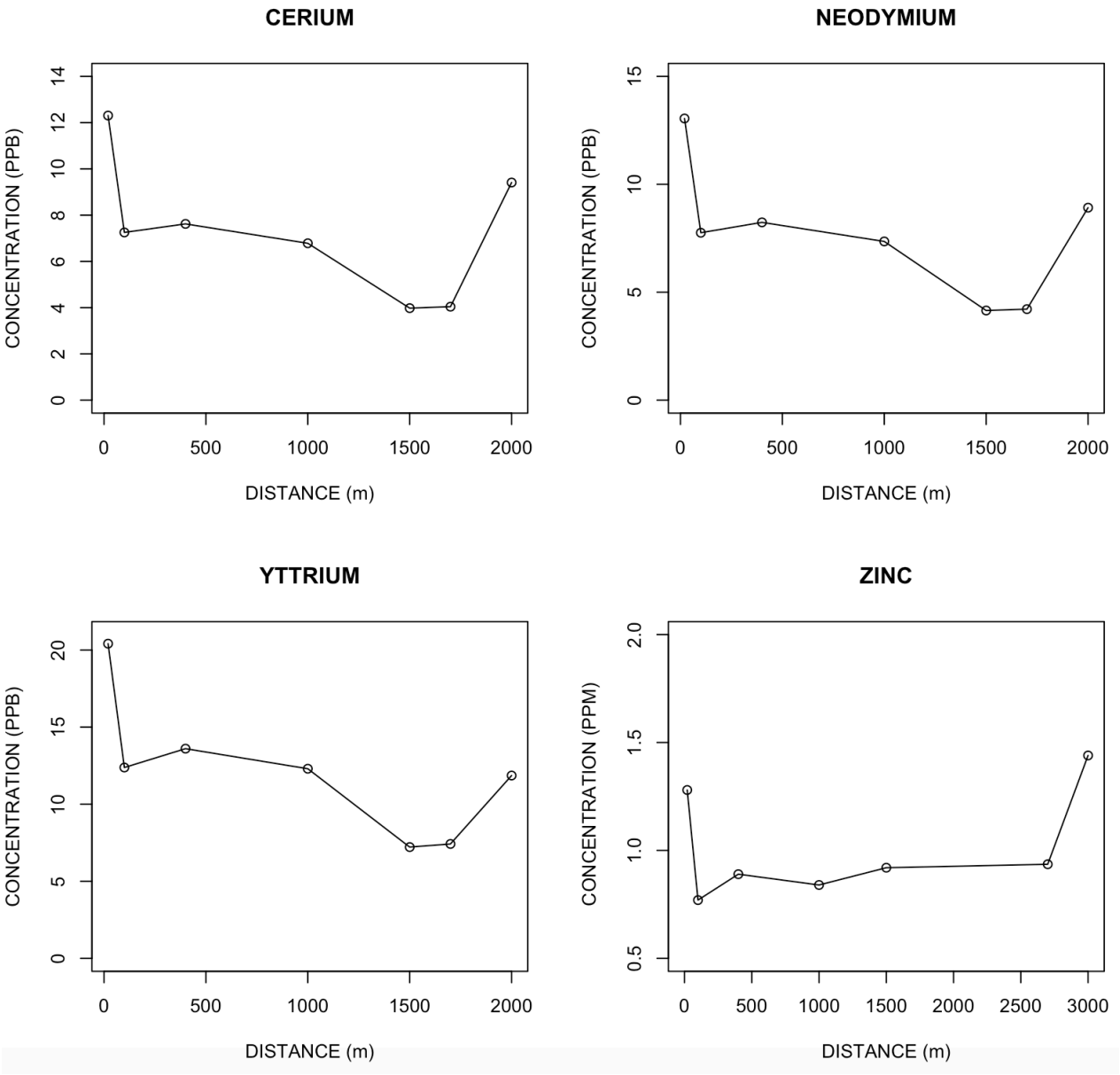


**Figure 3-7. Longitudinal variations in concentrations of the rare earth elements: Ce, Nd, and Y; Zn is included for comparison**

The concentrations decrease overall until reaching Peru Creek. A plot of Zn is included to compare similar behavior. The concentrations were higher at sites with lower pH such as SN2X20, and downstream of the Peru Creek confluence at SN8. The concentrations are lower at

sites with more neutral pH, such as SN6 and SN7. Despite small pH variation, the REE concentrations decreased by approximately half at SN3X120 due to Deer Creek's near equivalent inflow.

Figures 3-8, 3-9, and 3-10 depict observed concentrations of REEs over the duration of the tracer injection.

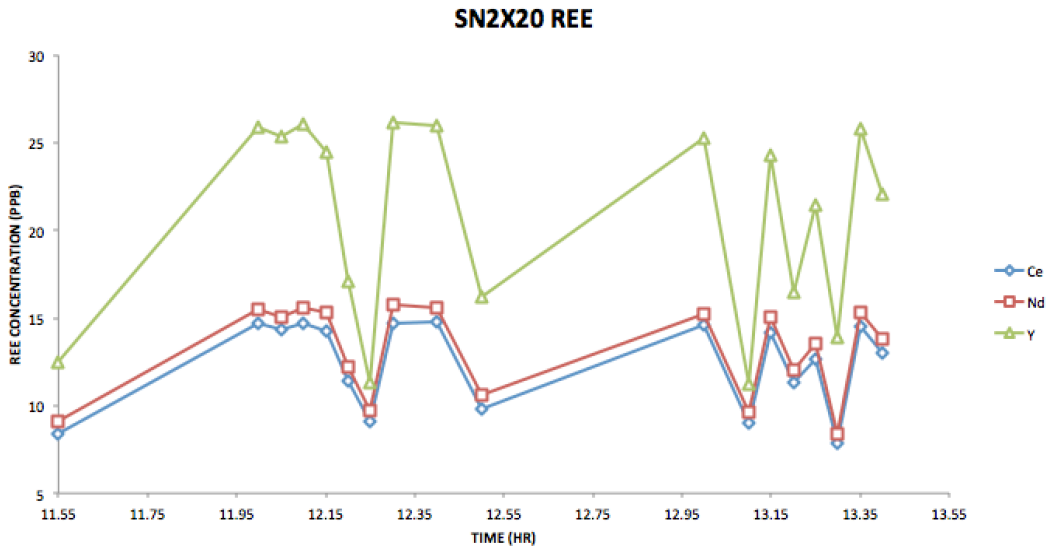


**Figure 3-8 Observed REE concentrations (ppb) of sampling site SN2X20 over duration of tracer injection. Variation in REE concentration reflects variable mixing with Deer Creek during sampling.**

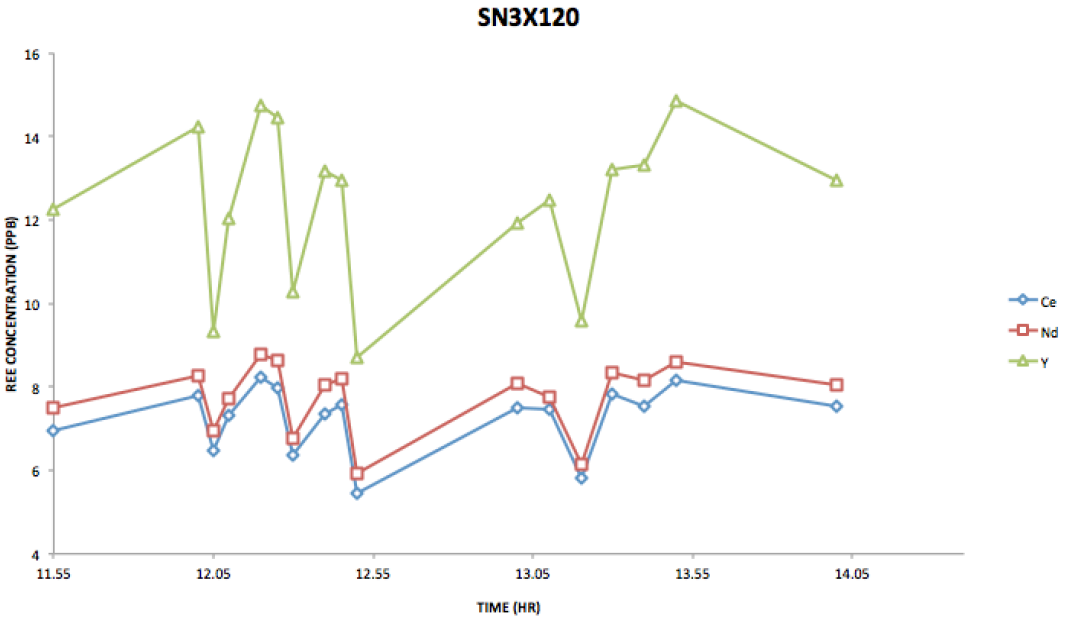


**Figure 3-9 Observed REE concentration (ppb) at site SN3X120 over duration of tracer injection. Variation in REE concentration reflects variable mixing with Deer Creek during sampling.**

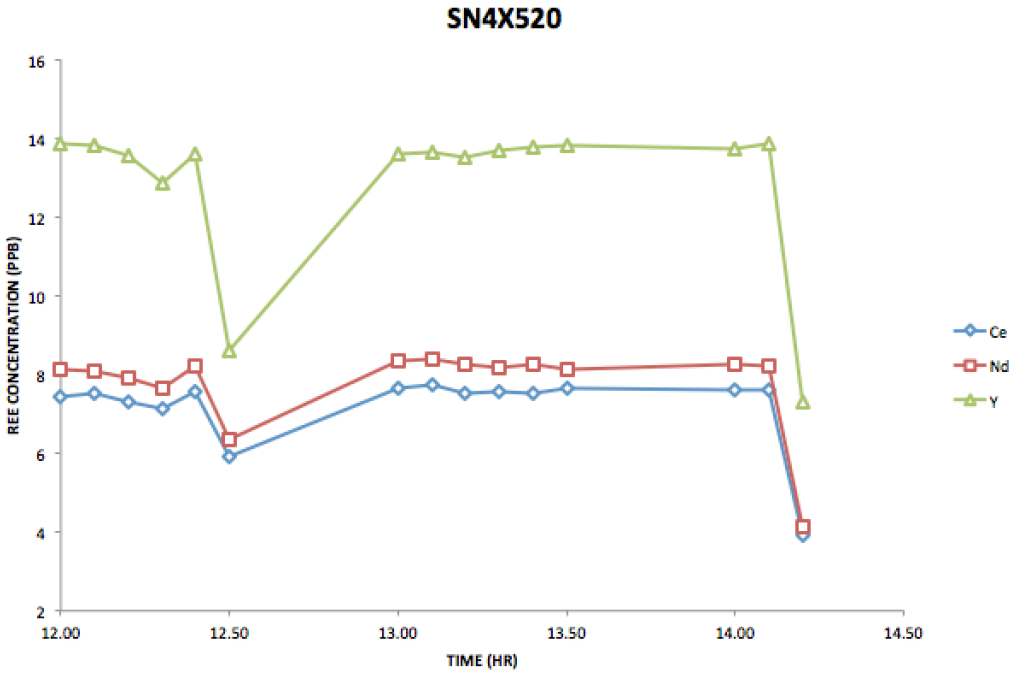


**Figure 3-10 Observed REE concentrations (ppb) at sampling site SN4X520 over duration of tracer injection**

The variance in concentrations decreases downstream indicating complete mixing of Snake River and Deer Creek water farther from the confluence. As concentrations of rare earth metals varied similarly to sulfate concentrations, the REE concentrations were corrected using the percent that sulfate deviated from expected conservative behavior; this is seen in Figures 3-11, 3-12, and 3-13.

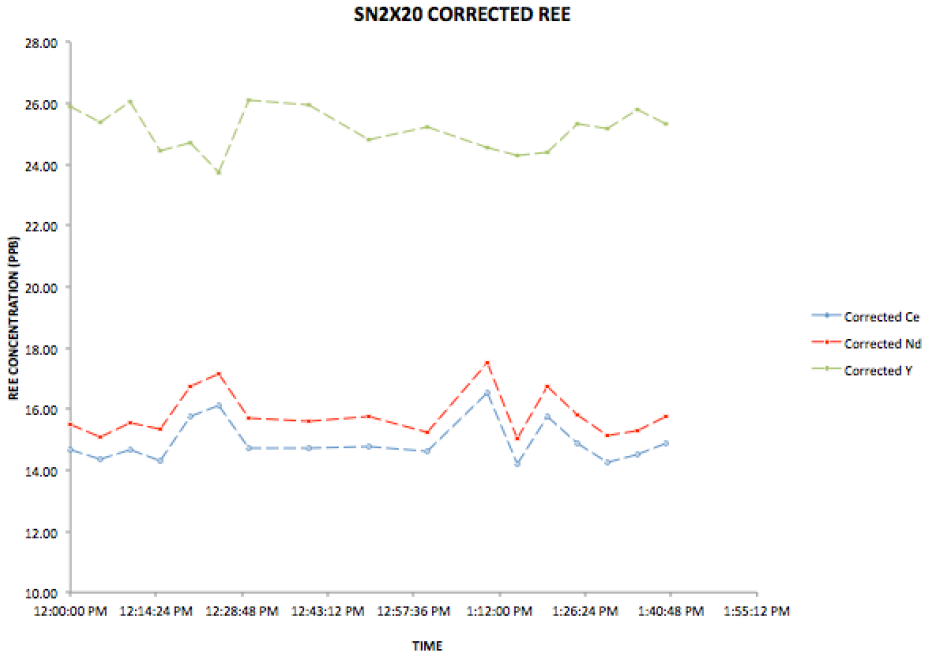


**Figure 3-11 Sulfate Corrected REE concentrations (ppb) of sampling site SN2X20 over duration of tracer injection**

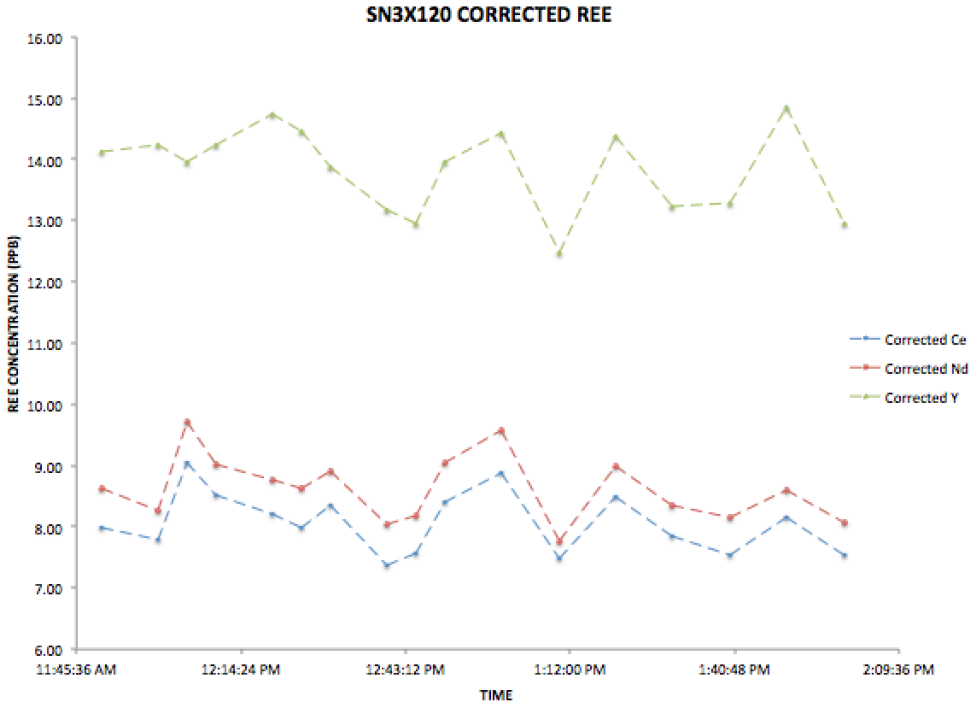


**Figure 3-12 Sulfate corrected REE concentration (ppb) at site SN3X120 over duration of tracer injection**

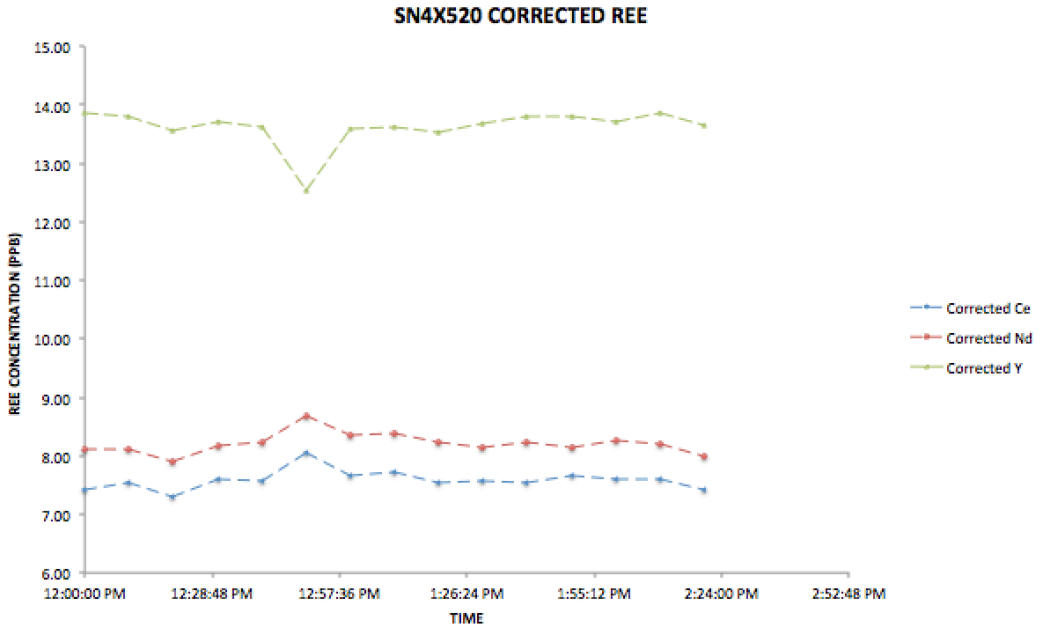


**Figure 3-13 Sulfate corrected REE concentrations (ppb) at sampling site SN4X520 over duration of tracer injection**

The conservative nature of REEs is further explored through direct correlation with sulfate concentrations. Generally in the Snake River, sulfate should vary little within each reach. Large fluctuations as seen in this tracer injection suggest sampling of less sulfate concentrated waters. The sulfate ratios used to correct lithium and chloride data were used to increase the minima displayed in REE concentration profiles. REE data is plotted against sulfate and can be seen in Figures 3-14, 3-15, and 3-16. The slope of each REE's trendline is very low, at each site, which supports Ce, Nd, and Y's conservative nature.

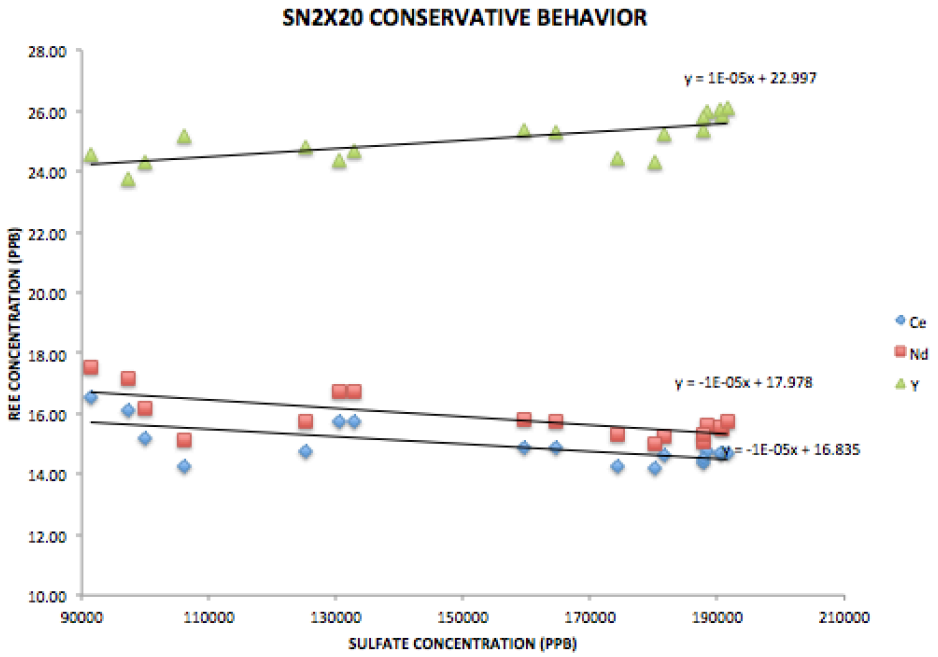


**Figure 3-14 Corrected REE concentrations (ppb) in relation to sulfate at SN2X20**

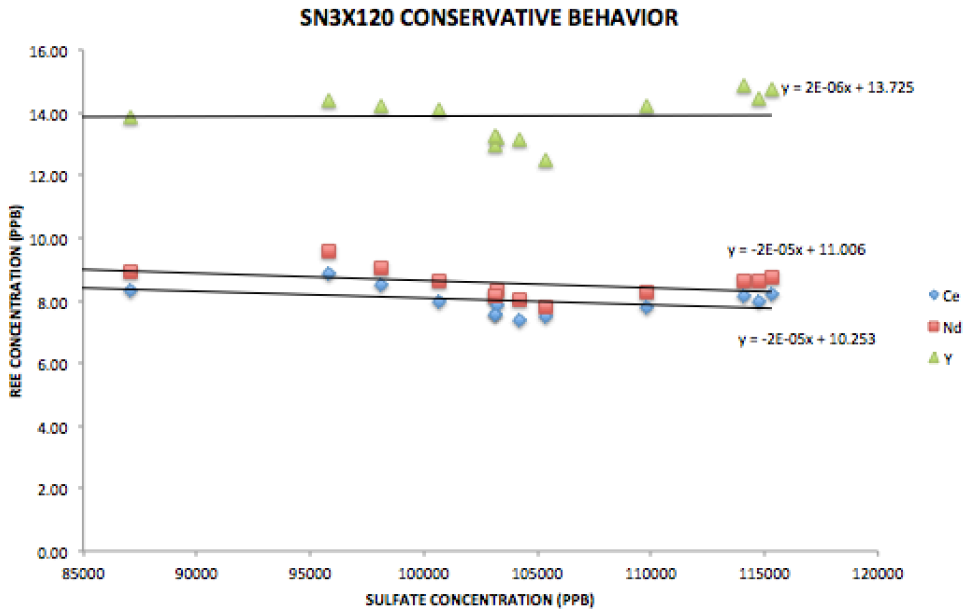


**Figure 3-15 Corrected REEs in relation to sulfate at SN3X120**

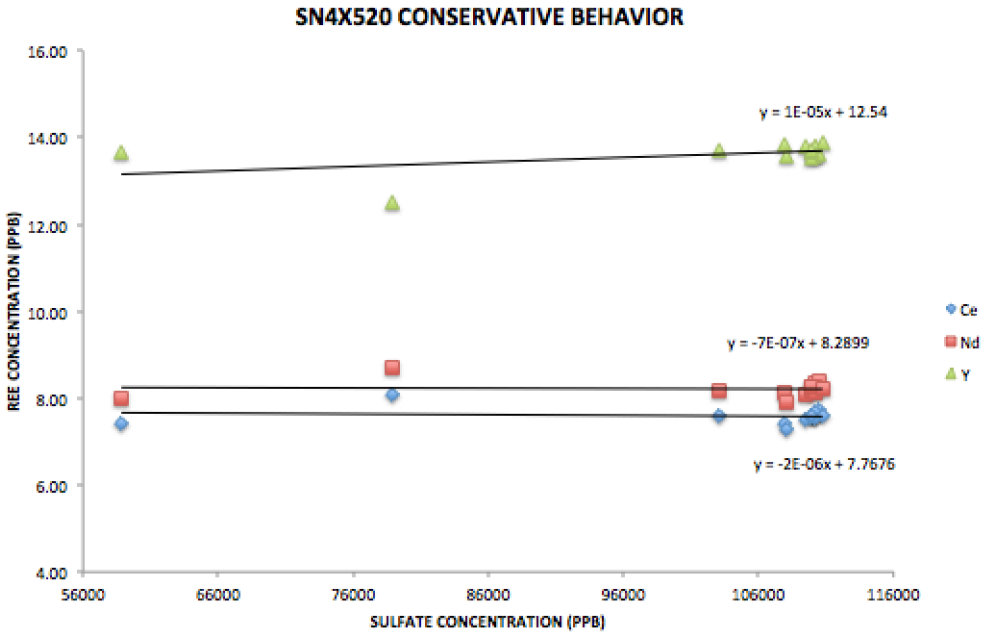


**Figure 3-16 Corrected REEs in relation to sulfate at SN4X520**

*3.6.5 Breakthrough Curve (BTC): Model Parameters*

The results of the tracer injection were modeled using OTIS based upon experimental Li and chloride Cl concentrations. Due to time restrictions in the field, sites below SN4X520 were not modeled, as the conservative tracer, LiCl, did not plateau and/or complete its descending limb in the allotted time for sampling.

In order to model and optimize the experimental data, smoothing had to be done to the plateau of the BTCs. Data collected at SN2X20 reflected sporadically sampled Deer Creek water, as seen in the raw breakthrough curve's (shown by solid line in Figure 3-17) oscillating plateau. The raw BTC (Figure 3-18) of SN3X120 also exhibits an oscillating plateau, which is most likely explained by close proximity to the Snake River-Deer Creek confluence. The dilution effect provided by Deer Creek's pristine inflow is generally about twofold. The BTC for SN4X520 (Figure 3-19) has a stable plateau, as it is far enough downstream to result in complete mixing of Snake River-Deer Creek water. Also, it should be noted that there was no significant inflow from SN3X120 to SN4X520.

In order to correct for oscillation of the SN2X20 and SN3120 plateaus, correction ratios were developed using the conservative behavior of sulfate and further applied to increase the minima within the Li BTCs. Given the assumption that sulfate concentration should vary little due to conservative nature, except in times of sampling error or changes in flow rate, the percent difference between the highest initial sulfate concentration of the plateau (within each reach) and the minimum of interest was determined. Then, this percent difference was applied

to the Li and Cl increasing the minima concentrations. This accounted for dilution effects and ultimately smoothed the plateau. The observed and corrected $Li^+$ breakthrough curves can be seen in Figures 3-17, 3-18 and 3-19 with sulfate included for comparison.


**Figure 3-17. Observed lithium BTCS shown with corrected BTCs and sulfate comparison at SN2X20**

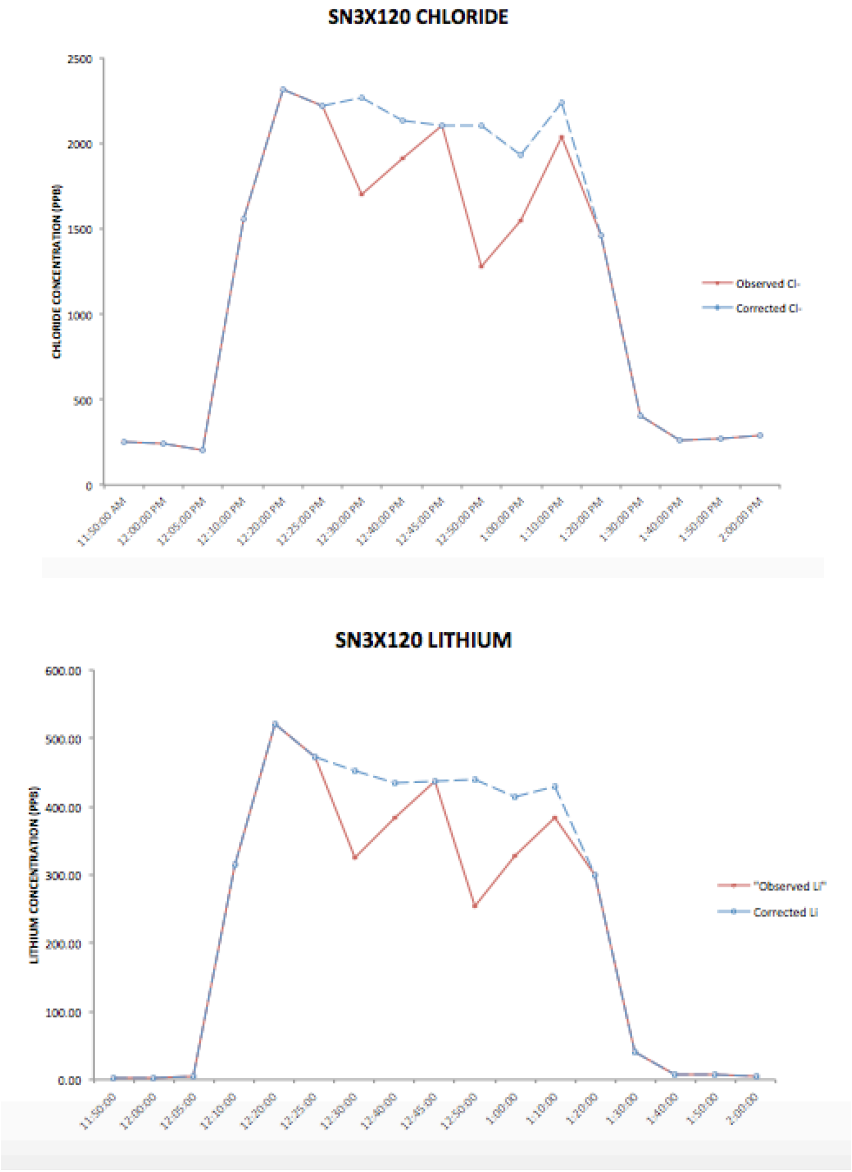


**Figure 3-18. Observed lithium BTCS shown with corrected BTCs and sulfate comparison at SN3X120**

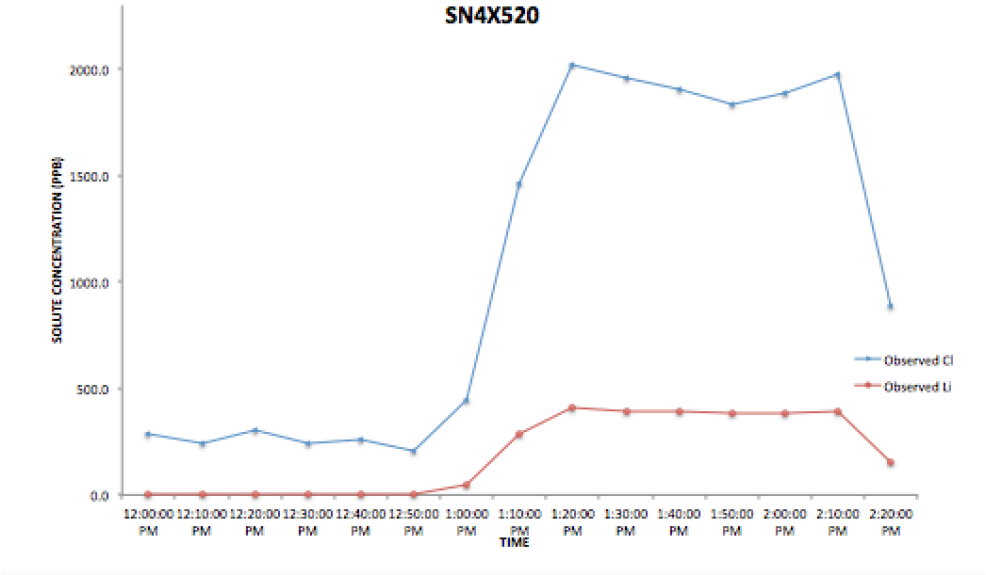


**Figure 3-19. Observed lithium BTCS shown with corrected BTCs and sulfate comparison at SN4X520**

In order to calculate each reach's flow rate (Q), averages of the corrected BTC concentrations were used, and are as follows: SN2X20 = 886 ppb, SN3X100 = 450 ppb; SN4X400 = 393 ppb.

Original parameters were estimated using field measurements discharge measurements with pygmy meters, and BTC analysis. The estimated parameters for lithium and chloride, respectively, are shown below:

**Table 3-1. Original field measurements of solute transport parameters**

Li+

| Reach | Distance from x = 0 m | Reach Length (m) | Q ($m^3/s$) | Q ($m^3/s$) (with pygmy) | $q_{Lin}$ ($m^2$/sec) | Travel time (sec) | Velocity (m/s) | A ($m^2$) |
|---|---|---|---|---|---|---|---|---|
| 1 (SN2-> Conf) | 20 | 20 | 0.06 | 0.03 | 0.00 | 60 | 0.33 | 0.18 |
| 2 (Conf-> SN3) | 140 | 100 | 0.12 | 0.09 | 0.00 | 420 | 0.33 | 0.36 |
| 3 (SN3->SN4) | 560 | 400 | 0.13 | 0.09 | 0.00E+00 | 4200 | 0.10 | 1.37 |
| 4 (SN4-> DSBC) | 2720 | 2000 | 0.13 | N/A | 0.00 | 20,000 | 0.10 | 1.30 |

Cl-

| Reach | Distance from x = 0 m | Reach Length (m) | Q ($m^3/s$) | Q ($m^3/s$) (with pygmy) | $q_{Lin}$ ($m^2$/sec) | Travel time (sec) | Velocity (m/s) | A ($m^2$) |
|---|---|---|---|---|---|---|---|---|
| 1 (SN2-> Conf) | 20 | 20 | 0.07 | 0.03 | 0.00 | 60 | 0.33 | 0.21 |
| 2 (Conf-> SN3) | 140 | 100 | 0.14 | N/A | 0.000 | 420 | 0.33 | 0.42 |
| 3 (SN3->SN4) | 560 | 400 | 0.16 | 0.09 | 5.00E-05 | 4200 | 0.10 | 1.68 |
| 4 (SN4-> DSBC) | 2720 | 2000 | 0.16 | N/A | 0.00 | 20,000 | 0.10 | 1.60 |

Original parameters were calculated for the previously defined five reaches; however only reaches 1, 3 and 4 were individually modeled due to issues with fitting the Li corrected plateaus. For example, instead of using reach 2 to reflect the Deer Creek tributary, reach 3 was adjusted to include Deer Creek as lateral inflow. Reaches were defined based on expected hydrological fluxes, and coincided with pre-determined sampling sites. The user-defined reaches are as follows: SN2X20 (x = < 20 m downstream from injection point), SN3X120 (x =120 m downstream) and SN4X520 (x = 520 m). The reach lengths were approximated using Google Earth. The closest site to the injection point, SN2X20, is an estimation of the characteristics delineating the Snake River's upper reaches. Farther downstream, another 95-100 m is SN3X120, which also encompasses inflows from both the headwaters of the Snake River and the pristine Deer Creek. Approximately 400 m farther downstream is site SN4X520, which could reflect parameters extending to the rest of the Snake River, or at least until metal-enriched inflow from Peru Creek. Also, it should be noted that the pygmy meter discharge measurements underrepresented the flow at SN2X20 and SN3X120, possibly due to

measurements being taken in areas lower than the sampling site with more narrow or shallow channels.

In order to calculate the remaining parameters (Q, $q_{lin}$, A, and the travel time), the sulfate corrected plateau values were averaged to obtain a single plateau concentration. This removed the smaller fluctuation caused by dilution and/or incomplete mixing leaving a single value. It is important to establish a firm plateau before modeling as this plateau concentration incorporates not only the solute moving through the main channel, but also the streambed and fluctuations arising from changing direction and unsteady velocity distributions that occur naturally within the bed material and boundary layer (Bencala, et al., 1990).

The flow rate (Q) was calculated using the tracer-dilution method and confirmed using pygmy meter discharge. The discharge measurements taken from the pygmy meter were within reason of those calculated using the BTCs providing confidence in using the more consistent discharge from each site's BTC. Q and $q_{lin}$ were calculated using the following equations, respectively:

$$\mathbf{Q_1=(Q_{inj}C_{inj})/(C_l-C_b)} \qquad \mathbf{(3\text{-}5)}$$

$$\mathbf{q_{lini}=(Q_i-Q_{i-1})/L} \qquad \mathbf{(3\text{-}6)}$$

where $C_l$ = concentration of solute at plateau (ppm), $C_b$ = concentration of solute in background (ppm). The travel time (sec) was estimated using the BTC, and defined as the time for the tracer to reach 50% of its plateau concentration. The velocity (m/s) was calculated as the distance

(x=0) divided by the travel time (m/s). Finally, the main channel area (A ($m^2$)) was calculated by dividing the reach's averaged discharge by the area.

The upstream boundary conditions (U.S.B.C.), designated as distance "0 m", were defined using SN2X20 parameters as there were no significant variations in hydrological parameters from x = 0 to 20 m. It should be noted that there is a moderate wetland between SN2X20 and Deer Creek. Being within 50 m of each other, the streams exhibited varying lateral fluxes, hyporheic exchange and storage. The U.S.B.C.s (used for lithium) are shown below

**Table 3-2. USBCS for Simulations**

| Q ($m^3$/s) | $C_B$ (ppm) | $C_P$ (ppm) |
|---|---|---|
| 0.06 | 1-6 | 886.2 |

$C_B$ refers to the background lithium concentration prior to injection, and $C_p$ is the lithium plateau concentration. Although the flow varied spatially at upper reaches and temporally within the Snake River, the upstream boundary conditions were modified to reflect steady-state flow.

*3.6.5 Model Results*

The calculations of the solute transport parameters using field data, per reach, were estimated using trial-and error. This was done by first manually changing the area to match the timing of

the rising limb of the observed BTC, and further confirmed using a visual best fit; the final parameter estimates for Li are shown in the table below:

**Table 3-3. Calculated Lithium Transport Parameters from Trial-and-Error and Visual Best Fi**

Parameters optimized for lithium

| Reach | Distance from x = 0 m | Reach Length (m) | Stream Cross Sectional Area, A ($m^2$) | Storage Area ($A_s$) ($m^2$) | $q_{Lin}$ ($m^2$/sec) | Dispersion Coefficient D ($m^2$/s) | Exchange Coefficient α (1/s) | $A_s$/A |
|---|---|---|---|---|---|---|---|---|
| 1 (SN2-> Conf) | 20 | 20 | 0.17 | 1.00E-03 | 0.00 | 1.34 | 1.00E-04 | 0.01 |
| 2 (Conf-> SN3) | 120 | 100 | 0.17 | 3.30E-02 | 6.27E-04 | 0.98 | 1.00E-04 | 0.19 |
| 3 (SN3->SN4) | 540 | 400 | 1.19 | 2.40E-02 | 2.50E-05 | 0.09 | 1.00E-04 | 0.02 |

The upper reaches contained the highest dispersion coefficients, and smaller areas as compared to the lower reach SN4X520. The simulated Li breakthrough results are shown in Figure 3-20.

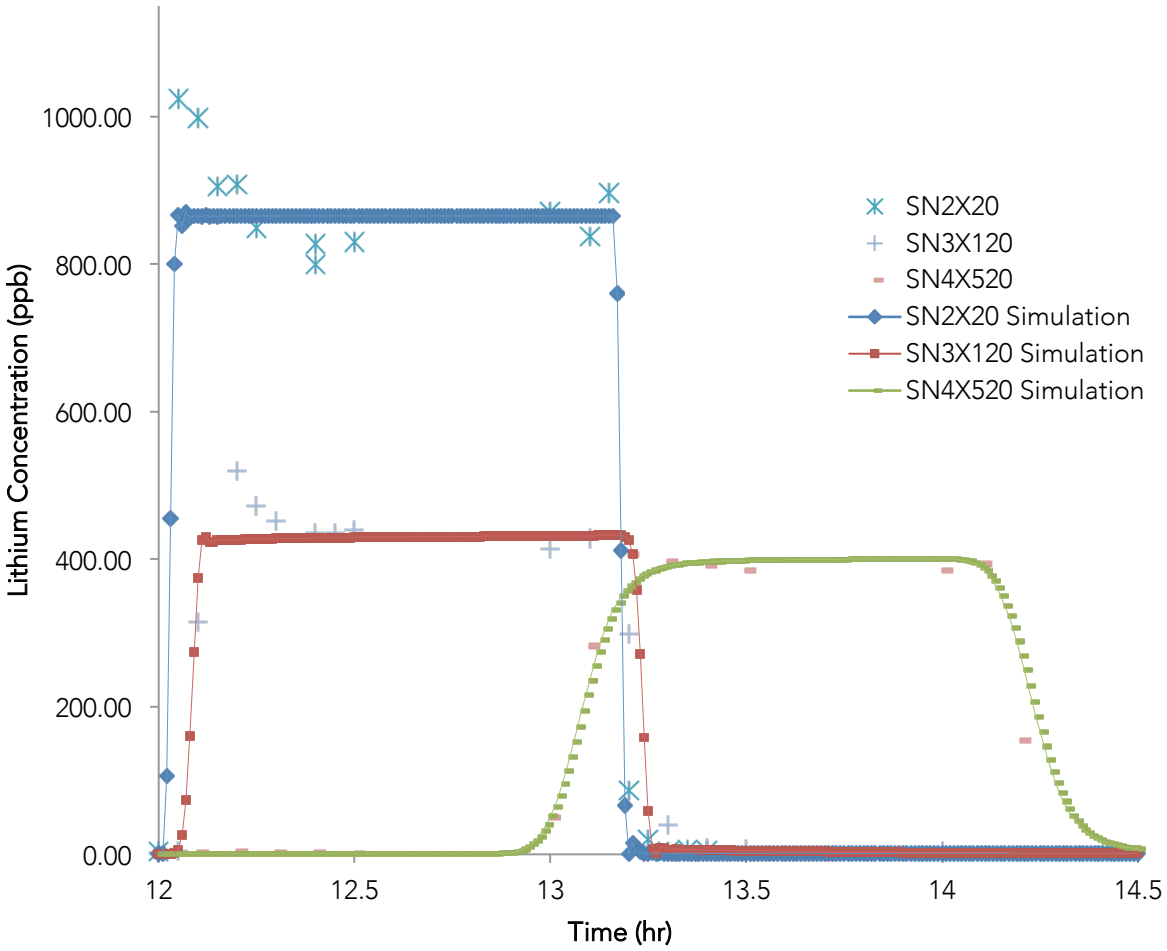


**Figure 3-20. Observed and simulated Li BTC at SN2X20, SN3X120, and SN4X520; sulfate corrected values are expressed as point values, and simulations seen as line**

The simulated values deviate the most from observed values in the upper reaches.

*3.6.6 Storage Zone*

In order to distinguish the degree to which the storage zone impacts the solute dynamics of each reach, $F_{med}$ and $A_s/A$ were calculated; shown in Table 3-5. $F_{med}$ is a metric developed by Runkel (2002) to understand temporal transport within the transient storage zone. $F_{med}$ is a

function of u, $A_s$, and α, thus provides a median travel time with respect to storage (Runkel, 2002). The equation is shown below (Runkel, 2002):

$$F_{med} \cong (1 - e^{-L(\alpha/u)}) \frac{A_S}{A + A_S}$$

where L represents the average reach length, set to 200 m (Runkel 2002) and u represents the advective velocity (Q/A). A high $F_{med}$ indicates a storage zone having significant effect on solute transport, and a low $F_{med}$ indicates storage zone have little effect on downstream transport (Runkel, 2002). $A_s/A$ determines the physical size of the storage zone relative to the main channel; the larger the value, the larger the storage zone relative to the main channel. Table 3-4 shows calculations for $A_s/A$ and $F_{med}^{200}$ :

**Table 3-4. $A_s/A$ and $F_{med}^{200}$ calculated values using estimated parameters**

| Reach | Discharge Q (m3/s) | Advective Velocity u (m/s) | $A_s/A$ | $F_{med}^{200}$ |
|---|---|---|---|---|
| 1 (SN2-> Conf) | 0.06 | 0.35 | 0.01 | 3.22E-04 |
| 2 (Conf-> SN3) | 0.12 | 0.71 | 0.19 | 4.54E-03 |
| 3 (SN3->SN4) | 0.13 | 0.11 | 0.02 | 3.31E-03 |

$F_{med}^{200}$ increases downstream to the Snake River – Deer Creek confluence, and then decreases slightly at the third reach.

*3.7 Discussion*

*3.7.1 pH*

One of the most influential variables affecting solute transport is pH. The pH of the system increases overall due to downstream flow contributions. The pH is low in the headwaters as this is where the majority of exposed pyrite is weathered producing low pH water. The pH controls the rates of biogeochemical reactions such as the role of ferrous oxidizing bacteria, as well as hydroxide and oxyhydroxide formation and precipitation. Fe and Al are the primary metals precipitating out in this system. Fe precipitates at pH > 3, and Al precipitates at pH > 4. The pH values of the simulated reaches (SN2X20 to SN4X520) are slightly below the Al precipitation and slightly above the Fe precipitation thresholds suggesting that the freshly produced Al-hydroxides and Fe-hydroxides create an environment where sorption of REEs could occur. The models created using OTIS define the general advection-dispersion parameters under conservative behavior. The model based upon lithium transport calculations, does not account for precipitation and therefore variance in Fe transport relative to the A-D model can be explained by sorption, redox reactions and other chemical reactions.

### *3.7.2 Sulfate*

Sulfate fluctuated significantly indicating intermediate sampling of Deer Creek at SN2X20. It should be noted that there is little observable inflow to SN4X520; these drops in sulfate concentration could indicate sampling a portion of the stream that inadequately reflects the channel's water chemistry.

### *3.7.3 Metal Transport and Behavior*

#### *3.7.3.1 Reactive Metal Transport*

The pH and metal concentration have an inverse relationship; as the pH increases, more reactive metals will decrease due to precipitation, co-precipitation, complexation and sorption. As previously mentioned, hydroxides of ferric iron precipitate at pH > 3.5. In the presence of oxygen, ferrous ions oxidize to ferric ions creating Iron (III) hydroxides as seen by orange-yellow precipitate known as 'yellow boy' at pH > 3.0. Al hydroxides precipitate at pH > 5.0, and then dissolves at pH > 9. Precipitation of manganese (Mn) generally occurs between pH 9.0 and 9.5.

The more reactive metals generally prone to redox, precipitation and sorption reactions such as iron are shown to display substantial fluctuations in concentrations at SN2X20 and SN3X120. After comparing the iron behavior with relatively conservative solutes such as sulfate, similar patterns of fluctuating concentrations were seen. The same patterns were also seen with Li, Cl, Al, and the REEs. These similarities would suggest sporadic sampling of the Deer Creek confluence (McKnight) in which concentrations of these metals are much lower. This could also indicate a high exchange rate between the hyporheic zone and main channel at SNX20.

*3.7.3.2 REE Transport*

The concentration of rare earth elements depends on the following: release due to weathering and erosion, pH and redox potential of the main channel and groundwater, adsorption, complexing ligands and varying flow paths and transient storage. The increased acidity resulting from acid mine drainage significantly effects the rare earth element behavior with concentration exhibiting an inverse relationship with pH (Goldstein and Jacobson, 1987; Johannesson, 2005).

As the pH of the Snake River increased downstream, the REE averaged concentrations decreased coinciding with the REEs with stronger sorption characteristics. The light REEs are, on average, more likely to be scavenged through sorption mechanisms as compared to heavier REEs (Johannesson, 2005). The concentrations of REEs displayed similar fluctuations as the more conservative solutes Cu and Zn, as shown by Figures 3-3 and 3-4, suggesting REEs can behave conservatively at higher pH. The iron concentrations in Figure 3-8 parallel the fluctuations of REE concentrations in Figures 3-9, 3-12, and 3-15. However, once effects of Deer Creek exchange were removed, through sulfate corrections, the rare earth elements varied little and closely resembled characteristics of other conservative solutes (Li, Cl, and sulfate). This conservative nature confirms previous studies in that REEs are generally conservative below pH of 6.0.

*3.7.4 Breakthrough Curve (BTC) Analysis*

Both Li and Cl are considered conservative ions (Bencala et al., 1990). However, due to Li's high solubility and low background concentration, the parameters were determined using Li BTCs and further used to define Fe transport and REE behavior. Also, Li was capable of quantifying flow more closely to values calculated using pygmy measurements (Table 3-1). For the purpose of this model, Li is assumed to be subject to the following four processes: advection, dispersion, lateral inflow, and transient storage. In general, Li concentration should exhibit little variation. However, oscillation of concentration was observed. The low points of the oscillating plateau reflect times in which very pristine waters were sampled. Sampling sites SN2X20 and Deer

Creek were within the confluence zone and it is likely that these sporadic minima reflected parcels of Deer Creek inflow and exchange.

Calculated parameters were compared to a previous LiCl injection study conducted by Bencala et al., 1990. Bencala (1990) provides an overview of a lithium tracer study conducted in 1983 which encompasses the sites used within this study (SN2X20, SN3X120, and SN4X520). Variations among the parameters obtained in this study and those of the 1983 study could be contributed to the variance in defined reach length and higher flow. The parameters are seen below:

**Table 3-5.** Parameters obtained from Bencala et al., 1990

Parameters obtained from Bencala et al., 1990

| Reach | Stream Cross Sectional Area, A ($m^2$) | Storage Area ($A_s$) ($m^2$) | $q_{Lin}$ ($m^2$/sec) | Dispersion Coefficient D ($m^2$/s) | Exchange Coefficient **α** (1/s) | $A_s$/A |
|---|---|---|---|---|---|---|
| 1605-2845 m (SN2X20) | 0.7 | 0.12 | 2.80E-05 | 0.2 | 2.00E-04 | 0.17 |
| 2913-3912 m (SN3X120) | 1.08 | 0.05 | 1.76E-04 | 0.2 | 5.00E-05 | 0.05 |
| 3912-3889 m (SN4X520) | 1.21 | 0.05 | 4.30E-05 | 0.2 | 5.00E-05 | 0.04 |

Parameters from Bencala et al. were also used to ensure reasonable parameters were calculated for the Snake River. Variance could be attributed to temporal change and the installation of a second culvert under Montezuma Road.

*3.7.4.a Storage Zone and Exchange Rate*

The storage zone, defined per reach, can play an important role in solute transport in streams. There are a number of transient storage mechanisms, but for the purpose of this study, transient storage is generally seen in the form of turbulent eddies, large but slowly recirculating zones along the sides of the pools, side pockets and the hyporheic zone (Harvey et al., 2012). In general, OTIS identifies the storage zone as being the stream subsurface and calculates solute concentrations based on exchange between the main channel and the hyporheic zone. Hyporheic exchange (HE) is the exchange of water between the main channel (at least 10%) and the storage zone; HE is often difficult to quantify as there are many routes for water to travel, generally re-entering the stream at some arbitrary point downstream (Harvey et al., 2012). Also, pool-riffle sequences and stream meandering can encourage hyporheic exchange.

The reach between the injection site to the upper Snake River (SN2X20) sampling site contains several pool-riffle sequences, where the lower sampling sites may be influenced by more intense meandering patterns. The main channel area increased downstream in concurrence with a decreasing slope. As main channel area (A) increased and stream slope decreased downstream, the area of transient storage increased to 0.033 $m^2$ below the Snake River-Deer Creek wetland, and then decreased to 0.024 $m^2$ upon reaching SN4X520, presumably due to decreasing influence of pool-riffle sequences and turbulence from tributary inflow.

The $A_s/A$ increases downstream to SN3X120, and then decreases throughout the SN4X520 reach. The increasing values of $A_s/A$ and $F_{med}$ downstream indicate the storage zone having greater significance downstream. The primary process is most likely hyporheic exchange

throughout SN3X120. This could be due to close proximity to the influential confluence area. The larger the storage zone, the longer the residence time for solute transport as dissolved metals can remain trapped in the slower moving storage or removed all together to only re-enter at an arbitrary point downstream.

The exchange rates (α), of this study, shown in Table 3-3, were chosen based upon typically seen exchange coefficients of high gradient streams. For this study, the exchange coefficients were kept constant, however, higher exchange rates could counteract the longer residence time provided by increased storage zone. The flow variables will change seasonally in this snowmelt driven system, and thus the underlying mechanisms defining transient storage vary temporally. These areas and exchange rates could be useful in defining the high-moderate gradient alpine streams during low flow conditions, post-snowmelt.

*3.7.4 b. Main Channel Flow and Lateral Inflows*

The main channel flow rates remained relatively constant throughout the Snake River, experiencing influences of nearly equivalent flow from Deer Creek and Peru Creek. However, the lateral inflows of each defined reach are not limited to the inflow from confluences, but encompass other sources of overland flow, interflow, and ground-water discharge. For this system, the model accounts for the Deer Creek overland flow averaged over 20 m, and lateral inflow between SN3X120 and SN4X520 taken as the difference in flow between each reach averaged over reach length. Also, the plateau concentration of the breakthrough curves decreased downstream, indicating dilution by lateral inflow. The largest difference in plateau

concentrations occurred between SN2X20 and SN3X120, highlighting the strong dilution effect of Deer Creek. Also, there was no significant inflow between SN3X120 and SN4X520

*3.7.4 c. Dispersion Coefficient*

The dispersion coefficient (D) provides insight into the degree of solute mixing within the main channel (Runkel, 1998). It should be noted that the lower resolution of the ascending and descending limbs of the obtained BTCS provide less confidence in dispersion coefficients. Comparing the coefficients to Bencala (1990) allowed for higher confidence in this model's calculation of reasonable values.

In general, the farther downstream a solute travels, the more spread out it becomes creating a broader and more uniform spatial profile. The dispersion behavior is also quantified in the direction of flow as OTIS assumes dispersion only occurs in the longitudinal direction with negligible variation in width and depth. The model for this system shows the highest level of dispersion occurring at SN2X20 and significantly decreasing in downstream sites shown in Table 3-3. The dispersion coefficients for this particular study were on average somewhat higher than those typically seen in high gradient streams and vary from values obtained in previous years (Bencala, et al., 1990). The optimized dispersion values of this experiment increased by 80% at SN2X20, increased by 74% at SN3X120 and decreased by 55% as compared to the similarly defined reaches in the 1983 Bencala et al. tracer injection. The contrast between these estimated parameters could be contributed to the smaller reach length outlined in this study of

which incorporates a smaller segment with more turbulence and less water chemistry variations.

Dispersion can also be quantified using the relative width of the simulated BTCs. A system with a wider BTC, will exhibit a higher degree of dispersion, where as systems with more uniform BTC will exhibit a lower degree of dispersion. It is estimated that SN2X20 and SN3X120 contain the widest BTC, which supports the model's higher dispersion coefficients; however, the resolution of data defining the ascending and descending limbs are low which introduces some uncertainty.

# CHAPTER 4:

# CONCLUSIONS

## *4.1 Conclusion*

In conclusion, AMD is mobilizing REEs as shown by higher concentrations in affected sites relative to pristine sites. Transport behavior of REEs shown to be relatively conservative at low pH (< 6) with solution chemistry playing a major role retarding scavenging mechanisms at low pH. As pH increases downstream (> 5), lower percent of Al and Fe in dissolved phase and variable percent in colloidal and particulate phases. Also, as pH increases, there is a higher degree of fractionation of REEs into colloidal and particulate phase.

Using sulfate corrections, solutes with conservative behavior can be identified. After corrections, Li, Cl and the rare earth metals showed little variation over duration of tracer suggesting conservative behavior at the confluence and farther downstream.

## *4.2 Future Work*

In order to develop a more accurate geochemical model of REE behavior, dissolved organic matter (DOM) should be considered. Previous studies suggest fractionation of REE is heavily influenced by the presence of humic acids (HA) (Rue, 2015). McKnight et al. (1992) found that humic acids are preferentially sorbed to Al and Fe hydroxides and oxides. The introduction of HA into the analysis may alter the scope of REE behavior due to competition of binding sites on

metal hydroxides with the weak carboxylic acid sites. As pH influences the availability of HA binding sites, this could provide another dimension explaining REE enrichment of lack thereof. Also, pH perturbation could provide greater modeling capacity to evaluate the effectiveness of remediation and possibility of selective recovery of metals. Slowly increasing the pH > 8.0 of the system through the use of a base such as sodium hydroxide could provide insight into the efficiency of REE and trace metal removal that result from using active remediation techniques.

*Literature Cited*

Allison, J. D., Brown, D. S. & Novo-Gradac, K. J. (1991) M1NTEQA2/PRODEFA2, and A geochemical assessment model for environmental systems: Version 3.0 User's Manual. Report EPA/600/3-91/021, US Environ. Prot. Agency, Washington, DC.

Akcil, A. & Koldas, S., (2006). Acid Mine Drainage (AMD): causes, treatment and case studies. *Journal of Cleaner Production*, 14(12–13 SPEC. ISS.), pp.1139–1145.

Balistrieri, B.L.S. et al., 1998. Chapter 6 — Impacts of historical mining in the Coeur d ' Alene River Basin.

Belanger, L. "Source and effect of acid rock drainage in the Snake River Watershed, Summit County, Colorado." (2002)

Bencala, K.E., McKnight, D.M. and Zellweger, G.W., (1990). Characterization of transport in an acidic and metal-rich mountain stream based on a lithium tracer injection and simulations of transient storage. Water Resources Research, 26(5), 989- 1000.

Bencala, K. E., and R. A. Walters, (1983) Simulation of solute transport in a mountain pool-and-riffle stream: A transient storage model, Water Resour. Res., 19, 718 – 724

Bencala, K.E., McKnight, D.M., Zellweger, G.W., and Goad, Julie, (1986), The stability of rhodamine WT dye in trial studies of solute transport in an acidic and metalrich stream: in Subitzky, Seymour, ed., Selected papers in the hydrologic sciences: U.S. Geological Survey Water-Supply Paper 2310, p. 87-95.

Bencala K. E. and McKnight D. M. (1987) Identifying instream variability: Sampling iron in an acidic stream. In Chemical Quality of Water and the Hydrologic Cycle (eds R. C. Averett and D. M. McKnight), pp. 255-269. Lewis Publishers, London.

Benner, S.G. et al., (1999). Geochemistry of a permeable reactive barrier for metals and acid mine drainage. *Environmental Science and Technology*, 33(16), pp.2793– 2799.

Bau, M., (1999). Scavenging of dissolved yttrium and rare earths by precipitating ironhydroxide: experimental evidence for Ce oxidation, Y–Ho fractionation, andlanthanide tetrad effect. Geochim. Cosmochim. Acta 63, 67

Boyer, Elizabeth W., et al. (1997): "Response characteristics of DOC flushing in an alpine catchment." *Hydrological processes* 11.12 :1635-1647.

Brooks, P. D., McKnight, D. M., & Bencala, K. E. (2001). *Annual maxima in Zn concentrations during spring snowmelt in streams impacted by mine drainage*. *Environmental Geology*, *40* (11-12), 1447-1454. DOI: 10.1007/s002540100338

Bau, M., 1999. Scavenging of dissolved yttrium and rare earths by precipitating iron oxyhydroxide: experimental evidence for Ce oxidation, Y-Ho fractionation, and lanthanide tetrad effect. Geochimica et Cosmochimica Acta 63, 67–77.

Broshears, R.E. et al., (1996). Reactive solute transport in an acidic stream: Experimental pH increase and simulation of controls on pH, aluminum, and iron. *Environmental Science and Technology*, 30(10), pp. 3016–3024.

Byrne R. H. and Sholkovitz E. R. (1996) Marine chemistry and geochemistry of the lanthanides. In Handbook on the Physics and Chemistry of Rare Earths, Vol. 23 (eds. K. A. Gschneidner Jr. and L. Eyring), pp. 497-593. Elsevier, Amsterdam.

Chapman, B.M., Jones, D.R., and Jung, R.F., (1983), Processes controlling metal ion attenuation in acid mine drainage streams: Geochimica et Cosmochimica Acta, v. 47, pp. 1957–1973.

Clow, D., (2010): Changes in the Timing of Snowmelt and Streamflow in Colorado: A Response to Recent Warming. J. Climate, 23, 2293–2306, doi: 10.1175/2009JCLI2951.1.

Colorado Department of Public Health and Environment Water Quality Control, 2008: 5 CCR 1002-93 Regulation # 93 Section 303(d) List Water-Quality-Limited Segments Requiring TMDLs. Available at: http://www.cdphe.state.co.us/regulations/wqccregs/100293wqlimitedsegtmdls.pdf

Colorado Mining Water Quality Task Force (1997) Report and recommendations regarding water quality impacts from abandoned or inactive mined lands, Department of Public Health and Environment. http://www.cdphe.state.co.us/op/wqcc/MWQTFreportword.PDF, last accessed February 14,

Crouch, Caitlin M., (2011) Hydrologic Change on Geochemistry in the Upper Snake River, a High Mountain Acid Rock Drainage Stream, ProQuest Dissertations Publishing

Crouch, C. M., McKnight, D. M., & Todd, A. S., (2013). Quantifying sources of increasing zinc from acid rock drainage in an alpine catchment under a changing hydrologic regime. *Hydrological Processes*. DOI: 10.1002/hyp.9650

DeBaar, H. J. W., Schijf, J., and Byrne, R. H. (1991) Solution chemistry of the rare earth elements in seawater. Euro. J. Chem. 28, 357-373.

De Carlo E. H., Resing J. A., Wen X. Y., and Cowen J. P. (1996) Rare earth elements in water samples collected over Loihi seamount during the August 1996 seismic event. Eos 77, 398.

De Carlo E. H., Wen X.-Y. and Irving M. (1998) The influence of redox reactions on the uptake of dissolved Ce by suspended Fe and Mn oxide particles. Aquat. Geochem. 3, 357– 389.

De Carlo, E.H., Wen X.Y., Cowen, J.P., (2000). Rare earth element fractionation in hydrogenetic Fe–Mn crusts: the influence of carbonate complexation and phosphatization on Sm/Yb ratios C.R Glenn, L. Prevot-Lucas, J. Lucas (Eds.), Marine Authigenesis: From Global to Micobial, 66, Society for Sedimentary Geology Special Publication, pp. 271–285

Dettinger, M.D., and D.R. Cayan, (1995): Large-scale atmospheric forcing of recent trends toward early snowmelt runoff in California. J. of Clim., 8, 606-623. (32)

Dupre, B., Gaillardet, J., Rousseau, D., Allegre, C.J., (1996). Major and trace elements of river-borne material: the Congo basin. Geochim. Cosmochim. Acta 96, 1301– 1321.

Dutta, T. et al., 2016. Global demand for rare earth resources and strategies for green mining. *Environmental Research*, 150, pp.182–190. Available at: http://dx.doi.org/10.1016/j.envres.2016.05.052.

Dzombak, D.A., and Morel, F.M.M., (1990), Surface complexation modeling—hydrous ferric oxide: John Wiley and Sons, New York, 393 pp.

Elderfield, J., Upstill-Goddard, R., Sholkovitz, E.R., (1990). The rare earth elements inrivers, estuaries and coastal seas and their significance to the composition ofocean waters. *Geochem*. Cosmochim. Acta 54, 971–991.

Folland C.K., Karl T.R., Christy J.R., Clarke R.A., Gruza G.V., Jouzel J, Mann M.E., Oerlemans J.,Salinger M.J., Wang S.W. (2001). Observed climate variability and change. In Climate Change 2001: The Scientific Basis, Houghton JT, Ding Y, Griggs DJ, Noguer M, van der Linder PJ,Dai X, Maskell K, Johnson CA (eds). Cambridge Univ. Press: Cambridge; 99–181.

Gleick, P.H., (2016). Water strategies for the next administration. *Science*, 354(6312).

Goldstein, S.J., Jacobsen, S.B., (1988). Rare earth elements in river waters. *Earth Planet.Sci*. Lett. 89, 35–47.

Hansen, J., M. Sato, R. Ruedy, K. Lo, D.W. Lea, and M. Medina-Elizade, (2006): Global temperature change. *Proc. Natl. Acad. Sci.*, 103, 14288-14293, doi:10.1073/pnas.0606291103.

Harvey, J. W., and K. E. Bencala (1993), The Effect of streambed topography on surface-subsurface water exchange in mountain catchments, Water Resour. Res., 29(1), 89–98, doi:10.1029/92WR01960.

Harvey, J. W., B. J. Wagner, and K. E. Bencala, (1996) Evaluating the reliability of the stream tracer approach to characterize stream-subsurface water exchange, Water Resour. Res., 32(8), 2441 – 2451

Harvey, J. W., Drummond, J. D., Martin, R., McPhillips, L. E., Packman, A. I., Jerolmack, D. J., Stonedahl, S. H., Aubeneau, A. F., Sawyer, A. H., Larsen, L. G., & Tobias, C. R. (2012). Hydrogeomorphology of the Hyporheic Zone: Stream Solute and Fine Particle Interactions With a Dynamic Streambed. Journal of Geophysical Research: Biogeosciences, 117 (G4), G00N11-. http://dx.doi.org/ 10.1029/2012JG002043

Haxel, Gordon B., James B. Hedrick, and Greta J. Orris., (2002) "Rare Earth Elements Critical Resources for High Technology | USGS Fact Sheet 087-02." Rare Earth Elements Critical Resources for High Technology | USGS Fact Sheet 087-02.

Henderson, P., 1984. Rare Earth Element Geochemistry. Elsevier, Amsterdam. 510

Hogsden, K.L. & Harding, J.S., 2012. Anthropogenic and natural sources of acidity and metals and their influence on the structure of stream food webs. *Environmental Pollution*, 162, pp.466–474. Available at: http://dx.doi.org/10.1016/j.envpol.2011.10.024.

Hole, W. & Hole, W., 1995. The Aquatic Chemistry of Rare Earth Elements in Rivers and Estuaries., (Iii), pp.1–34.

Jenne, E.A., (1968), Controls on Mn, Fe, Co, Ni, Cu, and Zn concentrations in soils and water—the significant role of hydrous Mn and Fe oxides; in Gould, R.F. (ed.),Trace Inorganics in Water, Advances in Chemistry Series No. 73: American Chemical Society, Washington, D.C., pp. 337–387.

Jenne, E.A., (1977), Trace element sorption by sediments and soils—sites and processes; in Chappell, W.R., and Peterson, K.K. (eds.), Molybdenum in the Environment, Vol. 2: Marcel Dekker, New York, pp. 425–553.

Johannesson, K. H. (2005). Rare earth elements in groundwater flow systems. Dordrecht: Springer.

Johnson CA (1986) The regulation of trace element concentrations in river and estuarine waters contaminated with acid mine drainage: the adsorption of Cu and Zn on amorphous Fe oxyhydroxides. Geochim. Cosmochim. Acta 50: 2433-2438

Jury W.A. (1988) Solute Transport and Dispersion. In: Steffen W.L., Denmead O.T. (eds) Flow and Transport in the Natural Environment: Advances and Applications. Springer, Berlin, Heidelberg

Kimball, B. A., D. M. McKnight, G. A. Wetherbee, and R. A. Harnish, (1992). Mechanisms of iron photoreduction in a metal-rich, acidic stream (St. Kevin Gulch, Colorado, U.S.A.), Chem. Geol., 96, 227 – 239.

Kimball, B.A., Broshears, R.E., Bencala, K.E., McKnight, D.M., 1994: Coupling of hydrologic transport and chemical reactions in a stream affected by acid mine drainage. Environmental Science and Technology 28, 2065-2073.

Kimball, B.A., Callender, E., and Axtmann, E.V., (1995). Effects of colloids on metal transport in a river receiving acid mine drainage, upper Arkansas River, Colorado, U.S.A. Applied Geochemistry, 10, p. 285-306.

Kimball, B.A., (1997). Use of tracer injections and synoptic sampling to measure metal loading from acid mine drainage: U.S. Geological Survey Fact Sheet 245-96, 4 p. (Available online at http://ut.water.usgs.gov/publications/fs245-96/)

Kimball, B.A., Runkel, R.L., Walton-Day, Katherine, and Bencala, K.E., (2002), Assessment of metal loads in watersheds affected by acid mine drainage by using tracer injection synoptic sampling—Cement Creek, Colorado, USA: Applied Geochemistry, v. 17, no. 9, p. 1183– 1207.

Kleinmann R.L.P., Crear, D. A., and Pacelli, R. R., (1981), Biogeochemistry of Acid Mine Drainage and a Method to Control Acid Formation: Mining Engineering v. 33, p. 300-304.

Koeppenkastrop D. and De Carlo E. H. (1992) Sorption of rare earth elements from seawater onto synthetic mineral particles: an experimental approach. Chem. Geol. 95, 251–263.

Taylor H., Taylor, R. Huff, A. Montaser (1998) Novel Applications of ICPMS. Inductively Coupled Plasma Mass Spectrometry (first ed.)Wiley-VCH, New York

Trenberth, K. E., (1999): Short-term Climate Variations. Recent accomplishments and issues for future progress. Storms Vol 1. R. Pielke Sr and R. Pielke Jr (Eds). Routledge Press. London. 126-141.

Landa, E.R., Cravotta, C.A., Naftz, D.L., Verplanck, P.L., Nordstrom, D.K., Zielinski, R.A.,(2000). Geochemical investigations by the USGS on uranium mining, milling and environmental restoration. Technology 7, 381–396.

Liu, F., M. W. Williams, and N. Caine (2004), Source waters and flow paths in an alpine catchment, Colorado Front Range, United States, Water Resour. Res., 40, W09401, doi:10.1029/2004WR003076.

Lovering, T.S., Goddard E.N., (1950), Geology and ore deposits of the Front Range, Colorado. U.S. Geological Survey Professional Paper 223, p. 319

Marmier N., Dumonceau A. J. and Fromage F. (1997) Surface complexation modeling of Yb(III) sorption and desorption on hematite and alumina. J. Contam. Hydrol. 26, 159–167.

Marmier N., Delise´e J. A. and Fromage F. (1999a) Surface complexation modeling of Yb(III) and Cs(I) sorption on silica. J. Colloid Interf. Sci. 212, 228–233.

McKnight, Diane M., AND G. L. Feder. (1984). The ecological effect of acid conditions and precipitation of hydrous metal oxides in a Rocky Mountain stream. Hydrobiology: 119:129–138.

McKnight, Diane M., and Kenneth E. Bencala. (1990) "The Chemistry of Iron, Aluminum, and Dissolved Organic Material in Three Acidic, Metal-Enriched, Mountain Streams, as Controlled by Watershed and in-Stream Processes." *Water Resources Research* 26.12: 3087-3100.

McKnight, Diane M., K. E Bencala, G. W. Zellweger, G. R. Aiken, G. L. Feder AND K. A.Thorn. (1992). Sorption of dissolved organic carbon by hydrous aluminum and iron oxides occurring at the confluence of Deer Creek with the Snake River, Summit County, Colorado. Environ. Sci. Technol. 26: 1388–1396.

McKnight, Diane M., Kimball, B.A. & Runkel, R.L., (2001). pH dependence of iron photoreduction in a rocky mountain stream affected by acid mine drainage. *Hydrological Processes*, 15(10), pp.1979–1992.

McKnight, Diane M., and Sabre M. Duren (2004). "Biogeochemical processes controlling midday ferrous iron maxima in stream waters affected by acid rock drainage." *Applied Geochemistry* 19.7: 1075-1084.

McLennan S.M. (1994). Rare earth element geochemistry and the “tetrad” effect Geochim. Cosmochim. Acta 58, 2025–2033

Mote, P. W. (2006). Climate-Driven Variability and Trends in Mountain Snowpack in Western North America. Journal of Climate, 19(23): 6209-6220

Music S. and Ristic R. (1988) Adsorption of trace elements or radionuclides on hydrous oxides. J. Radioanal. Nucl. Chem. 120, 289–304.

Neuerburg, G. and T. Botinelly, (1972), Map showing geologic and structural control of ore deposits, Montezuma District, Central Colorado. USGS Miscellaneous Geologic investigations, Map I-750.

Nordstrom, D.K. & Southam, G., (1997). Geomicrobiology of sulfide mineral oxidation. *Geomicrobiology: Interactions between Microbes and Minerals*, (August), pp.361–390.

Nordstrom, D Kirk, (2009), Acid rock drainage and climate change: Journal of Geochemical Exploration, v. 100, iss. 2–3, p. 97-104.

Pullin, M.J., and SE Cabaniss. (2003), The effects of pH, ionic strength, and iron-fulvic acid interactions on the kinetics of non-photochemical iron transformations. II: The kinetics of thermal reduction. Geochim. Cosmochim. Acta. 67:4079-4089.

Rabung T., Geckeis H., Kim J. and Beck H. P. (1998) Sorption of Eu(III) on a natural hematite: application of a surface complexation model. J. Colloid Interf. Sci. 208, 153–161.

Rue, Garrett P., and Diane M. McKnight (2015). Geologic Misfortune: The Sourcing, Fate, and Transport of Rare Earth Elements in the Snake River Watershed, Montezuma, Colorado, ProQuest Dissertations & Theses, Ann Arbor

Runkel, R.L., (1995). Simulation models for conservative and nonconservative solute transport in streams. *Effects of scale on interpretation and management of sediment and water quality. Proc. symposium, Boulder, 1995*, 226, pp.153–159. Available at: http://pubs.er.usgs.gov/publication/70018887.

Runkel, R. L., D. M. McKnight, K. E. Bencala, and S.C. Chapra, (1996) Reactive solute transport in streams, 2, Simulation of a pH modification experiment, Water Resour. Res., 32(2), 419-430.

Runkel, R.L., (1998), One-Dimensional Transport with Inflow and Storage (OTIS): A Solute Transport Model for Streams and Rivers: U.S. Geological Survey Water-Resources Investigations Report 98-4018, 73 p.

Runkel, R. L., Kimball, B. A., Mcknight D. M., Bencala, K. E., (1999), "Reactive solute transport in streams: a surface complexation approach for trace metal sorption." *Water Resources Research* 35.12 (1999): 3829-3840.

Runkel, R.L. & Kimball, B.A., (2002), Evaluating Remedial Alternatives for an Acid Mine Drainage Stream: Application of a Reactive Transport Model. *Environmental Science & Technology*, 36(5), pp.1093–1101. Available at: http://pubs.acs.org/doi/abs/10.1021/es0109794.

Runkel, R.L., (2010), One-dimensional transport with equilibrium chemistry (OTEQ) — A reactive transport model for streams and rivers: U.S. Geological Survey Techniques and Methods Book 6, Chapter B6, 101 p.

Runkel, R.L. et al., 2013. Journal of Hydrology Estimating instream constituent loads using replicate synoptic sampling. *Journal of Hydrology*, 489, pp.26–41. Available at: http://dx.doi.org/10.1016/j.jhydrol.2013.02.031.

Runkel, R.L., 2015. On the use of rhodamine WT for the characterization of stream hydrodynamics and transient storage. Water Resour. Res. 51 (8), 6125–6142. http://dx.doi.org/10.1002/2015WR017201

Salomons, W., (1995). Environmental impact of metals derived from mining activities: Processes, predictions, prevention. *Journal of Geochemical Exploration*, 52(1–2), pp.5–23.

Saunders, Steven, Montgomery, Charles and Easley, Tom (2008). The West's Changed Climate. Rocky Mountain Climate Organization

Schemel, L. E., Kimball, B. A. & Bencala, K. E. (2000). Colloid formation and metal transport through two mixing zones affected by acid mine drainage near Silverton, Colorado. Applied Geochemistry, 15, 1003–1018.

Sholkovitz E. R. (1995) The aquatic chemistry of rare earth elements in rivers and estuaries. Aquat. Geochem. 1, 1-34.

Smedley, P.L. (1991). The Geochemistry of Rare Earth Elements in Groundwater from the Carnmenellis Area, Southwest England. Geochim. Et Cosmochim. Acta. V. 55, pp. 2767-2779

Smith, K.S., Ranville, J.F., Plumlee, G.S., and Macalady, D.L., (1998), Predictive double-layer modeling of metal sorption in mine-drainage systems; in Jenne, E.A. (ed.), Adsorption of Metals by Geomedia: Academic Press, San Diego, Calif., pp. 521– 547.

Smith, K. .S. and Huyck, H. L. O. (1999) An overview of the abundance, relative mobility, bioavailability, and human toxicity of metals; in Plumlee, G.S., and Logsdon, M.J. (eds.), The Environmental Geochemistry of Mineral Deposits, Part A: Society of Economic Geologists, Reviews in Economic Geology, v. 6A, pp. 29-70.

Stewart, I. T., Cayan, D. R., and Dettinger, M. D.: (2003), 'Changes towards Earlier Streamflow Timing across Western North America', in preparation.

Stumm, W. & Morgan, J.J., (1981). *Aquatic chemistry: an introduction emphasizing chemical equilibria in natural waters*, Wiley. Available at: https://books.google.com/books?id=EvZOAAAAMAAJ.

Sullivan, Annett B., James I. Drever, and Diane M. McKnight, (1998), "Diel variation in element concentrations, Peru Creek, Summit County, Colorado." *Journal of Geochemical Exploration* 64.1: 141-145.

Tang J. and Johannesson K. H. (2005) Adsorption of rare earth elements onto Carrizo sand: experimental investigations and modeling with surface complexation. Geochim. Cosmochim. Acta 69, 5247–5261.

Taylor, S.R., Lennan, M.M. & Mccxr, M.T., 1983. Geochemistry of loess , continental crustal composition and crustal model ages. , 41, pp.1897–1905.

Theobald, P.K., Lakin, H.W., Hawkins, D.B., (1963), The precipitation of aluminum, iron and manganese at the junction of Deer Creek with the Snake River in Summit County, Colorado. Geochim. Cosmochim. Acta 27, 121–132.

Todd, A., McKnight, D., & Wyatt, L. (2003). Abandoned mines, mountain sports,and climate variability: implications for the Colorado tourism economy. *Eos, Transactions American Geophysical Union*, *84*(38), 377-386. *DOI*: 10.1029/2003EO380002

Todd, A.S., 2005: Mining legacies in the Snake River watershed: the interaction of biogeochemistry, stream ecology, and human use. Doctor of Philosophy Thesis, University of Colorado at Boulder. Todd,

Todd, Andrew S., McKnight, D. M., and Duren S. M., (2005), Water Quality Characteristics for the Snake River, North Fork of the Snake River, Peru Creek, and Deer Creek in Summit County, Colorado: 2001 to 2002, vol. no. 57.;57.; University of Colorado, Institute of Arctic and Alpine Research, Boulder, Colo.

Todd A.S., Manning A.H., Verplanck P.L., Crouch C.M., McKnight D.M., R. Dunham, (2012), Climate-change-driven deterioration of water quality in a mineralized watershed Environ. Sci. Technol., 46, pp. 9324–9332

Trenberth, K. E., (1999), Short-term Climate Variations. Recent accomplishments and issues for future progress. Storms Vol 1. R. Pielke Sr and R. Pielke Jr (Eds). Routledge Press. London. 126-141.

Tweto, Ogden, and Sims, P.K., (1963), Precambrian ancestry of the Colorado mineral belt: Geological Society of America Bulletin, v. 74, no. 8, p. 991-1014.

Verplanck, P. L., R. C. Antweiler, D. K. Nordstrom, and H. E. Taylor, (2001), Standard reference water samples for rare earth element determinations, *Appl. Geochem.*, **16**, 231–244

Verplanck P.L., Nordstrom D.k. Taylor H.E. and Kimball B.A. (2004) Rare earth element partitioning between hydrous ferricoxides and acid mine water during iron oxidation. Applied Geochemistry 19 (2004) 1339–1354

Webster, J.G., Nordstrom, D.K., and Smith, K.S., (1994), Transport and natural attenuation of Cu, Zn, As, and Fe in the acid mine drainage of Leviathan and Bryant Creeks; in Alpers, C.N., and Blowes, D.W., (eds.), Environmental Geochemistry of Sulfide Oxidation: American Chemical Society Symposium Series 550, American Chemical Society, Washington, D.C., pp. 244–260

Webster, J.G., Swedlund, P.J. & Webster, K.S., (1998), Trace Metal Adsorption onto an Acid Mine Drainage Iron (III ) Oxy Hydroxy Sulfate. *Environmental Science and Technology*, 32(Iii), pp.1361–1368.

Yoshida T., Ozaki T., Ohnuki T. and Francis A. J. (2004) Adsorption of rare earth elements by c-Al2O3 and Pseudomonas fluorescens cells in the presence of deferrioxamine B: implication of siderophores for the Ce anomaly. Chem. Geol. 212, 239–246

Zhang Z., Fenter P., Cheng L., Sturchio N. C., Bedzyk M. D., Predota M., Bandura A. V., Kubicki J. D., Lvov S. N., Cummings P. T., Chialvo A. A., Ridley M. K., Benezeth P., Anovitz L., Palmer D. A., Machesky M. and Wesolowski D. J. (2004b) Ion adsorption at the rutile–water interface: linking molecular and macroscopic properties. Langmuir 20, 4954–4969.

Zhao, F., Cong, Z., Sun, H., Ren, D., 2007. The geochemistry of rare earth elements (REE) in acid mine drainage from the Sitai coal mine, Shanxi Province, North China. International Journal of Coal Geology 70, 184–192.